Diplomarbeit

Determination of the mobile ion fraction in molding composite materials: influence of time and temperature

Ausgeführt am Institut für
Chemische Technologien und Analytik
der Technischen Universität Wien

unter der Betreuung von

Univ.Prof. Dipl.-Ing. Dr.techn. Andreas Limbeck

durch

Tobias Raphael Schöberl, BSc

Datum

Unterschrift (Student)

"Aber an K.s Gurgel legten sich die Hände des einen Herrn, während der andere das Messer ihm tief ins Herz stieß und zweimal dort drehte. Mit brechenden Augen sah noch K., wie die Herren, nahe vor seinem Gesicht, Wange an Wange aneinandergelehnt, die Entscheidung beobachteten. »Wie ein Hund!« sagte er, es war, als sollte die Scham ihn überleben."

"Der Proceß" by Franz Kafka, 1925

Danksagung

An dieser Stelle möchte ich all jenen danken, die mich während der Zeit meines Studiums und bei dieser Diplomarbeit unterstützt haben. Beginnend bei Lukas Brunnbauer, der immer ein offenes Ohr für meine Anliegen und Probleme hatte und durch seine langjährige Erfahrung in jeder Schieflage weiterhelfen konnte. Des weiteren möchte ich meinem Betreuer, Andreas Limbeck, danken, der es mir ermöglicht hat in seiner Gruppe meine Diplomarbeit zu absolvieren. Ich möchte mich auch bei meinen Betreuern bei Infineon, Steffen Jordan und Stefan Schwab, bedanken, die immer ein offenes Ohr für Problemstellungen hatten und mit Informationen zu dem Probenmaterial selbst immer weiterhelfen konnten. Zusätzlich gilt ein großer Dank an Silvia Larisegger, welche mich immer organisatorisch und menschlich unterstützt hat.

Auch all den anderen Gruppenmitgliedern sei an dieser Stelle gedankt: Barbara Umfahrer, Birgit Achleitner, David Gibbs, Jakob Willner, Laura Kronlachner, Maximilian Podsednik und Zuzana Gajarska. Danke für den fachlichen Input und die Hilfe, wenn Geräte nicht funktioniert haben. Auch danke für die vielen lustigen Mittagessen und post-Seminar Biere in der Küche. Ohne euch hätte diese Zeit nur einen Bruchteil so viel Spaß bereitet.

Ein besonderes Danke geht an Anne Kasper-Giebl und Hong Huang für die Möglichkeit, IC, pH und Leitfähigkeitsmessungen durchzuführen und die Daten gemeinsam besprechen zu können. Durch diese weiteren Daten, konnte ein konkreteres Bild zum Verständnis der Ionenmobilität in Abhängigkeit von Zeit und Temperatur geschaffen werden.

Danke auch an all meine Freund:innen außerhalb des Studiums. Danke für das ewige ertragen meines Jammers und den unzähligen Malen meiner Absagen, wenn das Studium mal wieder mehr Zeit in Anspruch genommen hat. Danke für so viele schöne und unvergessliche Erinnerungen die ich doch inhärent mit diesem Studium verbinde.

Abschließend möchte ich hier all meinen Studienkolleg:innen danken, die mich über die letzten sechs Jahre begleitet haben. Danke für das Verschönern meiner Studienzeit. Danke für die viele Ausarbeitungen und das gemeinsame Lernen. Danke für die mentale Unterstützung, wenn das Leben an der Universität gerade alles andere als Spaß gemacht hat. Danke für die unzähligen Male mit Bier und Wein nach den Vorlesungen und getaner Arbeit. Danke, Alena, Anna, Benedikt, Johannes, Marlene, Nico, Nicole, Sarah und Stefan. Ohne euer Dasein, hätte dieses Studium nicht mit einem Abschluss geendet.

Kurzfassung

Halbleiter werden heutzutage in fast allen Lebensbereichen eingesetzt und sind ein treibender Faktor für Innovation. Dementsprechend wird von Geräten mit integrierten Halbleiterelementen erwartet, dass sie eine konstante Leistung erbringen und eine lange Lebensdauer vorweisen, bevor erste Anzeichen von Materialermüdung auftreten. Je nach Umgebung kann die Lebensdauer jedoch stark verkürzt werden, da Produktausfälle wahrscheinlicher werden, wenn die verwendeten Bauteile extremen Bedingungen ausgesetzt sind. Daher ist es von großem Interesse, diese Halbleiterelemente (Mikrochips, Transistoren), die auf Leiterplatten (PCBAs) eingesetzt werden, zu schützen. Hierfür können verschiedene Materialien verwendet werden, darunter auch Molding Kompositmaterialien, auch Molding Compound genannt. Molding Compound ist ein Verbundwerkstoff aus Siliziumdioxidpartikeln und verschiedenen (an)organischen Zusatzstoffen, die in einer synthetischen Polymermatrix eingebunden sind. Durch das Zusetzen dieser (an)organischen Verbindungen wird der Ionenanteil im Molding Compound drastisch erhöht. Auf dem Halbleiterbauelement selbst werden elektrische Felder induziert, die eine Ionenmigration und -anreicherung an den Elektroden bewirken. Da nicht jede Verunreinigung oder jeder Zusatzstoff im Feststoff mobil ist, ist es von großem Interesse, den Anteil an mobilen Ionen zu bestimmen.

Für die industrielle Anwendung wird das Extraktionsverfahren nach der Norm SEMI G29 verwendet, die 48 h Extraktionszeit unter Verwendung von 100 mL Wasser und 10 g (1:10 Verhältnis) Molding Compound bei 120 °C mit anschließender Analyse des gewonnenen Extrakts mittels induktiv gekoppelter Plasma Massenspektrometrie/Optischer Emissionsspektroskopie (ICP-MS/OES) vorsieht. Hierbei ergeben sich vor allem zwei Nachteile: eine lange Probenvorbereitung und ein hoher Probenverbrauch, was zu einem geringen Probendurchsatz führt. Infolgedessen neigen Hersteller dazu, das Standardverfahren zu variieren, was zu unvergleichbaren Ergebnissen führt.

In dieser Arbeit wurde eine Methode zur Quantifizierung des Gesamtionengehalts in Molding Compound durch mikrowellenunterstützten Säureaufschluss und anschließender ICP-MS-Analyse entwickelt. Für die Bestimmung des Gehalts an mobilen Ionen wurde eine mikrowellengestützte Extraktion und anschließender ICP-OES-Analyse entwickelt, welche anschließend mit der Norm SEMI G29 verglichen wurde. Die Extraktionszeiten und -temperaturen wurden von 30 min bis 48 h und von 60 °C bis 225 °C variiert. Die Ergebnisse zeigen, dass die Elemente Na, Mg & Ca bereits innerhalb von 30 min der Extraktion mobil sind und dass kürzere Extraktionszeiten und höhere Temperaturen bereits eine hohe Extraktionseffizienz aufweisen, was einen höheren Probendurchsatz erlaubt. Mit diesen Ergebnissen können weitere Experimente durchgeführt werden, um das Auslaugungsverhalten von Molding Compound zu untersuchen.

Abstract

Nowadays semiconductors are used in almost every aspect of a person's life and drive innovation within the industrial sector. Logically so, devices that use semiconductors are expected to perform on a constant level with a long life-time before first signs of fatigue show. Depending on the environment, the life-time can be rather short, as product failure increases when these devices are exposed to harsh conditions, i.e. radiation and high temperatures. Therefore, it is of great interest to protect these semiconductor devices (microchips, transistors) implemented on Printed Circuit Board Assemblies (PCBAs). Various materials for protection can be used, one of it being molding compound. Molding compound is a composite material made of silica particles and various (in)organic additives bonded into a synthetic polymer matrix. By introducing these (in)organic compounds, the ion fraction within the molding compound increases. On the semiconductor device itself, electrical fields are induced and cause ion migration and accumulation at the electrodes, which accelerates corrosion. As not every impurity or additive is mobile within molding compound, it is of great interest to determine the mobile ion fraction from the total and mobile ion content.

For industrial application, the standard SEMI G29 is used as an extraction procedure which requires 48 h of extraction time using 100 mL of water and 10 g of molding compound at 120 °C with subsequent analysis of the derived extract using Inductively Coupled Plasma Mass Spectrometry/Optical Emission Spectroscopy (ICP-MS/OES). This brings two disadvantages: long sample preparation and great sample consumption, resulting in low sample throughput. As a result, manufacturers tend to vary the standard procedure leading to incomparable results.

In this work, a method for ion quantification within molding compound using microwave assisted acid digestion with subsequent ICP-MS analysis was developed. A microwave-based extraction method employing ICP-OES was developed for mobile ion determination which was then compared to the standard SEMI G29. Extraction times and temperatures were varied from 30 min to 48 h and 60 °C to 225 °C. Results show that elements Na, Mg & Ca are mobile within already 30 min of extraction as well as shorter extraction times and higher temperatures are favorable, yielding a higher sample throughput. With these results, further experiments can be conducted, investigating the short-term leaching behavior of molding compound.

Contents

1 Introduction

Composite materials are per definition at least made of two different types of components, that are mixed but still distinguishable by phase separation. By combining these components, they gain properties that could not be achieved by employing the two materials as their own. Composite materials find a wide application range from aerospace structures to housing material for microchips. Due to these ranges, the material mixtures employed also vary. In this work, the focus lays upon the characterization of epoxy resin based composite material (molding compound) used for housing and protection in Printed Circuit Board Assemblies (PCBAs)[1]. Due to its application in technical fields, polymer based composite materials may come into contact with materials subject to corrosion (microchips, metals of various kind). Because of changes in temperature and humidity within the housing of a semiconductor device, water may condensate, which can then lead to the diffusion of mobile ions within this housing material into the liquid phase[2]. Wherever humidity as well as an accumulation of ions can be found, fatigue occurs due to various corrosion processes[3–5]. On microchips themselves, electrical fields are induced. With a trend towards miniaturisation, these fields only get stronger as the electrical field is defined as $F \propto \frac{U}{d}$ where U is the voltage and d the distance between the line spacings. This plays a factor within the fatigue of these parts, as higher electrical fields yield an accelerated corrosion process and ion migration[2,6].

As a long lifetime of electronic products is favored by costumers and producers, it is of great interest to understand the corrosion processes/ ion migration and minimize fatigue. One part of this is to determine which ions and how much of them are mobile within this epoxy resin based molding compound. In general, molding compound is a challenging materials to analyze as it consists of two different phases which are of organic (epoxy resin) and inorganic (silica particles) nature. Additionally, molding compound, as it is used for housing materials, is made in a way that it withstands even harsh environments, so sample preparation is tedious. For the organic, continuous phase of the molding compound, general approaches for polymer characterization can be employed such as Fourier Transform Infrared Spectroscopy (FT-IR), Raman Spectroscopy, Matrix Assisted Laser Desorption Mass Spectrometry (MALDI-MS) as well as Pyrolysis Gas Chromatography (Py-GC)[7,8]. These principles may yield information about the type of epoxy resin or degradation products. However, elemental information cannot be extracted as well as little to no spatial information about the distribution within the composite material. For spatial elemental information, Laser Ablation Inductively Coupled Plasma Mass Spectrometry (LA-ICP-MS), Laser Induced Breakdown Spectroscopy (LIBS), Scanning Electron Microscopy Energy Dispersive X-ray spectrometry (SEM-EDX) as well as Secondary Ion Mass Spectrometry (SIMS) can be employed to characterize molding compounds[9]. As these methods use probes which can be focused from the μm to nm range, they come with the advantage of almost no sample preparation as well as easy generation of qualitative data. However, gaining information about the bulk content and quantification of the analytes in general poses a challenge, as the interaction of the laser with the sample strongly depends on the sample matrix, making it necessary to use matrix matched standards. For common materials, these standards can be bought.

However, with a less common sample material, they need to be prepared in-house. Preparations of matrix matched solid standards is a difficult task, as homogenization of solids is difficult. Additionally, resulting Relative Standards Deviations for good measurements lay around 10 %, which is significantly higher than its liquid counterpart[10–12] .

In this thesis, different approaches have been applied to determine the mobile ion fraction within six different molding compound samples provided by Infineon Technologies. For total ion quantification, Microwave Assisted Acid Digestion (MAAD) was performed to dissolve the polymer matrix and its additives besides added silica. MAAD is an easy and quick method for accelerated sample digestion, being able to dissolve complex solid samples matrices within a view hours due to the ability to raise the temperature higher than the boiling point of the acid mixture at 1 atm, as these digestions are performed in pressure stable Teflon vessels. Ideally, the complete sample is mineralized during the digestion for reasons of reproducibility. If a sample is not mineralized completely, these fragments may cause unwanted matrix effects later in the analysis or cause analyte loss due to adsorption[13] .

Analytes were then quantified using Inductively Coupled Plasma Mass Spectrometry (ICP-MS). ICP-MS poses as one of the most sensitive methods for elemental quantification with a Limit Of Detection (LOD) in the sub-pg g^{-1} range for most elements. ICP-MS has found its way into many application fields from the fields of biomedical, nuclear, environmental, geological to material science. Additionally, elemental quantification is an easy task due to mostly matrix-independent ionization within the plasma, making it possible to simply use inorganic elemental standards for external calibration. The measurement of liquid samples has been approached since the upcoming of the first commercial instrument in 1983, thus, with years of experience, making it an off-the-shelf bench-top technique with resulting RSDs below 1-2 %[14] .

After determination of the total amount of ions of interest within the molding compound, aqueous extractions were performed in order to determine the mobile ion fraction. These extracts were then further characterized using various techniques: Inductively Coupled Plasma Optical Emission Spectroscopy (ICP-OES) for cation and carbon detection, Ion Chromatography (IC) for the quantification of acetate, formate, lactate, chlroride, nitrate and sulfate and additional measurements of the pH-value as well as the conductivity for further characterization. ICP-OES poses a less sensitive but more robust quantification method when being compared to ICP-MS with a LOD in the $\mu g\, g^{-1}$ to ng g^{-1} range, depending on the element, respectively. In addition, ICP-OES instruments are cheaper and better suited for samples with a possible wide range of concentration, whereas ICP-MS instruments may face a detector overload and show further difficulties due to isobaric interferences, depending on the analyte. As well as ICP-MS, ICP-OES is also employed in many different fields of sciences and considered an off the shelf benchtop technique since its first commercial instrument in 1974[15] .

IC is a well established method for ion quantification. Depending on the column material, cations or anions of inorganic and organic nature can be separated and analyzed depending on the charge of the ion as well as the overall charge distribution. IC is widely applied and a laboratory staple, as it allows easy and fast separation of ion and LODs in the low ng g^{-1} range. Though cations and an anions can be analyzed, in this work, only the anions were determined using the IC system, as ICP-OES allows an easy and quick approach with simultaneous detection of 75 of the 92 naturally occurring elements. The main focus for IC was the determination of the chloride content within the prepared extracts. However, as other anions (inorganic and organic) may also be involved in corrosion processes, external calibration for acetate, formate, lactate, chlroride, nitrate and sulfate was performed overall[15,16] .

2 Theoretical Aspects

As multiple instrumental analytical techniques were employed for this thesis, the following chapters will focus on an overview about the techniques applied as well as thorough explanation of their principles. Methods applied range from sophisticated instruments such as Inductively Coupled Plasma Mass Spectrometry (ICP-MS) to more simple principles such as the measurement of pH value and conductivity. Overall five different instrumental methods were used to characterize the mobile ion fraction in molding composite material: Inductively Coupled Plasma Mass Spectrometry / Optical Emission Spectroscopy (ICP-MS/OES) for easy elemental quantification, ion chromatography for the detection of anions as well as pH value and conductivity to further characterize the extracts yielded. In addition to the methods and principles applied in the course of this thesis, the following chapters will also discuss the sample type analyzed: molding compound.

2.1 Inductively Coupled Plasma Mass Spectrometry / Optical Emission Spectroscopy (ICP-MS/OES)

Nowadays, the analytical usage of a sustained Ar plasma is applied in many fields from geochemistry over biology to material sciences. On the contrary to different analytical principles such as Flame Atomic Absorption Spectrometry (F-AAS) or Graphite Furnace Atomic Absorption Spectrometry (GF-AAS) an inductively coupled Ar plasma reaches temperatures above 10 000 K which then allows for an easy matrix-independent multi-element quantification method[14] . Depending on the demanded Limit of Detection (LOD) as well as lab infrastructure, instruments for Inductively Coupled Plasma Mass Spectrometry (ICP-MS) or Inductively Coupled Plasma Optical Emission Spectroscopy (ICP-OES) are employed. The sample material is introduced into the instrument in form of a fine aerosol, either of liquid or solid nature. For its routine application ICP-MS/OES is mostly coupled to a liquid sample introduction system, offering LODs in the ng g^{-1} to sub-ng g^{-1} range and a Relative Standard Deviation (RSD) below 1 to 2 %. Using this set-up, in combination with beforehand (liquid) sample digestion, an average analyte concentration within a wide range of sample materials can be analyzed to a high certainty. However, as mentioned, only an average information can be yielded. If spatial or depth-resolved measurements are of interest, coupling to a laser is necessary in order to achieve this goal. Laser Ablation ICP-MS/OES (LA-ICP-MS/OES) has gained big popularity in the last 10 to 20 years as it, together with Laser Induced Breakdown Spectroscopy (LIBS), allows for fast and easy acquisition of elemental information with almost no sample preparation needed. Nonetheless, this has its price, as every sample interacts different with the laser photons applied, resulting in strong matrix effects, thus quantification poses a clear challenge when it comes to LA-ICP-MS/OES and LIBS. In this section, the principles and details of ICP-MS/OES will be explained. For this, the topics are split into to three parts: the inductively coupled plasma itself and the processes evoked, the mass analyzer and the optical system to analyze the emitted photons from the plasma[14,15,17] .

2.1.1 Inductively Coupled Plasma (ICP)

Before going into detail about plasma generation, the term plasma needs do be defined first. A plasma is a gas which macroscopically can be described as of neutral charge, however on a microscopical basis, the gas is made up of free charges, ions and electrons, as well as neutral species. Due to additional forces being employed when these free charges interact with each other, the gas itself gains new properties which would not be achievable if the gas consisted of only neutral atoms. Because of these newly gained properties, a plasma is thus considered as its own state of matter, often referred to as the fourth state of matter besides gaseous, liquid and solid[18] . Inductively Coupled Plasma (ICP) is the most commonly used type of generated plasma, other examples being Direct Current Plasma (DCP) as well as Microwave Induced Plasma (MIP). For ICP generation three components are necessary, a Radiofrequency (RF) generator, a plasma torch and the plasma gas itself. In almost every case, Ar is used as the plasma gas as its high ionization energy (15.76 eV) is high enough to ionize almost every element (exceptions being He, Ne and F). As an inert gas, Ar does not tend to react with analyte ions present (compared to other non-inert gases) as well as its abundance of 1 % in the atmosphere, making it the most abundant of all noble gases[15,19,20] . The plasma torch is made up of three concentric tubes of different diameter usually made of quartz glass or corundum. A schematic picture of the plasma torch arrangement can be seen in Figure 1,.[14]

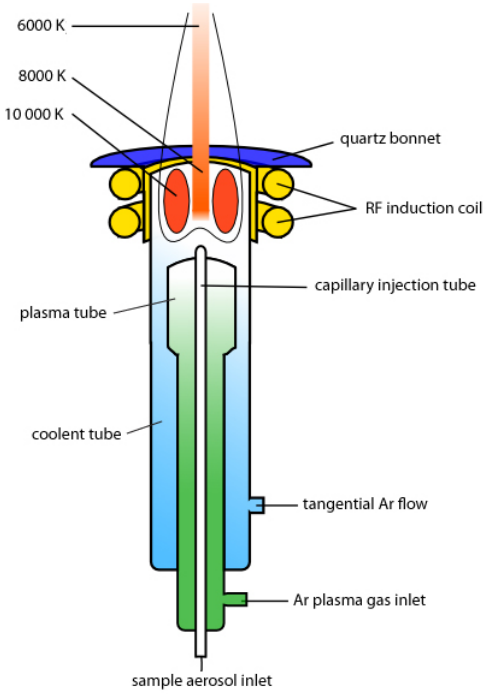

Figure 1: Schematic drawing of the design of an ICP torch[21]

Through these tubes, Ar is flushed at different velocities. The gas flow between the outer and middle tube is called cooling gas and is usually regulated from 12 to 17 $\mathrm{L\,min^{-1}}$. The flow between the middle and the inner tube is called auxiliary gas flow and has a flow of ca. 1 $\mathrm{L\,min^{-1}}$. Via the inner tube, the sample aerosol is transported introduced into the system using

the nebulizer gas flow of ca. $1\,\mathrm{L\,min^{-1}}$. In conclusion, an overall gas stream of 14 to $19\,\mathrm{L\,min^{-1}}$ is used when the instrument is at work[14]. With the RF generator, an alternating current at, in our case, 27 MHz is put through a copper coil which, in combination of its impedance, induces a magnetic field, perpendicular to the flow direction of the current, with the same frequency as the current. When the plasma is ignited a short high voltage spark ionizes Ar atoms and the ions and electrons are then accelerated in the magnetic field, gaining energy and colliding with other Ar atoms and eventually ionizing them. The different processes induced by collisions in the plasma can be seen in Equation 1 to Equation 3, where e^-... electron, Ar^+... Ar ion, Ar^*... excited Ar atom and Ar^m... metastable Ar atom. After a certain time (10 to 20 min), an equilibrium between new ion formation and recombination processes is reached[14,15].

$$\mathrm{e^- + Ar \rightarrow Ar^+ + 2\,e^-} \tag{1}$$

$$\mathrm{e^- + Ar \rightarrow Ar^* + e^-} \tag{2}$$

$$\mathrm{e^- + Ar \rightarrow Ar^m + e^-} \tag{3}$$

As can be seen in Figure 1, the plasma has a strong temperature gradient. The hottest zone (Induction Zone (IZ)) is in the red doughnut shaped region at the coil, where the temperature exceeds 10 000 K. Going 10 to 20 mm above the coil, we find the Normal Analytical Zone (NAZ) where the temperature ranges from 6000 to 8000 K. In this zone, mostly ions can be found and resulting emission lines also mostly respond to those of relaxed ions. Ions and photons yielded for analytical use, are mostly taken from this region of the plasma. Going further, the temperature only decreases and recombination processes take place, forming polyatomic ions and oxides. During the analysis, the sample is introduced as a fine wet aerosol which then undergoes different processes in the plasma: the fine droplets are desolvated and form solid particles, which are then vaporized and atomized. After the sample has been broken down to its atomic components, collisions with the plasma gas can now either excite or ionize the atoms. The possible reactions caused by the collision with mostly electrons can be seen in Equation 4 to Equation 10., where M... analyte atom, M^+... analyte ion, M^*... excited analyte atom, M^{+^*}... excited analyte ion[14,15]. During recombination processes, a continuous spectrum of Bremsstrahlung is emitted which creates a background signal in mostly the visible part of the electromagnetic spectrum. Because of this Bremsstrahlung, cold plasma conditions (power supply of 0.7 to 0.9 kW) are necessary for the measurement in order so increase the Signal to Noise Ratio (SNR) of elements emitting in this energy range such as Na and K[15].

$$M + e^- \rightarrow M^+ + 2\,e^- \quad (4)$$

$$M + e^- \rightarrow M^* + e^- \quad (5)$$

$$M + Ar^* \rightarrow M^* + Ar \quad (6)$$

$$M + Ar^* \rightarrow M^+ + Ar + e^- \quad (7)$$

$$M + Ar^* \rightarrow M^{+^*} + Ar + e^- \quad (8)$$

$$M + Ar^+ \rightarrow M^{+^*} + Ar \quad (9)$$

$$Ar^+ + e^- \rightarrow Ar + h\nu \quad (10)$$

2.1.2 Analytical use of ions in ICP-MS

During an ICP-MS measurement, a liquid sample is introduced into the system where it is then nebulized into a fine aerosol. This aerosol is then transported into the Ar plasma with an efficiency of 1 to 3 %. In the plasma itself, the wet aerosol is desolvated into small particles which are then further atomized. During the different collisions in the plasma of the analyte atoms with the electrons and Ar ions, they are then ionized/ excited and the resulting ions can then further be excited as well. The analyte ions are then extracted into the mass spectrometer through an interface made of two Ni cones (sampler and skimmer cone) using electronic lenses as well as the pressure gradient. There is a strong pressure difference between the Ar plasma (ambient pressure) compared to the mass spectrometer (10^{-7} bar). This vacuum is maintained using a differential pumping system via an oil rotary pump in addition to turbo molecular pumps in the mass spectrometer. The ions then pass a collision cell (see paragraph 2.1.2.3) and are then separated according to their mass to charge ratio before they are detected using a Secondary Electron Multiplier (SEM). A schematic picture of the general measurement set-up for an ICP-MS measurement can be seen in Figure 2[22].

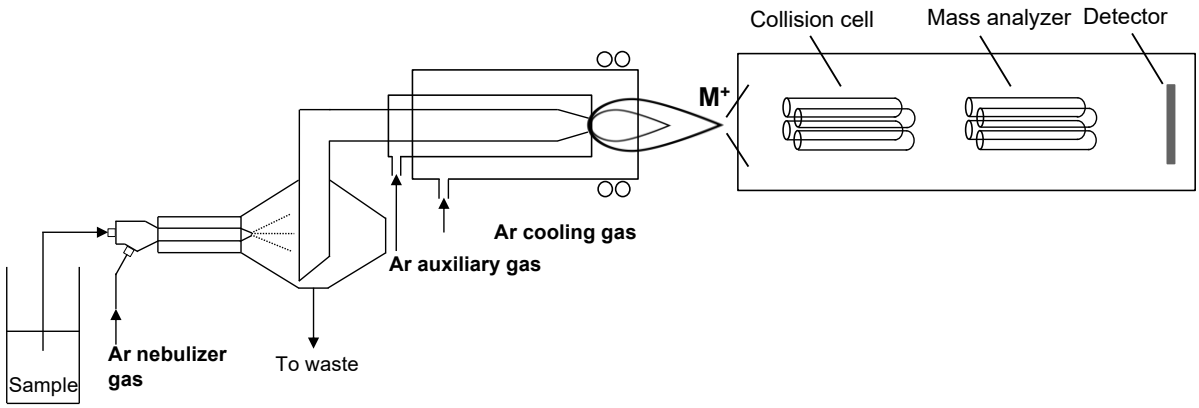

Figure 2: Schematic picture of the general setup for an ICP-MS measurement if coupled to a liquid sample introduction system

2.1.2.1 Interface in ICP-MS

In ICP-MS, the produced ions are then further extracted into a mass spectrometer using an axially positioned interface which can be seen in Figure 3. The ions must be extracted sufficiently into the mass spectrometer, using electronic lenses as well as the pressure gradient between the plasma (1.013 bar) and mass spectrometer ($<10^{-7}$ bar). The ions pass through two cones made of Ni or Pt, where a pressure of ca. 10^{-3} bar is maintained. The first cone (sampler cone) has an orifice with a diameter of 0.8 to 1.2 mm and shortly after comes the skimmer cone with a diameter of 0.4 to 0.8 mm, these cones further focus the extracted ion beam. As not only ions, but also photons and uncharged particles can be introduced into the mass spectrometer system, these can damage the detector system/ falsify measurements (depending on the detector). To avoid this, electronic lenses are used to the deflect the ion beam by 90° or slightly off axis. As only the ion beam trajectory can be manipulated using electronic fields, the uncharged particles and photons collide with the walls of the system and can no further influence the measurement,.[14,15]

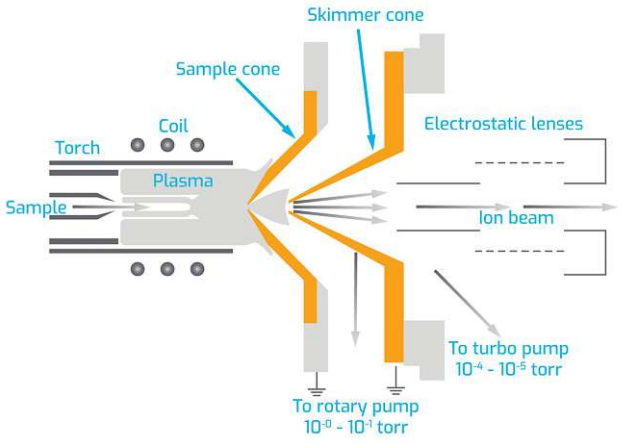

Figure 3: Design of an ICP-MS interface using a sampler and skimmer cone[23]

2.1.2.2 Mass Analyser

Different mass analyzers are applied in ICP-MS such as quadrupole, Time Of Flight (TOF) and Sector Field (SF) instruments. As a quadrupole mass analyzer instrument was used for this work, the following chapter will further focus to highlight the working principle of such. A quadrupole consists of four metal rods in each corner of a square which are either made of stainless steel or Molybdenum. A Direct Current (DC) and a Alternating Current (AC) at 2 to 3 MHz are placed through opposite rods with a positive and negative bias. The result of this is then a complex electrical field which forces the ions into certain trajectories. For a given DC/AC ratio a mass to charge ration (m/z) exists, which trajectory passes through the quadrupole wheres other m/z ions collide with the rods and are neutralized, thus unable to reach the detector. The principle ion trajectory during mass separation can be seen in Figure 4. By scanning over different DC/AC ratios, it is possible to scan a certain range of m/z ratios. Most quadrupoles work in a mass range of 1 to 300 Da with a mass resolution of approx. 300,

allowing the separation of integer mass differences. During analysis, the quadrupole can either scan over the whole mass range sequentially or just perform in peak hopping mode where certain m/z values are selected and the instrument switches from one to another, resulting in a more efficient usage of the measurement time. For statistical purposes, a certain DC/AC ratio is maintained for usually 10 ms and the registered counts are then extrapolated to one second, resulting in the derived unit Counts Per Second (cps). The time for which the DC/AC ratio is held constant is referred to as dwell time and the repeats of each dwell time are then called sweeps[14, 15, 22] .

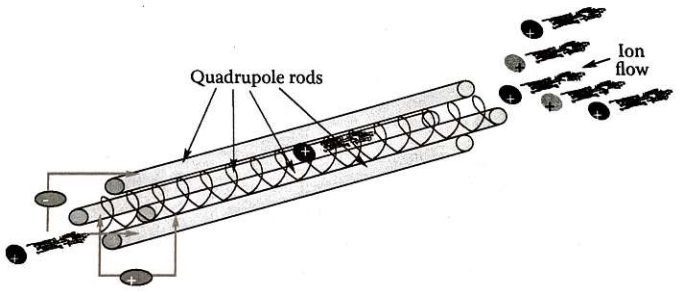

Figure 4: Schematic principle of a quadrupole mass analyzer including the ion trajectory during mass separation[14]

2.1.2.3 Kinetic Energy Discrimination (KED)

In the plasma, the introduced sample gets atomized and ionized and monoatomic species are further extracted into the mass spectrometer. Besides those monoatomic species, also polyatomic species form in the plasma, though the probability is rather low. However, if the constituents are present in a large amount within the plasma mixture, even a small probability results in a large amount of such polyatomic species. Using an Ar plasma in combination with an aqueous sample, O from the water or acid can easily react with the Ar atoms and thus species such as $^{40}Ar^{16}O^{+}$ are formed. Of course, $^{40}Ar^{16}O^{+}$ is only a mere example of the great amount of polyatomic species formed. Nominally, the mass to charge ratio (m/z) of $^{40}Ar^{16}O^{+}$ is 56, the same as $^{56}Fe^{+}$. Using a quadrupole mass analyzer only integer masses can be separated due to its low mass resolution (approx. 300), meaning that $^{40}Ar^{16}O^{+}$ cannot be separated from $^{56}Fe^{+}$, though their exact mass differs due to the mass defect. Of course, these problems are no issue when a high resolution mass analyzer such as a double focusing Sector Field (SF) instrument is employed. Throughout the years, different approaches were applied in order to minimize the formation of these so-called isobaric interferences as well as techniques were developed to eliminate these interferences from the ion beam. For example, for single quadrupole instruments, the application of cold plasma conditions (lower plasma temperatures) results in less formation of polyatomic interferences. However, this approach is prone to matrix effects. Nowadays, mainly collision cell technology as well as reaction cell technology is applied for the reduction of isobaric interferences in quadrupole based instruments. As many different versions are applied in different instruments, only the mechanism which was applied during this work will be further discussed. The ion beam is introduced into a quadrupole where only an alternating current is applied (radio frequency only mode) for ion beam stabilization & focusing and a gas is flushed

through collision cell, for example H_2 mixed with He. Comparing the isobaric interference with the analyte ion (see Figure 5), it is obvious that the cross section of the interference is much greater compared to the analyte[14,22]. This is visualized for the $^{40}Ar^{16}O^+$ & $^{56}Fe^+$ example in Figure 5.

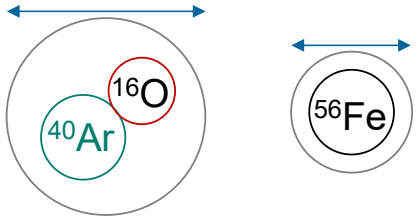

Figure 5: Comparison of the cross sections of $^{40}Ar^{16}O^+$ and $^{56}Fe^+$ (not to scale)

When the ion beam passes through the collision cell, the ions collide with the gas atoms. During these collisions, they lose kinetic energy. As polyatomic interferences have a greater kinetic cross section compared to the monoatomic analytes, statistically they collide more often and thus lose more energy as of the inelastic nature of these collisions. After the collision cell, an energy barrier is placed and only ions with an energy high enough can pass further to the quadrupole mass analyzer. However, ions with lesser energy are eliminated out of the ion beam. The applied collision gas flows and energy barrier applied at the end of the cell needs to be optimized for the application for either multi-element analysis or specific analytes. This technology is called Kinetic Energy Discrimination (KED) and all analyte ions are measured at their expected mass to charge ratio. The collision cell can also be flushed with a reactive gas where the analyte ions can react with the gas, whereas the polyatomic interferences cannot, and a mass shift occurs. This is called reaction cell technology and different gasses are applied such as NH_3 or O_2 mixed with He. Further developments include the application of a triple quadrupole ICP-MS system, accounting for even better elimination of isobaric interferences[14,22].The graphic principle for KED can be seen in Figure 6.

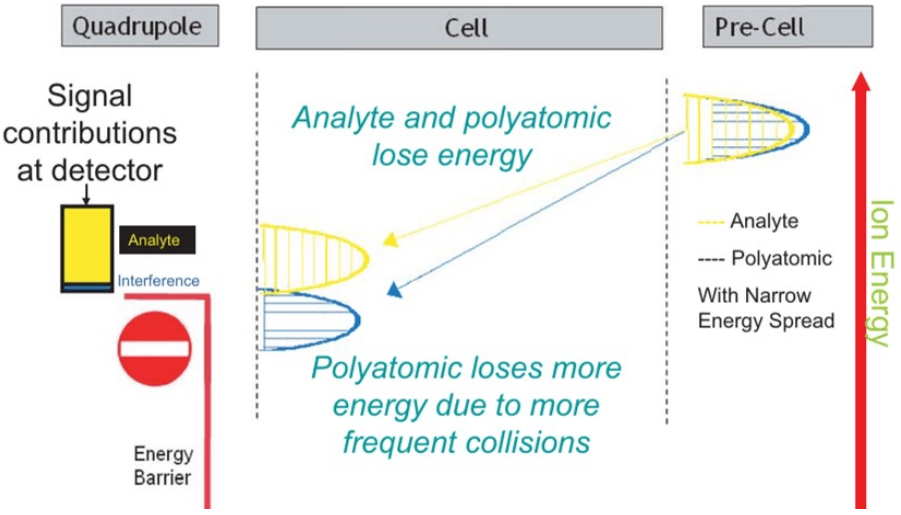

Figure 6: Graphic principle of Kinetic Energy Discrimination (Courtesy of ThermoScientific)[24]

2.1.2.4 Secondary Electron Multiplier (SEM)

After the ions are separated using the mass analyzer, they then need do be detected. As for ion detection devices, different types can be employed such as a Faraday cup or a Secondary Electron Multiplier (SEM). As latter one was employed during this work, this chapter aims to highlight the working principle of a SEM detector. After mass separation the ions go further to the detector, where they first hit a conversion dynode and electrons are emitted and accelerated towards a second dynode where additional electrons are emitted and further accelerated, resulting in an electron cascade and signal amplification. Thus, the SEM converts a positive ion current into a negative electron current. The dynode material is usually made of CuBe and AgMg alloys and high work functions are of interest so only minimal dark current is obtained (noise reduction). The electrons are accelerated to 10 to 14 dynodes using sequentially higher potentials at each dynode with an overall potential difference between the first and last dynode ranging from 3 to 6 kV. After the last electrode, the current is then measured and amplification factors range from 10^5 to 10^8. As for multi-element approaches, the concentration of the analyte can vary drastically. For this, dual ion detectors using SEM are implemented in modern ICP-MS instruments. Here two different kinds of detection modes are possible, analog mode and counting mode. Using the counting mode for low ion intensities, all dynodes are used for signal amplification. On the opposite, the analog mode is used for high ion intensities, where at a certain dynode the signal is read out already to increase the lifetime of the SEM as the dynode material is a consumable. Using this combination, a dynamic range for linear calibration of 10^9 can be achieved.[14,15,22] The schematic principle of a SEM can be seen in Figure 7 and the schematic principle for the counting and analog mode implemented into one SEM can be seen in Figure 8.

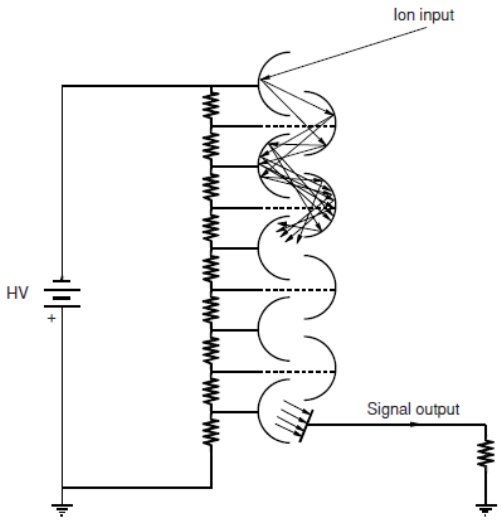

Figure 7: Schematic principle of a Secondary Electron Multiplier (SEM) with discrete dynodes[25]

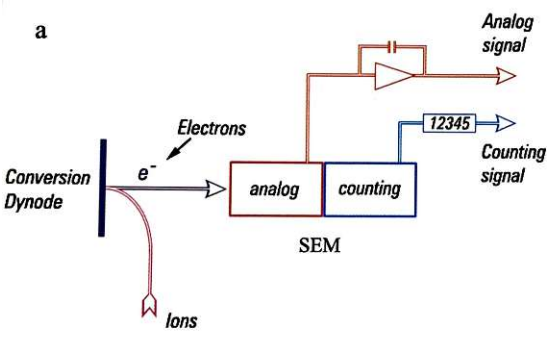

Figure 8: Schematic principle of a Secondary Electron Multiplier (SEM) in dual detection mode: analog and counting[22]

2.1.3 Analytical use of emitted photones in ICP-OES

Before an ICP was used as an ion source for mass spectrometry, the emitted photons of the analytes were analyzed in order to gain elemental data from the introduced sample. The use of an ICP for optical emission spectroscopy was firstly described by Greenfield et al. In ICP-OES, atoms or ions are excited from a ground state S_0 to an excited state S_n and relax back to S_0 within a time frame of 10^{-7} s, resulting in the emission of photons. As energy levels are discrete and characteristic for each element, these emitted photons are also characteristic and can be used for elemental identification. However, energy levels and transitions in different elements may not differ a lot in energy, thus photons differ only a few pm in wavelength and it may be not possible to resolve photons of such similar energy. It is assumed that the amount of emitted photons depends linearly on the amount of analyte atoms present in the plasma which depends on the concentration of the analyte within the sample solution. In ICP-OES two measure modes are possible, radial viewing and axially viewing of the plasma. In radial viewing the entrance slit for the optics lays perpendicular to the axis of the plasma and with axial viewing mode it lays in the same axis[15,22,26]. In this work a radial ICP-OES instrument was used and a schematic picture of this instrument setup can be seen in Figure 9.

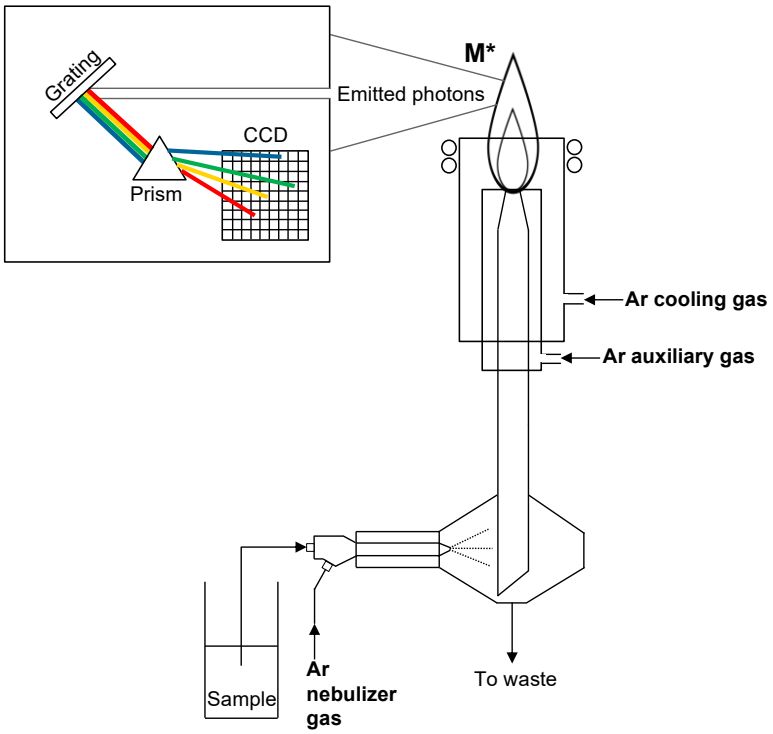

Figure 9: Schematic picture of the general setup for a radial ICP-OES measurement if coupled to a liquid sample introduction system

2.1.3.1 The spectrometer

A continuous spectrum (Bremsstrahlung) together with various line spectra of photons is emitted from the plasma coming from Ar itself, various impurities and the analyte atom/ ions. Each element atom/ ion serves a line spectrum with emission lines which can then be selected for the

analysis. For trace element analysis, lines are chosen which have a high emission intensity as well as low interference with other elements, allowing easy quantification. Before detection, the polychromatic emitted light needs to be separated according to the energy of the resulting photons. For this, dispersive devices are applied using diffraction or refraction. Depending on the spectrometer used, the photons are either detected simultaneously or sequentially[15,27]. Though every emitted line is characteristic for each element, some lines either overlap in their peak shape or lay very close to each other on the energy spectrum. For example, Cr emits at 267.716 nm and Pt emits at 267.715 nm. This obviously demands the use of high resolution spectrometers[15,19]. In general, three different types of spectrometers are used in ICP-OES analysis: the Czerny-Turner monochromators (diffraction), echelle polychromators (diffraction and refraction) and a polychromator in the Paschen-Runge design (diffraction). In this work, an instrument with echelle optics was used and thus only the echelle polychromator will be further explained[15,27,28].

Using echelle optics, the emitted light enters the spectrometer through the entrance slit and is further collimated before it hits the echelle grating. The grating usually has 30 to 300 grooves mm^{-1} and opts for higher diffraction orders compared to a grating used in a Czerny-Turner monochromator with 600 to 1200 grooves mm^{-1} which opts for a diffraction order of $n = 1$. After the echelle grating, the diffraction orders still overlap and need to be further separated using a refractive element (prism). For the prism, ideally a material is employed which has low to no absorption in the energy range of the photons (160 to 800 nm), for example CaF_2. After passing through the prism, this two dimensional picture of the diffraction orders (vertical) and wavelengths (horizontal) hits a solid state detector such as a Charged Coupled Device (CCD) or a Charge Injection Device (CID), explained below. Using echelle optics, a resolution of a couple of pm or below can be achieved[15,29–31]. The schematic principle of a echelle optical system can be seen in Figure 10.

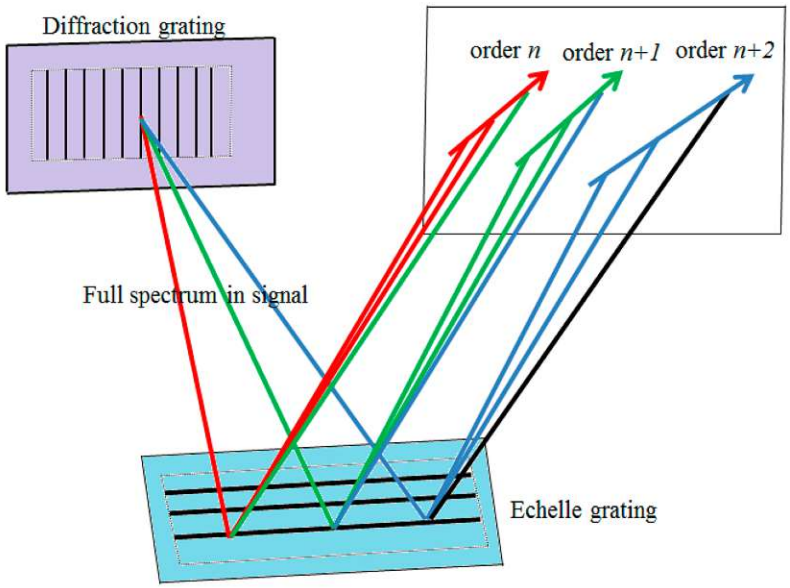

Figure 10: Schematic principle of wavelength separation using an echelle polychromator with an echelle grating in combination with a diffraction grating[32]

2.1.3.2 Solid state detectors

After the photons are separated according to their energy in the spectrometer, they need to be detected. Before the uprising of solid state detectors, Photo Multiplier Tubes (PMTs) were used which work similar to a Secondary Electron Multiplier (SEM) but instead of ions, the arriving photons excite electrons into the vacuum where they are then further accelerated to discrete dynodes[15,22,28]. Further details to a SEM can be found in paragraph 2.1.2.4. PMTs are still used today, for example in Czerny-Turner spectrometers[15]. Using echelle optics, mainly solid state detectors with a similar working principle are employed, mainly Charge Coupled Devices (CCDs), Charge Injection Devices (CIDs) and Segmented-Coupled Devices (SCDs)[27,33]. These solid state detectors consist of a n or p doped semiconductor substrate, an insulator film and gate electrodes in form of pixels in a range of a couple of μm. The gate electrodes as well as the insulator film are translucent so that the arriving photons can only interact with the substrate. In the substrate, electrons are excited from the valence band to the conduction band if the photon energy exceeds the band gap, resulting in electron-hole pairs[27,28,33]. For wavelengths ranging from ultraviolet to the visible range, Si with a band gap of 1 eV is suitable[15]. At the gate electrode, a bias voltage is applied and the free charges are collected as the arrangement of a Metal-Oxide-Semiconductor (MOS) resembles a capacitor where under each gate electrode (pixel) a small potential well forms where the charges are stored during the time of light exposure. In a CCD, p-doped Si is used as substrate, SiO_2 is used for the insulator film, poly-crystalline Si is used as gate electrode material and electrons are collected in the potential well. The schematic principle can be seen in Figure 11, where the cross section of one pixel is presented. After the exposure time, the pixel in a CCD is read out sequentially, pixel after pixel[27,34]. One potential well can only hold a certain amount of charges. When too many photons hit one pixel, an effect called "Blooming" can be observed where the excess charges then hop into the neighboring potential wells (pixels). This issue is overcome in a CID, where n-doped Si is used as a substrate, SiO_2 is used for the insulator film, poly-crystalline Si is used as gate electrode material and the positive holes are "collected". In a CID, each pixel can be read out individually. When the charge capacity of a pixel is reached, the pixel is read out during the exposure time, eliminating the possibility of "Blooming"[15,27,28,34]. Using such solid state detectors, wavelengths in the range of 160 to 800 nm can be monitored[15,31].

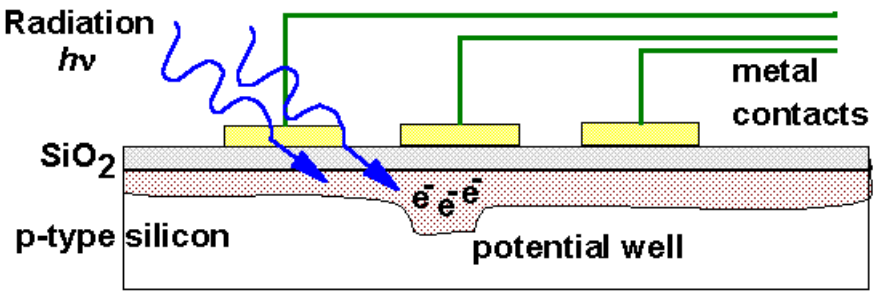

Figure 11: Cross section of a pixel in a CCD detector. The arrangement for a CID detector would be similar, with n-type Si and positive holes being collected in the potential well[35]

2.2 Microwave assisted acid digestion

In order to analyze solid samples, they need to be digested beforehand. To avoid interferences and energy consumption in the plasma, it is opted to mineralize the sample material during the digestion. Depending on the material, this dissolution may be tiresome and time intensive. For sample digestion, various methods are used nowadays, such as open vessel digestion, closed vessel digestions using Tölg bombs (Teflon vessels in a pressure stable stainless steel mantle) or Microwave Assisted Acid Digestion (MAAD). In an open vessel digestion, the sample is placed into a vessel and an oxidizing agent such as HNO_3, H_2O_2 or $HClO_4$ is added and the mixture may be heated in a water bath until the sample is completely dissolved. For a lot of materials, especially metals with an reduction potential lower than that of nitric acid $E_0 = 0.957\,\mathrm{V}$ (see Equation 11), an open vessel digestion is sufficient for sample digestion. However, open vessel digestion are unsuitable if volatile species such as As, Si, Ge or Pb are to be determined[15,19,36] .

$$NO_3^- + 4\,H^+ + 3\,e^- \longrightarrow NO + 2\,H_2O \tag{11}$$

In addition, many materials such as organic mater, ceramics and glasses often demand harsher conditions and suited acids such as hydrufluoric acid (HF) or fluoride containing alternatives such as NH_4F, and HBF_4[36,37] . MAAD is a widely used technique for sample digestion and has been employed ever since its first introduction in 1975 and further development in the 1990s. Using MAAD, temperatures above the boiling temperature of the acid can be achieved at high pressures using pressure stable vessels made of Teflon or quartz glass. Additionally, the microwave radiation offers a more precise heating source and does not result in cracking processes in the gas phase, as mostly the liquid phase heats up during the digestion due to the rotation and friction of dipoles.This makes MAAD more favorable compared to closed vessel digestions. As can be seen in Figure 12, using a microwave heating source, the liquid is ca.100 K hotter than the gas phase as compared to the convection oven, where the gas phase is hotter than the liquid phase which may cause cracking processes in the gas phase[15,36,38] .

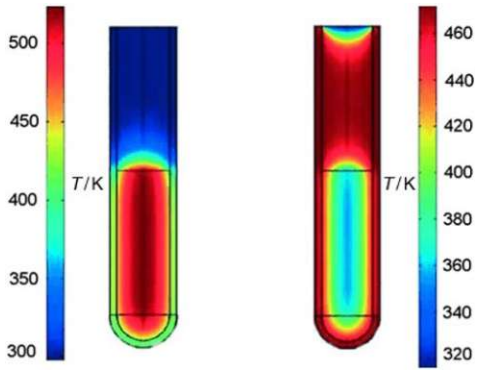

Figure 12: Temperature distribution of a heated liquid in a closed vessel using a microwave heating source (left) and a convection oven (right)[38]

2.3 Ion Chromatography

Since its first introduction in 1975, Ion Chromatography (IC) has become an important analytical tool for both anion and cation separation and subsequent detection. The most basic IC principle uses ion exchange columns, where the analyte ions interact with the oppositely charged groups of an ion exchange resin as a stationary phase[39]. For anion IC mostly resins with quarternary ammonium groups are used. The resin material can be made of different synthetic polymers, for example poly(styrene-co-divinylbenzene)-based materials which are then functionalized with quartenary ammonium ions. As an eluent, for anion IC mostly bicarbonate systems (HCO_3^-) are used. As the anions differ in size and charge as well as electronegativity, they interact differently with the stationary phase, thus they are retained on the column, making separation possible. The principle of interaction stays the same, but the equilibrium constant differs for each anion. The interaction between two arbitrary anions C^- and D^- with the stationary phase can be seen in Equation 12 and Equation 13[16,40].

$$\text{Resin}{-}NR_3^+HCO_3^- + C^- \overset{K_1}{\rightleftharpoons} \text{Resin}{-}NR_3^+C^- + HCO_3^- \tag{12}$$

$$\text{Resin}{-}NR_3^+HCO_3^- + D^- \overset{K_2}{\rightleftharpoons} \text{Resin}{-}NR_3^+D^- + HCO_3^- \tag{13}$$

The equilibrium constant can then be defined as:

$$K = \frac{[A^-]_s \cdot [HCO_3^-]_m}{[A^-]_m \cdot [HCO_3^-]_s} \tag{14}$$

Where K is the equilibrium constant, $[A^-]_s$ the concentration of the anion A in the stationary phase, $[HCO_3^-]_m$ the concentration of bicarbonate in the mobile phase, $[A^-]_m$ the concentration of the anion A in the mobile phase and $[HCO_3^-]_s$ the concentration of bicarbonate in the stationary phase[40]. A visualized principle for the interaction of analyte with the stationary phase can be seen in Figure 13.

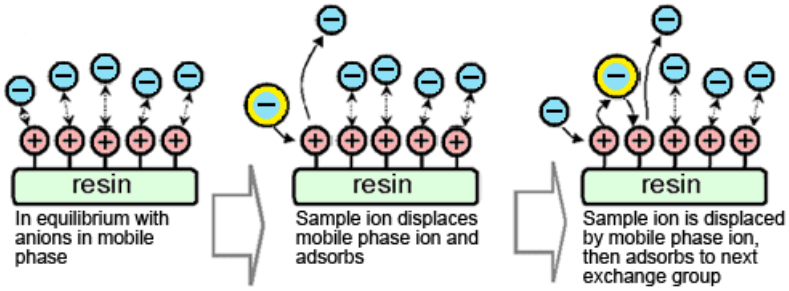

Figure 13: Separation principle for the interaction of analyte with the stationary phase with the mobile and stationary phase in equilibrium (left), injection of analyte (middle) and further interaction and retention of analyte on the stationary phase (right)[41]

For a functioning IC system, a pump, injection valve, separator column and a detection system are needed[40]. A general IC setup can be seen in Figure 14.
For an eluent either diluted mineral acids or bases are used, making it necessary to use chemically inert materials for all parts of the IC system such as Polyether Ether Ketone (PEEK), as parts made of stainless steel would start to corrode over time and have a strong negative influence on

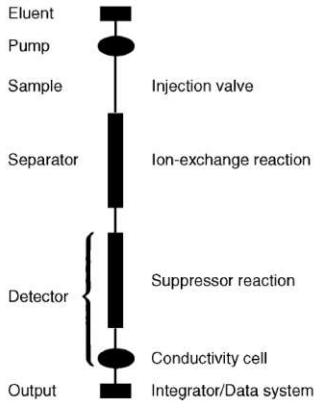

Figure 14: General setup for an Ion Chromatography (IC) system[40]

the IC measurements. The most employed detection principle for both anion and cation IC is the change in conductivity[40]. As the eluent has a high base conductivity itself, this needs to be suppressed after separation using a suppressor before the mixture of analyte and eluent can pass through the detection system. In the suppressor unit, the eluent flows through a hollow fiber in countercurrent to the regenerate flow, separated by a semipermeable membrane. In anion IC, diluted sulfuric acid (H_2SO_4) can be used as regenerate. Protons and sodium ions can pass through the membrane. In the suppressor, the bicarbonate system reacts with the protons and forms carbonic acid which has only a weak dissociation, thus an decrease in conductivity is achieved. To remain the ionic balance, the sodium ions pass through the membrane into the regenerate flow and are eliminated from the eluent flow[16,39,40]. A schematic drawing of the reaction in the suppressor can be seen in Figure 15.

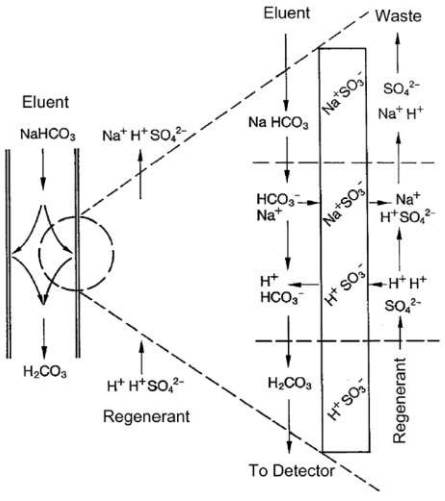

Figure 15: Schematic principle of the reaction taking place in a suppressor for anion Ion Chromatography (IC)[40]

After the suppressor unit, the eluent is then further directed into detection system. The most commonly used principle is the change in electrical conductivity as it is a sensitive and fairly cheap system, though amperometric detectors are employed as well. Generally, conductometric detectors can be considered general detectors, as every ion will result in change of the electric conductivity, although some ions have a greater/ lesser impact on the increase in conductivity,

hence sensitivity varies from ion to ion. More sophisticated detection devices include Electrospray Ionization Mass Spectrometry (ESI-MS) as well as Inductively Coupled Plasma Mass Spectrometry (ICP-MS) as detection devices. Mass Spectrometer (MS) systems as detectors offer various advantages due to a second dimension added to the separation resulting in easier identification of co-elution of ions. However, MS systems are expensive and have high operation costs as well as high to ultra high vacuum needs to be maintained permanently[16,39,40].

In an electric conductivity detector, the post-suppressor eluent flows between two electrodes with an area A and a distance d while an electrical field is applied with the voltage V.The solution has a certain electrical conductivity due to the movement of the ions towards cathode and anode, thus a current I can be measured and the resistance r can be calculated from Ohm's law ($V = r \cdot I$)[16,42,43]. The conductance G is then defined as[16]:

$$G = \frac{1}{r} \tag{15}$$

G has the SI unit Siemens (S) which is equal to reciprocal Ohm (Ohm^{-1}). Considering the area A and the distance d between the electrodes, the specific conductance k can be calculated as follows[16]:

$$k = G \cdot \frac{d}{A} \tag{16}$$

with the unit $\mathrm{S\,cm}^{-1}$. $\frac{d}{A}$ can further be defined as the cell constant K resulting in[16]:

$$k = G \cdot K \tag{17}$$

Thus, by knowing the cell dimensions, the cell constant can be calculated. Generally, the conductance of a solution depends on the applied field, the temperature of the solution and the concentration of ions. When the applied field and the temperature are being held constant, only the concentration of ions in the eluent flow affect the measured conductivity. For quantification using an electrical conductivity detector, external standards with the ions of interest are prepared and measured before or after the samples[16,40,42,43]. In Figure 16 a schematic principle of an electrical conductivity measurement can be seen.

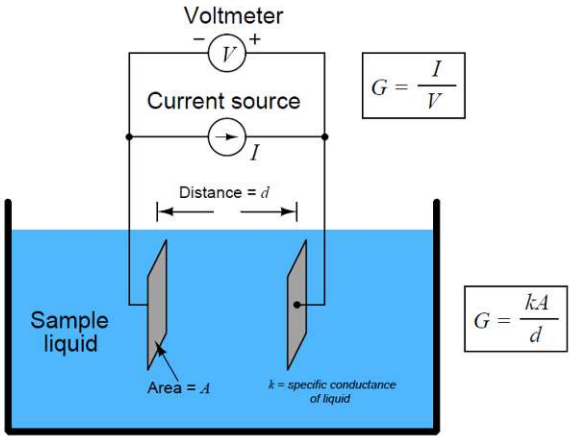

Figure 16: Schematic principle of an electrical conductivity detector employed in Ion Chromatography (IC)where V is the voltage, I is the measured current, d is the distance between the electrodes, A is the area of the electrodes, G is the conductivity of the liquid and k is the specific conductivity of the liquid[44]

2.4 pH electrode

The pH electrode marks an example for an ion selective membrane electrode, as only the concentration of H_3O^+ is measured[45] . In a pH electrode, the potential difference between an indicator electrode and the sample solution compared to a reference electrode such as a silver/ silver chloride electrode is measured. In Figure 17 the schematic principle of a pH electrode can be seen.The glass membrane separates the sample solution from the internal reference solution. When a glass membrane is put into water or an acidic solution, the H_3O^+ ions attach onto the glass surface, replacing other positively charged ions on the surface, thus making it sensitive towards H_3O^+ ions[46] . The sample solution has an unknown activity of H_3O^+ a_1 and the internal reference solution has a known activity of H_3O^+ a_2. The internal reference solution has a fixed pH value between 6 to 8 using a buffer system of NaH_2PO_4 / NaOH. The potential difference E only depends on the difference in H_3O^+ activity and can be described using the Nernst equation:

$$E = \frac{R \cdot T}{z \cdot F} \cdot ln(\frac{a_1}{a_2}) \tag{18}$$

Where R is the universal gas constant ($8.314\,\mathrm{J\,mol^{-1}\,K^{-1}}$), z is the charge of the H_3O^+ ion ($+1$) and F is the Faraday constant ($9.648\,\mathrm{C\,mol^{-1}}$). Assuming a Temperature T of 298 K and using a factor of 2.303 to convert the ln to log, the Nernst equation can be rewritten as:

$$E = 0,0592 \cdot log(\frac{a_1}{a_2}) \tag{19}$$

Looking at this simplified Nernst equation, it is clear that if the H_3O^+ activity of the internal reference solution is known, the activity within the sample solution and furthermore its pH value can easily be calculated. For a glass membrane, different types can be used with various advantages and disadvantages. The composition of the glass membrane has a great influence on the measurement as a high concentration of ions such as Na^+ or Ca^{2+} in a basic solution can influence the pH measurement, due to the great difference in activity between the competing

ions mentioned above and the H_3O^+ ions. For example, in a solution of sodium hydroxide with a concentration of $1\,\mathrm{mol\,L^{-1}}$, there is a Na concentration of $1\,\mathrm{mol\,L^{-1}}$ and a concentration/ activity of H_3O^+ of $10^{-14}\,\mathrm{mol\,L^{-1}}$. The influence of such processes can be minimized using glass membranes where the Na^+ and Ca^{2+} ions are replaced by Li^+ and Ba^{2+}. However, these influences occur only when solutions with a pH value of 9 or greater are being measured[39,45].

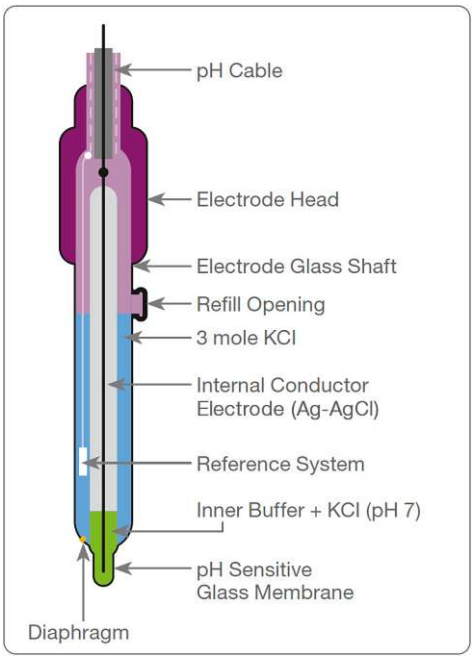

Figure 17: Schematic principle of a pH electrode using silver/ silver chloride electrodes[47]

2.5 Molding Composite Materials

Composite materials are a mixture of two different components or more which are distinguishable by phase separation. These components are mixed together with the goal of achieving properties which the materials could not have achieved employed in their own. Wherein a normal mixture, a blend, these two materials become unrecognizable, in a composite material they can still be clearly differentiated from one another. These two different phases are defined as the matrix phase and dispersed/ reinforcing phase. The matrix phase is continuous and binds everything together and is most likely more ductile and less hard, for example a polymer binding the mixture together. The dispersed phase is embedded into the matrix in discontinuous matter. An example for the embedding can be seen in Figure 18 (kindly provided by Veronika Zeller) as dispersed silica particles (light) are embedded into a epoxy resin matrix phase (dark). Simple and easy known examples for everyday composite materials would be wood (cellulose fiber in a lignin matrix) or ferro-concrete (steel lattice in a concrete matrix). Besides polymer matrix composites, also metal matrix composites as well as ceramic matrix composites are widely employed.[1] Additional to the used matrix phase, composite materials can also be classified according to their dispersed/ reinforced phase such as particulate composites (e.g. the presented epoxy resin composite with dispersed silica particles (see Figure 18)) and fibrous composites which can then be divided into additional subcategories[1,48]. Further looking into polymer composite materials, of course various kind of polymers are employed in these kind of materials. Depending on the used polymer, there are differences in the behaviour[48]. Hence, these materials can be divided into thermoplastic (become more ductile while heating up) and thermosetting (once heated to a certain temperature, the polymer becomes irreversible brittle and hard) polymer composite materials[49,50]. An example for the thermosetting polymer composite poses epoxy resin matrix composite materials, whereas Polyether Ether Ketone (PEEK) is an example for a polymer matrix categorized as thermoplastic[48–50].

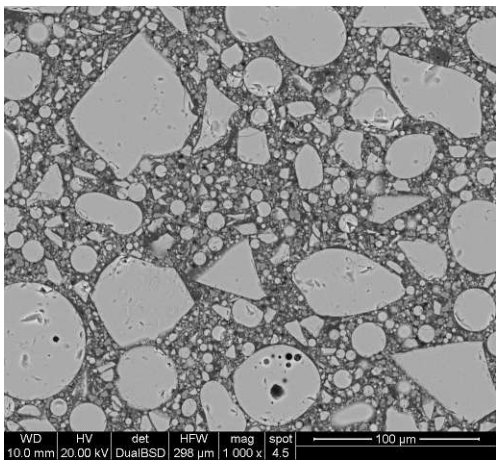

Figure 18: Example for the general structure of a composite material with silica as dispersed phase (light) and black carbon added epoxy resin (dark) as matrix phase

2.5.1 Silica-filled epoxy-composites

Though many different polymer based composite materials exist, the focus in this work lays upon the characterization of silica-filled epoxy-composites, thus only this sample type will be discussed further. When silica is mixed with polymers, it can interact with other silica particles at the surface using unsaturated silanol groups via hydrogen bonding, forming aggregates, thus increasing the viscosity of the mixture. Due to this interaction, silica particles add a thixotropic behavior and are used as a viscosity control agent to avoid sagging of any kind. For epoxy based composite materials, especially silica gel and fused silica is used[1,51]. Fused silica brings advantages such as a low thermal expansion coefficient, good dielectric properties and chemical as well as thermal stability, though fused silica is much more expensive compared to other forms of silica such as silica mineral and fumed silica. Hence, efforts are being made for the use of cheaper forms of silica as a mean of cost minimization[52]. Parameters that influence the behavior of the composite are the volume fraction of the filler, the particle size, the particle form, the modulus and strength of the filler, the resin-filler adhesion and additional properties of the epoxy resin matrix[52,53]. Before the composite material can be employed in its application, first the material has to be cured/ molded. Generally, an epoxy polymer consists of two parts: the epoxy resin and a hardening agent. An epoxy resin is defined as low-molecular weight pre-polymers consisting of more than one epoxy group[54,55]. Different epoxy resins are employed, for visualization, the diglycidyl ether of bisphenol-A (DGEBA) can be seen in Figure 19.

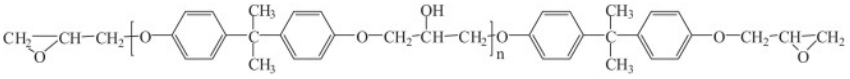

Figure 19: Chemical structure of the diglycidyl ether of bisphenol-A (DGEBA)[54]

During the curing process the hardener reacts with the epoxy resins and acts as a cross linker resulting in a hard thermosetting epoxy polymer.Overall, four different types of curing agents exist: amine curing agents, alkali curing agents, anhydride-based curing agents and catalytic curing agents. Curing agents need at least two functional groups in order to act as a cross linker[54,55]. This is shown in Figure 20 for amine based curing agents 4,4'-diaminodiphenyl methane (DDM) and 4,4'-diaminodiphenyl sulfone (DDS)

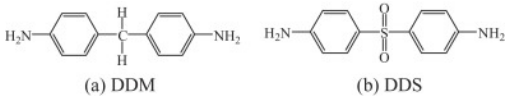

Figure 20: Chemical structures of (a) 4,4'-diaminodiphenyl methane (DDM) and (b) 4,4'-diaminodiphenyl sulfone (DDS)[54]

The curing reaction/ process can be initiated via different mechanisms such as photo or thermal initiation. The reaction mechanism during the curing process is visualized in Figure 21[54,56]. The most common curing process for epoxy molding compound is compression molding, where uncured material is placed between molding forms and is then pressed into the shape of interest which can be seen in Figure 22[57]. In addition to compression molding, transfer molding processes are also employed when it comes to curing processes of thermosetting materials such as

epoxy resin based molding compound. Transfer molding and compression molding are similar techniques, only that with transfer molding, the mold is closed, making it less wasteful. In addition, higher precision and more complex parts can be molded using transfer molding[58]. The material is loaded into a chamber (solid or liquid) and is then pressed into a heated mold cavity and can then be cooled for ideal thermoset curing[59]. The principle of transfer molding is depicted in Figure 23.

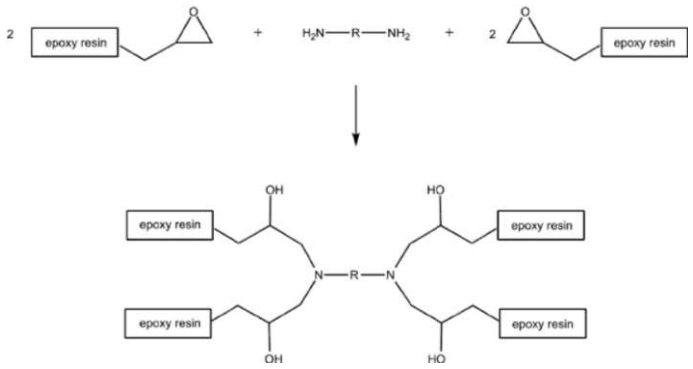

Figure 21: General reaction of a epoxy resin with an amine based curing agent during the curing process[60]

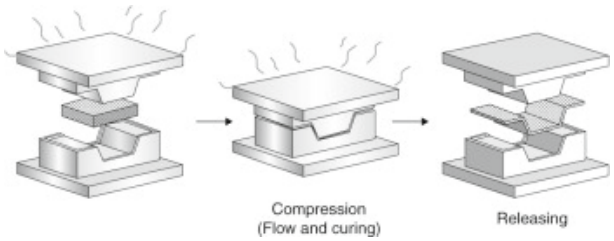

Figure 22: Schematic principle of the compression molding process[57]

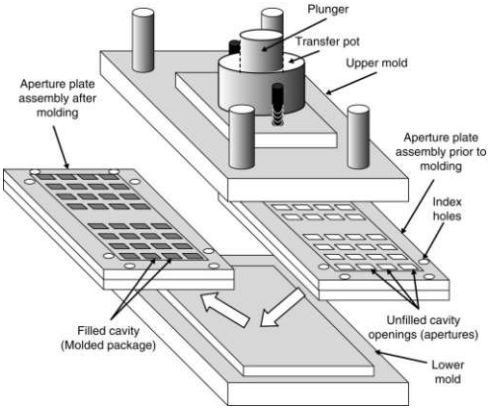

Figure 23: Principle of transfer molding[59]

3 Samples, materials and instruments

In the following chapter the analyzed samples, used materials and instruments are listed. As the employed materials in many different experiments do not differ, this accounts for a more oversee-able experimental part following.

3.1 Samples

Samples were provided by Infineon Technologies. All samples are epoxy resin based molding compounds with silica as filler particles. Overall, 12 sample were provided, cured (molded) and uncured (unmolded) versions of 6 different molding compounds, namely MCA to MCF including one model molding compound named MCF1.

3.2 Materials

The used materials in this thesis include:

- Antistatic weighing boats (VWR, Darmstadt, Germany)
- Antistatic polypropylene spatulas (VWR, Darmstadt, Germany)
- HVT Teflon digestion vessels with a maximal pressure of p_{max} =40 bar (Anton Paar, Graz, Austria)
- 50 mL metal free centrifuge tubes max. 12 500 xg (VWR, Darmstadt, Germany)
- 15 mL sterile centrifuge tubes max. 20 000 xg (VWR, Darmstadt, Germany)
- HCl 37 % and HNO_3 65 % in EMSURE® quality (Merck, Darmstadt, Germany)
- HF 40 % in Suprapur ® quality (Merck, Darmstadt, Germany)
- Teflon extraction vessels in a Polyether Ether Ketone mantle with a maximal pressure p_{max} =20 bar (Anton Paar, Graz, Austria)

3.3 Instruments

The used instruments/ devices in this thesis include:

- Analytical balance ENTRIS® II BCE224I-1S (Sartorius, Göttingen, Germany)
- Microwave Multiwave 5000 (Anton Paar, Graz, Austria)
- EASYPURE II (Thermo Scientific, Bremen, Germany) water system for ultrapure water with a resistance of 18.2 MΩcm
- HERAEUS Megafuge 16 (Thermo Scientific, Bremen, Germany)
- In-house built metal heating block (resistance heating) with an in-house built temperature logic and control unit

- Convection oven UNB 500 (Memmert, Schwabach, Germany)
- Heated magnetic stirrer MONOTHERM (H+P Labortechnik, Oberschleißheim, Germany)

4 Experimental

This thesis focused on three major points: the digestion of molding compound, the extraction of mobile ions and the instrumental analysis using Inductively Coupled Plasma Mass Spectrometry/ Optical Emission Spectroscopy (ICP-MS/ OES), Ion Chromatography (IC) and the measurement of pH-value & conductivity. The different approaches for digestion and extraction as well as the instrumental parameters are stated in the following chapter.

4.1 Milling of the molding compound

6 different kind of molding compound samples were analyzed in this thesis. For each molding compound sample both, cured and uncured molding compound were analyzed. The sample material was delivered as uncured pressed pellets or cured plates. Before analysis, these had to be milled into a fine powder. This was carried out using a triturator ball mill M400 (Resch, Haan, Germany). For milling, a 50 mL steel vessel with a steel ball (Retsch, Haan, Germany) was used. Before milling, the steel vessel was cooled using liquid nitrogen.

For the uncured molding compounds, the vessel was cooled for 90 s and milled for 90 s at 25 Hz. The plates of the cured molding compounds were broke apart using clean room wipes Series 1000 0909 (b-wipes, Langenargen, Germany) and a hammer. The broken apart pieces were then put into the vessel and were then cooled for 45 s and milled for 180 s at 25 Hz. The milled powders were stored in a Polypropylene (PP) vessel at −20 °C.

4.2 Sieving of molding compound powder

In order to investigate the influence on size distribution of the molding compound powder, a portion of the milled molding compound MCF1 was sieved using a 180 μm sieve (Fritsch, Idar-Oberstein, Germany) and a shaking tower 03.502 (Fritsch, Ida-Oberstein, Germany) set to permanent shaking at an amplitude setting of 4 for 10 min. Hence, two powders could then be characterized and compared using microwave assisted acid digestion and extraction.

4.3 Determination of size distribution

To characterize the approximate size distribution of the milled powders, the size distribution of the molding compound MCF1 was measured and it was assumed, that the rest of the powders have a similar size distribution, as sample material was limited for powders MCA-MCF. The size distribution was measured using the Mastersizer 2000 (Malvern Instruments, Malvern, United Kingdom). The size distribution was measured 15 times and for each measurement, the vessel containing the powder was shaken to avoid systematic sampling errors. The refractive index of silica (opal) (1,44) was assumed for the sample material[19] .

4.4 Microwave assisted acid digestion of molding compound

For sample digestion, 40 mg of milled molding compound sample were weighed onto weighing boats to 0.1 mg accuracy via a spatula using an analytical balance. The weighed sample was then put into HVT Teflon vessels. To the sample, different acids mixtures were added (see section below). The closed vessels were then put into the microwave and digestion was started with a controlled temperature program (see sections below). The digestion was considered unsatisfactory if the temperature range at the highest temperature was grater than ±20 °C. For each round of digestions (parameter variation or sample), 5 replicates were produced to account for reproducibility and homogeneity of the sample material. For experiments of parameter variation, the molding compound MCF unmolded was analysed.After the digestion, each digested sample solution was rinsed into a 50 mL centrifuge tube. The Teflon vessel was rinsed three times with ultrapure water. The solution was then diluted to a total volume of 45 mL and homogenized. As a precipitate/ residue was visible, the samples were centrifuged at 10 000 xg for 15 min. After centrifugation, 10 mL sample aliquote were taken for subsequent Inductively Coupled Plasma Mass Spectrometry (ICP-MS) analysis.

4.4.1 Acid variation

Different acid mixtures of HNO_3, HCl and HF were used in order to find the optimum. Though a total sample digestion can only be achieved by dissolution of the silica particles, also acid mixtures without HF were used.

4.4.1.1 Digestion using HNO_3 and HF

Different mixtures of HNO_3 and HF were used in order to evaluate the influence of HF content on the digestion behavior of the sample. For a total volume, it was always opted for 3.1 mL of acid mixture. The HF concentration ranged from 0 Vol − % to 13 Vol − % resulting in an added volume of HF of 0 mL, 0.025 mL, 0.05 mL, 0.1 mL, 0.15 mL, 0.2 mL and 0.4 mL. To get to 3.1 mL, HNO_3 was added. For the temperature program, the temperature was ramped up to 200 °C for 15 min and was then held constant at 200 °C for 45 min (hold time) and was afterwards cooled down to 60 °C which took about additional 20 min. In Figure 24 the temperature program can be seen.

4.4.1.2 Digestion using HNO_3

Digestions were performed using 3.1 mL of HNO_3. For the temperature program, the temperature was ramped up to 200 °C for 15 min and was then held constant at 200 °C for 45 min (hold time) and was afterwards cooled down to 60 °C which took about additional 20 min. In order to evaluate the influence of time and temperature on the digestion, additional digestions at 200 °C with 90 min hold time and 220 °C with 45 min hold time were performed. In Figure 25 the temperature programs can be seen.

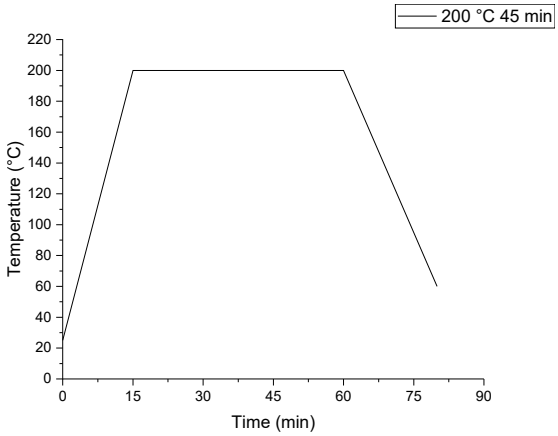

Figure 24: Temperature program applied with a 15 min temperature ramp to 200 °C and a hold time of 45 min with a cool off period of 20 min to 60 °C

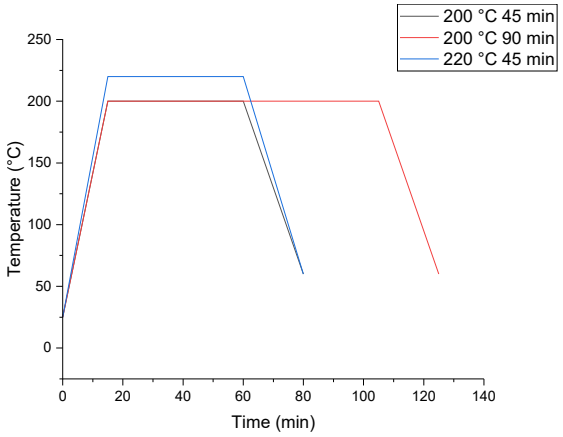

Figure 25: Temperature programs applied with grey: a 15 min ramp to 200 °C and a hold time of 45 min with a cooling off period of 20 min to 60 °C; red: a 15 min ramp to 220 °C and a hold time of 45 min with a cooling off period of 20 min to 60 °C; blue: a 15 min ramp to 200 °C and a hold time of 90 min with a cooling off period of 20 min to 60 °C

4.4.1.3 Digestion using HNO_3 and HCl

Digestions were performed using 3.1 mL of a 1:1 ratio of HCl and HNO_3 (1.55 mL HCl + 1.55 mL HNO_3), a 3:1 ratio of HCl and HNO_3 (2.325 mL HCl + 0.775 mL HNO_3) and a 1:3 ratio of HCl and HNO_3 (0.775 mL HCl + 2.325 mL HNO_3). The temperature program is described in paragraph 4.4.1.1 and can be seen in Figure 24.

4.5 ICP-MS measurement

In this work, a quadrupole ICP-MS $iCap^{TM}Qc$ (Thermo Scientific, Bremen, Germany) was used. Sample solutions were introduced via a double pass cyclonic spray chamber and an autosampler SC-2DX (Elemental Scientific, Omaha, United States). The instrument was tuned for maximum intensity for ^{115}In in standard mode using a solution with 1 ng g^{-1} ^{7}Li, ^{115}In and ^{238}U. For Kinetic Energy Discrimination (KED) mode, He gas with 7 Vol % H_2 (Linde, Dublin, Ireland)

was used. Before measurement, 20 min were taken into account for plasma stabilization and 15 min for the stabilization of the gas flow in the collision cell for KED mode. In Table 1, the instrument parameters can be seen. The calibration ranged from 0.1 ng g^{-1} to 160 ng g^{-1}. Standards were prepared gravimetrically using diluted acid (3 % HCl, 3 % HNO_3 vol/vol) and purchased standards of highest quality with a concentration of 1000 μg g^{-1} (Merck, Darmstadt, Germany). In Figure 26, a picture of the instrument is depicted.

Table 1: Instrumental parameters for the Inductively Coupled Plasma Mass Spectrometry (ICP-MS) measurement

Parameter	Value
RF Power	1550 W
Auxiliary gas flow	0.8 L min^{-1}
Cooling gas flow	12 L min^{-1}
Nebulizer gas flow	1 L min^{-1}
KED gas flow	4.5 mL min^{-1}
Dwell time	10 ms
Analytes	^{7}Li, ^{9}Be, ^{11}B, ^{23}Na, ^{24}Mg, ^{27}Al, ^{44}Ca, ^{50}Cr, ^{52}Cr, ^{55}Mn, ^{56}Fe, ^{58}Ni, ^{60}Ni, ^{59}Co, ^{63}Cu, ^{65}Cu, ^{64}Zn, ^{66}Zn, ^{68}Zn, ^{69}Ga, ^{71}Ga, ^{86}Sr, ^{88}Sr, ^{111}Cd, ^{112}Cd, ^{121}Sb, ^{125}Te, ^{126}Te, ^{137}Ba, ^{138}Ba, ^{139}La, ^{141}Pr, ^{143}Nd, ^{146}Nd, ^{178}Hf, ^{203}Tl, ^{205}Tl, ^{208}Pb, ^{209}Bi
Cone material	Ni
Sample Flow	0.4 mLmin^{-1}
Number of replicates	4
Total sample consumption	4 to 5 mL

Figure 26: Picture of the Inductively Coupled Plasma Mass Spectrometry (ICP-MS) instrument used in this work: $iCap^{TM}Qc$ (Thermo Scientific, Bremen, Germany)

4.6 Extraction of mobile ion fraction

The extraction of the mobile ions focused on three points: the heating source (heating block & microwave radiation), the extraction temperature and the extraction time. As the norm SEMI G29 foresees an extraction time of 48 h, an additional external heating device was necessary, as the employed microwave system is not designed for such long working times.

4.6.1 Heating block experiments

As the first goal was to properly perform the industrial standard SEMI G29, a heating block was used as primary heating source, as the standards calls for 48 h of extraction time, making it impossible to use the microwave later employed in this work. Additionally parameters of time and temperature could also be varied using this set-up before further extractions were performed using the microwave.Extractions were carried out in pressure stable Teflon vessels with a Polyether Ether Ketone (PEEK) mantle made for extraction studies with a maximal pressure of 20 bar. A metal heating block was used as a heating source with the principle of resistance heating using an in-house logic and control unit with a calibration range of 140 °C to 200 °C. To ensure the right temperature during the extraction, the outer mantle temperature of the extraction vessel was measured using an IR thermometer 62 MAX (Fluke, Everett, United States) and the offset of approx. 20 °C was considered adequate for future extractions. For example, for an extraction at 120 °C, the control unit had to be set to 140 °C to ensure the right temperature. For lower temperatures than 120 °C, a convection oven UNB 500 (Memmert, Schwabach, Germany) was used and no offset was necessary. After the vessels were put into the hot oven or heating block, 30 min were considered as stabilization time so the final temperature was reached. From that point on, the timer for the set extraction time was started.
For the extraction, 2 g of molding compound powder were weighed into the Teflon vessel to 0.1 mg accuracy using an analytical balance.To this, 20 g of ultrapure water were added. The closed vessel was put into the oven (60 °C and 90 °C experiment) or heating block (120 °C and 150 °C). For parameter optimization, a model molding compound MCF1 (molded) was used. Per extraction round, 3 replicates were produced to account for reproducibility. After the extraction, each yielded extract was put into a 50 mL centrifuge tube and centrifuged for 15 min at 12 000 xg. After that, the extracts were aliquoted for the IC, pH and conductivity measurement (9 mL) and the ICP-OES measurement (3 mL).

4.6.1.1 Extraction according to SEMI G29

The SEMI G29 is used as an industrial standard in order to evaluate the extraction behaviors of molding compound. According to the SEMI G29, the molding compound needs to be milled and sieved, so that the particle size distribution lays between 150 μm and 400 μm. For this work, the sieving part was ignored. The SEMI G29 states further that a 1:10 of molding compound to water should then be used for the analysis (e.g., 10 g of molding compound and 100 mL of water or 2 g of molding compound and 20 g of water). The suspension should then be placed at 120 °C for 48 h and the yielded extract should the be characterized using ICP-OES and IC.

4.6.1.2 Heating Block: influence of time

In order to optimize the extraction time and speed up the extraction process, different times were evaluated. At a temperature of 120 °C, extractions were performed using the sample MCF1 (molded) for 6 h, 12 h, 24 h, and 48 h. In addition to the influence of temperature, it was tested whether the use of a magnetic stir bar has a significant influence on the overall extraction behavior. For this, the molding compound was extracted at 120 °C and 150 °C for 24 h with the addition of a 3 cm magnetic stir bar which was set to 150 rpm using a magnetic stir plate. The stir bar was visibly stirring when only ultra-pure water was put into the vessel. However, due to the blackness of the molding compound, it was not possible to see whether the stir bar was stirring during the experiment itself.

4.6.1.3 Heating block: influence of temperature

After time optimization, the influence of temperature was investigated. As the extraction vessels were only stable up to 20 bar, the extraction temperature could only be raised up to 150 °C. For low temperature behavior, extractions were performed at 60 °C and 90 °C using a convection oven for 24 h of extraction time. For higher temperature behavior, experiments were conducted at 120 °C and 150 °C for 24 h using the metal heating block.

4.6.2 Microwave assisted extraction

For the HVT Teflon vessels, the manufacturer states a maximal pressure of 40 bar. This higher maximal pressure allows for higher extraction temperatures. By increasing the temperature, the extraction time could be decreased in order to increase the sample throughput.
For the extraction, 2 g of molding compound powder were weighed into the Teflon vessel to 0.1 mg accuracy using an analytical balance.To this, 20 g of ultrapure water were added. The closed HVT Teflon vessels were put into the microwave and the extraction was started. For parameter optimization, again the model molding compound MCF1 was used. Per extraction round, 4 replicates were produced to account for reproducibility. After the extraction, each yielded extract was put into a 50 mL centrifuge tube and centrifuged for 15 min at 12 000 xg. Afterwards, 14 mL were transferred into a 15 mL centrifuge tube and centrifuged for 30 min at 17 000 xg. For a final centrifugation step, 13 mL were transferred into a fresh 15 mL centrifuge tube and were centrifuged for 45 min at 18 000 xg.- After that, the extracts were aliquoted for the IC, pH and conductivity measurement (9 mL) and the ICP-OES measurement (3 mL).

4.6.2.1 Microwave assisted extraction: influence of temperature

In order to evaluate the influence of temperature on the extraction behavior, extractions at 150 °C, 175 °C, 200 °C and 225 °C were performed. The hold time at the maximal temperature was held constant for 90 min for all temperature variation experiments. For the temperature program, the temperature was ramped up to the desired maximal temperature in 15 min, was then held constant for 90 min and afterwards cooled down to 60 °C, which took about additional 30 min. After extraction and work-up IC, pH, conductivity and ICP-OES measurements

followed. The temperature programs applied can be seen in Figure 27.

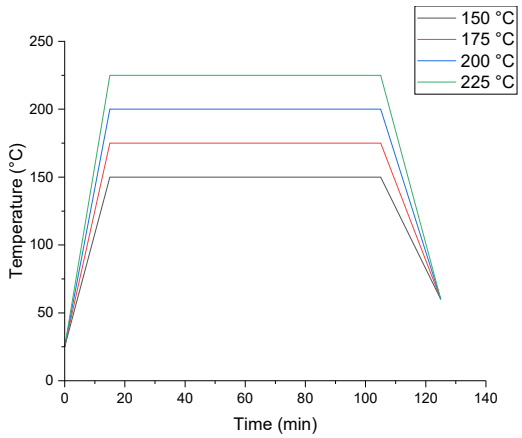

Figure 27: Temperature programs applied for the variation of the temperature for the microwave assisted extraction with a 15 min ramp to 150 °C (grey), 175 °C (red), 200 °C (blue) and 225 °C (green) and a hold time of 45 min at desired max. temperature with a cooling off period of 20 min to 60 °C

4.6.2.2 Microwave assisted extraction: influence of time

In order to evaluate the influence of extraction time, extractions at a constant temperature and different hold times at maximal temperature were performed. The times varied from 30 min, 60 min, 90 min to 180 min of extraction time. According to Anton Paar, the microwave should not be employed for longer than 90 min of hold time. Hence, for the extraction time of 180 min, the 90 min temperature program was performed two times in a row, which results in an additional heating and cooling phase for the extracts. For the temperature program, the temperature was ramped up to 175 °C in 15 min and this temperature was then held constant for the times mentioned above. Afterwards, the extracts were cooled to 60 °C which approximately took additional 30 min. After extraction and work-up IC, pH, conductivity and ICP-OES measurements followed. The temperature programs applied can be seen in Figure 28 and Figure 29.

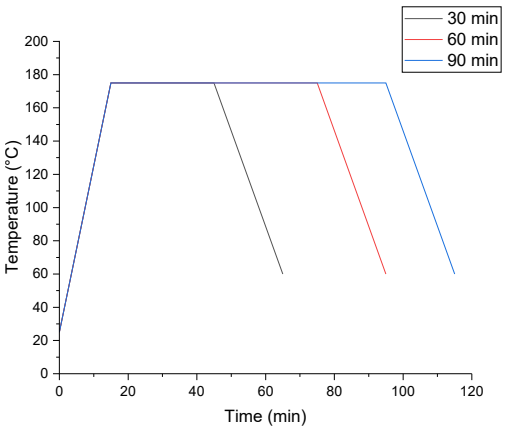

Figure 28: Temperature programs applied for the variation of time for the microwave assisted extraction with a 15 min ramp to 175 °C and hold time of 30 min (grey), 60 min (red) and 90 min (blue) with a cooling off period of 20 min to 60 °C

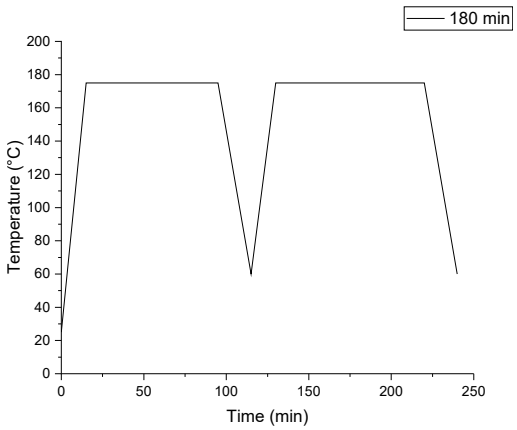

Figure 29: Temperature program applied for the variation of time for the microwave assisted extraction with a 15 min ramp to 175 °C and hold time of 90 min with a cooling off period of 20 min to 60 °C and an additional second run time with the exact same temperature program

4.6.2.3 Testing of completeness of extraction

Performing extractions in general, the question remains whether the extraction was complete or incomplete. To test this, an extraction was performed as stated above. However, after the extraction, the extract was worked up as described in subsubsection 4.6.2 but the sediment at the bottom of the vessel was not discarded but fresh 20 g of ultrapure water were added and another extraction was performed. This was then repeated two additional times, resulting in overall 4 consecutive extractions. For the temperature program, the temperature was ramped up to 225 °C in 15 min and the temperature was then held constant at 225 °C for 90 min. Afterwards, the temperature was cooled to 60 °C which approximately took additional 30 min. In Figure 27 (green line) the applied temperature program can be seen.

4.6.2.4 Influence of particle size on the extraction behavior

According to SEMI G29, the powder used for extraction should have a particle size distribution of 150 μm to 500 μm. For all experiments, this was ignored and the yielded powder after milling (subsection 4.1) was used for the experiments. To evaluate whether the particle size has an influence on the extraction behavior, the molding compound MCF1 was sieved according to subsection 4.2 after all other experiments were finished. After sieving, two powder fractions were yielded: $>180\,\mu$m and $<180\,\mu$m. For the temperature program, the temperature was ramped up to 225 °C in 15 min and the temperature was then held constant at 225 °C for 90 min. Afterwards, the temperature was cooled to 60 °C which approximately took additional 30 min. In Figure 27 (green line) the applied temperature program can be seen.

4.7 ICP-OES measurement

After extractions were performed, the yielded extracts were analyzed using an iCAP 6500 RAD (Thermo Scientific, Bremen, Germany) equipped with an ASX-520 autosampler (CETAC Technologies, Nebraska, USA), using a concentric nebulizer (Thermo Scientific, Bremen, Germany) and a single pass cyclonic spray chamber. For each element, at least two emission lines were chosen to account for spectral interferences except for Lithium, Potassium, Gallium, Thallium, Antimony, Praseodymium, Neodymium, Tellurium, Lead and Bismuth, as only one emission line delivered a linear response. The instrument parameters can be seen in Table 2 and the emission lines used can be seen in Table 3. Due to the different diffraction orders in the Charge Injection Device (CID) detector, the instrument can either detect Ultraviolet (UV) or Visible (VIS) lines, the measurement had to be optimized for UV and VIS individually, hence parameters may differ for the UV and VIS measurement mode stated in the following tables. The UV measure mode was optimized for Carbon quantification, as most other elements showed emission lines measurable using the VIS detection mode of the instrument.

Table 2: Instrumental parameters for the Inductively Coupled Plasma Optical Emission Spectroscopy (ICP-OES) measurement

Parameter	Value
RF Power UV/VIS	1550 W / 1100 W
Auxiliary gas flow	1.2 L min^{-1}
Cooling gas flow	14 L min^{-1}
Nebulizer gas flow UV/VIS	0.65 L min^{-1} / 0.7 L min^{-1}
Viewing height UV/VIS	8 mm / 12 mm
Integration time	10 s
Number of replicates	3
Sample flow	0.8 mL min^{-1}
Background correction	Constant shift from analytical line
Total sample consumption	approx. 2.5 mL

Table 3: Elements and used wavelengths for the Inductively Coupled Plasma Optical Emission Spectroscopy (ICP-OES) measurement

Element	WL I (nm)	WL II (nm)
Lithium (Li)	670.784	-
Beryllium (Be)	313.042	234.861
Boron (B)	249.773	249.678
Carbon (C)	193.091	247.856
Sodium (Na)	589.592	819.482
Magnesium (Mg)	279.553	280.270
Aluminum (Al)	167.079	396.152
Potassium (K)	766.490	-
Calcium (Ca)	393.366	373.690
Chromium (Cr)	267.716	284.325
Manganese (Mn)	257.610	259.373
Iron (Fe)	259.940	238.204
Cobalt (Co)	228.616	238.892
Nickel (Ni)	231.604	221.647
Copper (Cu)	324.754	213.598
Zinc (Zn)	213.856	202.548
Gallium (Ga)	294.364	-
Strontium (Sr)	407.771	421.552
Cadmium (Cd)	228.802	226.502
Tellurium (Te)	214.281	-
Barium (Ba)	455.403	233.257
Lanthanum (La)	412.323	379.478
Praseodymium (Pr)	414.311	-
Neodymium (Nd)	401.225	-
Thallium (Tl)	190.856	-
Lead (Pb)	220.353	-
Bismuth (Bi)	223.061	-

4.8 IC measurement

Measurements were carried out using a Dionex ICS-90 Ion Chromatography System (Thermo Scientific, Bremen, Germany) equipped with a Dionex ACRS 500 supressor (Thermo Scientific, Bremen, Germany) and a Dionex DS5 conductivity detection system (Thermo Scientific, Bremen, Germany). A Dionex IonPac AG14A guard column (Thermo Scientific, Bremen, Germany) with dimensions of 4 mm × 50 mm and a Dionex IonPac AS14A analytical column (Thermo Scientific, Bremen, Germany) with dimensions of 4 mm × 250 mm was used. For subsequent ion detection, an DS5 electric conductivity detector (Dionex, California, USA) was used.As an eluent a Na_2CO_3 / $NaHCO_3$ solution with a concentration of 1 mmol L^{-1} / 8 mmol L^{-1} was used. For the supressor, a solution of sulfuric acid with a concentration of 144 mmol L^{-1} was used. The pump rate was set to 1 mL min^{-1} at a pressure of 1630 psi. Formiate, Acetate, Lactate, Chloride, Nitrate and Sulfate were chosen as analytes. For Chloride, Nitrate and Sulfate bought standards with a concentration of 1000 $\mu g\, g^{-1}$ (Thermo Scientific, Bremen, Germany) were used. For ions Formiate, Acetate and Lactate stock solutions with a concentration of 1000 $\mu g\, g^{-1}$ were

prepared using Sodiumformate p.a. (Sigma Aldrich, Missouri, USA), Sodiumacetate trihydrate p.a. (Fluka, Buchs, Switzerland) and Sodiumlactate p.a. (Sigma Aldrich, Missouri, USA). The powders were weighed to an accuracy of 0.1 mg using an analytical balance CUBIS® MSE224S (Sartorius, Göttingen, Germany). For the calibration, solutions in a range from $0.05\,\mu g\,g^{-1}$ to $5\,\mu g\,g^{-1}$ were prepared.For data treatment, the provided software CHROMELEON version 6.60 was used. Data acquisition for each chromatogram lasted 12 min. Samples were injected manually.

4.9 Measurement of pH-value and conductivity

In order to further characterize the yielded extracts, the pH value and the conductivity were measured. As the work up process was further developed during the course of this thesis, the work-up procedure for some samples was too poor in order to measure the pH value and conductivity, as the particles in the suspension would have had a negative influence on the used electrodes and thus the measurement.

4.9.1 pH-value

For the pH value measurement, a combination electrode InLab Pure Pro-ISM (Mettler-Toledo, Columbus, USA) was used. The electrode was calibrated using solutions with a pH value of 4 and 7 purchased from VWR (Delaware Valley, USA). For signal output, a multimeter SevenCompact Duo S213 (Mettler-Toledo, Columbus, USA) was used. Measurements were conducted at a reference temperature of 25 °C.

4.9.2 Conductivity

For the conductivity measurement, a conductivity cell InLab 720 (Mettler-Toledo, Columbus, USA) for a range of 0 to $500\,\mu S$ in a temperature range of 0 to 100 °C was used. For signal output, a multimeter SevenCompact Duo S213 (Mettler-Toledo, Columbus, USA) was used. Measurements were conducted at a reference temperature of 25 °C.

5 Results & Discussion

This thesis consists of three major points: the digestion of molding compound, the extraction of mobile ions and the instrumental analysis using Inductively Coupled Plasma Mass Spectrometry/ Optical Emission Spectroscopy (ICP-MS/ OES), Ion Chromatography and the measurement of pH-value & conductivity. The results of the different approaches for digestion and extraction are stated in the following chapter. The discussion of latter results will focus on the digestion and extraction of molding compounds and the various influences of different parameters on elemental behavior. Additionally, the total elemental content as well as the extractability of ions within different molding compounds will be compared.

5.1 Microwave assisted acid digestion of molding compound

As this thesis shows a multi-element approach, the results for every element cannot be depicted graphically. Because of this, 8 elements (Li, Na, Mg, Al, Ca, Cr, Sr and Bi) were chosen to showcase the influence of the used acids on the quantified elemental content. These elements represent a broad range of concentrations within the sample material, ranging from impurities and thus trace elements to additives (minor components).

5.1.1 Acid variation

Experiments with different acids and acid mixtures were performed. For a digestion of the embedded silica particles, the use of hydrofluoric acid (HF) was necessary. However, as stated in literature, the addition of HF results in the formation of other precipitates such as AlF_3, MgF_2, $Na_{0,88}Mg_{0,88}Al_{1,12}(F,OH)_6 \cdot H_2O, CaF_2$ or $CaAlF_5$ in addition to possible co-precipitation of other elements such as Na and Ba[61]. Further attempts to dissolve the residue could be the treatment with HCl and evaporation of the resulting HF, as HCl forms stable Chlorides with the Fluoride-species while HF is a volatile byproduct which can evaporated off during this process. To properly investigate which acid mixture and conditions were optimal, digestions were performed using higher temperatures or longer extraction times as well as different acid mixtures. For an oxidizing agent, HNO_3 was employed in all performed digestions. Additionally, HF and HCl were used for total digestion of silica and/ or ion stabilization in solution. The results as well as the discussion of these acid variations can be seen in the following. Data points in graphs represent the mean of 5 overall repeats and their resulting standard deviation.
To evaluate the digestion results, all molding compound samples were sent to an external lab, which performed a Wickbold combustion. Afterwards, the residue was digested using aqua regia and the Na and K content within molding compound was quantified. As Na and K display important elements in corrosion studies, the quantified Na and K content were used as a benchmark in order to compare the yielded results. As with the addition of HCl to the digestions, K became not analyzable due to the formation of $^{37}Cl^1H^1H^+$ and $^{38}Ar^1H^+$ in the plasma. Because of that, only the Na content was used to compare the results. The external lab quantified a Na content for unmolded molding compound MCF of $86\,\mu g\,g^{-1}$.

5.1.1.1 Digestion using HNO_3 and HF

As it was unclear, whether HF has an influence on the determined elemental content, digestions with different ratios of HF to HNO_3 were conducted. The HF concentration during the digestion ranged from 0 Vol − % to 13 Vol − %. The results of these experiments can be seen in Figure 30 to Figure 37.

Elements can be sorted into three groups: heavily influenced by the addition of HF (Mg and Al), moderately influenced by the addition of HF (Na, Ca, Cr and Bi) and elements, that show a an optimum for a certain HF content (Li and Sr). It was expected for elements Mg and Al to be influenced heavily as these form various insoluble Fluoride-precipitates[61]. For elements Li and Sr an optimal HF content of ca. 4 Vol − % can be seen, which would suggest the usage of HF for sample digestion, if only these two elements were of interest. However, almost all elements showed a moderately negative influence of HF addition during digestion due to possible co-precipitation and adsorption. Of course, with a multi-analyte approach to sample characterization, an optimum for all elements cannot be achieved but rather an average condition which fits all needs to be chosen. Al, Mg and Cr show an exponential decrease, suggesting a reaction order of 1. However, the quantified Cr content only decreases by 30 % as compared to Al (96 %) and Mg (80 %). Na shows a somewhat negative trend with increasing HF content, however no such exponential decrease is visible. Elements least influenced by HF addition are Ca and Bi, which show little to no trend which may results from a solubility determined concentration in the solution after digestion. However, comparing the quantified content at 0 Vol − % with 13 Vol − % a certain negative trend is visible.

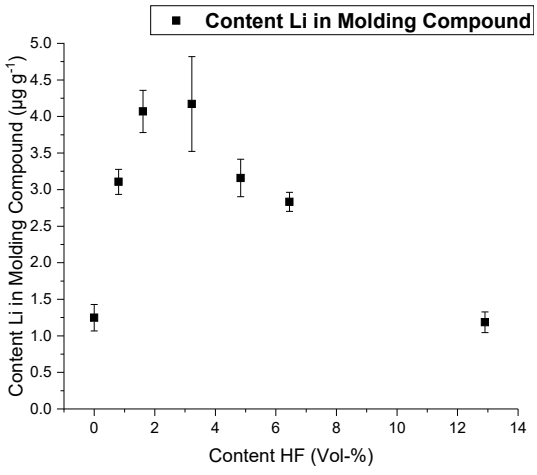

Figure 30: Results for the influence of HF on the quantified content of Lithium (Li) after acid digestion at 200 °C and a hold time at maximal temperature of 45 min

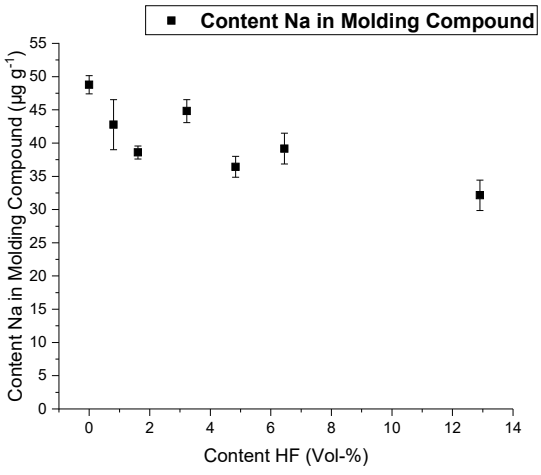

Figure 31: Results for the influence of HF on the quantified content of Sodium (Na) after acid digestion at 200 °C and a hold time at maximal temperature of 45 min

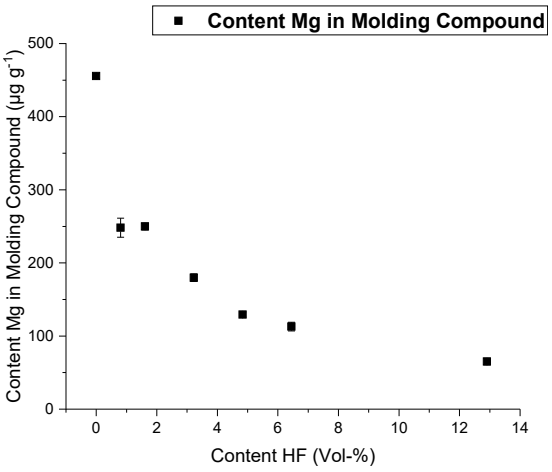

Figure 32: Results for the influence of HF on the quantified content of Magnesium (Mg) after acid digestion at 200 °C and a hold time at maximal temperature of 45 min

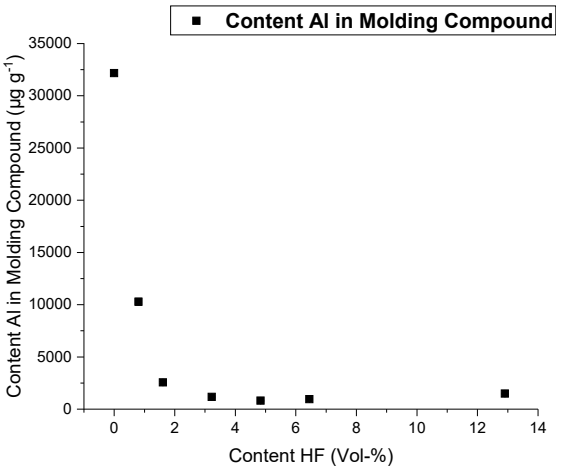

Figure 33: Results for the influence of HF on the quantified content of Aluminum (Al) after acid digestion at 200 °C and a hold time at maximal temperature of 45 min

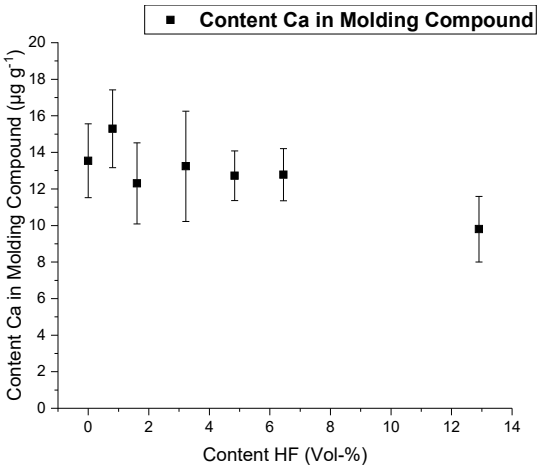

Figure 34: Results for the influence of HF on the quantified content of Calcium (Ca) after acid digestion at 200 °C and a hold time at maximal temperature of 45 min

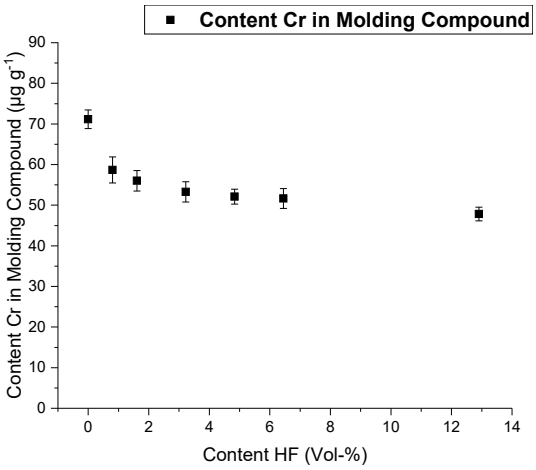

Figure 35: Results for the influence of HF on the quantified content of Chromium (Cr) after acid digestion at 200 °C and a hold time at maximal temperature of 45 min

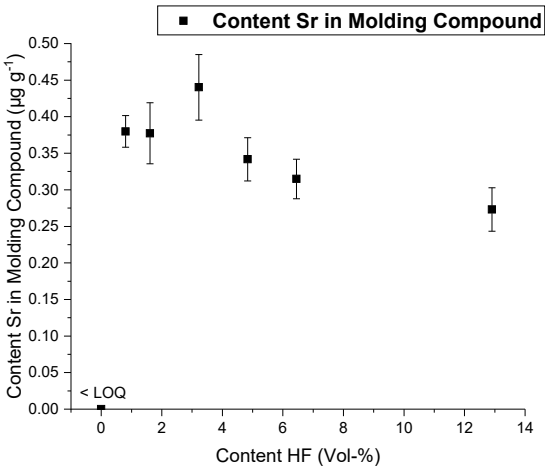

Figure 36: Results for the influence of HF on the quantified content of Strontium (Sr) after acid digestion at 200 °C and a hold time at maximal temperature of 45 min

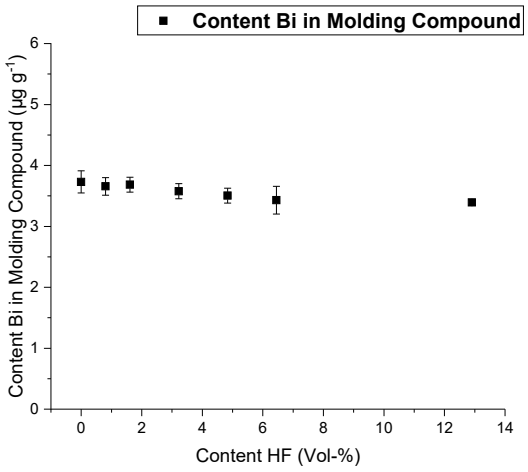

Figure 37: Results for the influence of HF on the quantified content of Bismuth (Bi) after acid digestion at 200 °C and a hold time at maximal temperature of 45 min

5.1.1.2 Digestion using HNO_3

Time and temperature have a strong influence in the digestion itself. As for temperature, an increase can result new possible reactions or a acceleration of the reactions in general, as a rule of thumb is that with every 10 °C the reaction time is split in half. Of course, lower temperature and longer extraction times may also yield a satisfying digestion. Because of these influences, time and temperature were varied using HNO_3 only during digestion. Results can be seen in Figure 38 and Figure 39, respectively.

In order to dissolve and digest the synthetic material in the molding compound (epoxy resin), nitric acid should be satisfactory. However, this offers only a partly digestion of the molding compound, as silica particles form a residue after digestion. On these silica particles, ions can be adsorbed and lead to a lower than expected quantification result. The question remained, whether a higher digestion temperature or longer hold time at maximum temperature have an influence on the quantifiable elemental content. Comparing the results in Figure 38 and Figure 39, no element shows a significant influence on digestion time and temperature. As all digests go through the same cooling off process, it is unclear whether higher temperatures and longer hold times actually account for higher concentrations in solution, as during the cooling off period, all additionally present analytes may be adsorbed onto the silica. With the use of only nitric acid for the digestion a Na content of ca. $40\,\mu g\,g^{-1}$ can be quantified, which is more than 50 % less compared to the results of the external lab.

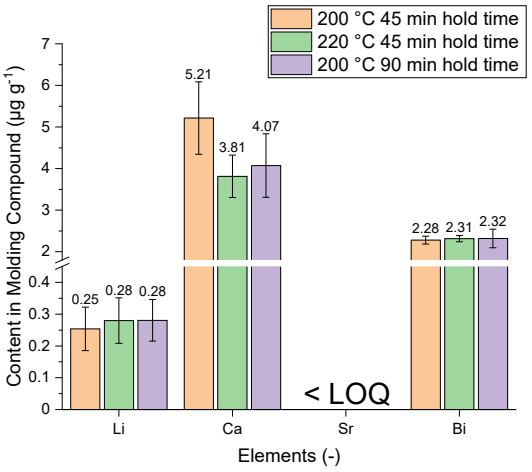

Figure 38: Quantified elemental contents for Li, Ca, Sr and Bi using only HNO_3 for acid digestion at 200 °C and 45 min hold time at maximum temperature (orange); 220 °C and 45 min hold at maximum temperature (green); 200 °C and 90 min hold time at maximum temperature (purple)

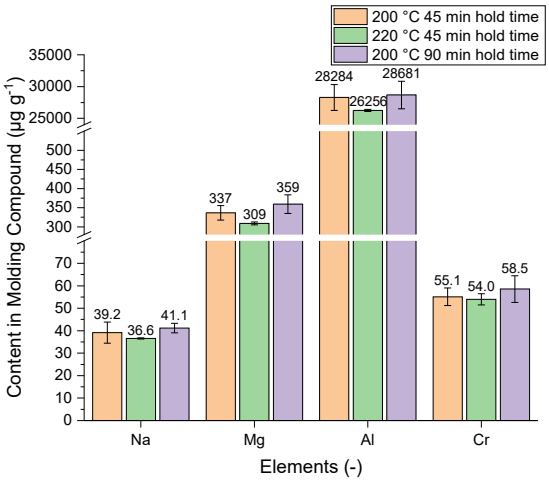

Figure 39: Quantified elemental contents for Na, Mg, Al and Cr using only HNO_3 for acid digestion at 200 °C and 45 min hold time at maximum temperature (orange); 220 °C and 45 min hold at maximum temperature (green); 200 °C and 90 min hold time at maximum temperature (purple)

5.1.1.3 Digestion using HNO_3, HCl and HF

In order to display the results for the digestions using different acid mixtures, all results for the elements for all acid variations were plotted into one graph. All digestions were performed at 200 °C and 45 min hold time at maximum temperature.

A different approach for the digestion was to use additional acids as the acid mixture has a strong effect on the overall digestion behavior of the sample. Additional HCl may stabilize ions in solution instead of being adsorbed to the silica during the cooling process. To compare this, digestions with different acid mixtures and ratios were performed using 1:1, 3:1 and 1:3 ratios of HCl:HNO_3 (v/v), a mixture with a ratio of 7.25:7.25:1 of HCl:HNO_3:HF(v/v), a mixture with a ratio of 14.5:1 of HNO_3:HF (v/v) and HNO_3 only. These different ratios may not only account for further stabilization but also to maybe promote new and different reactions to further digest the sample material. Results for this comparison can be found in Figure 40 for elements Li, Ca, Sr and Bi as well as in Figure 41 for elements Na, Mg, Al and Cr.

Starting with Li, the overall positive influence using HF during digestion is clearly visible, yielding a 20 times greater quantified content when comparing the HCl:HNO_3:HF mixture with the digestion using HNO_3 only. The mere addition of HCl has a positive effect as well as a 3 times greater content can be determined compared to the HNO_3 only mixture. Comparing the HCl:HNO_3:HF and the HNO_3:HF mixtures, the combination of HCl and HF shows the greatest effect on the quantified Li content. This may come from either better stabilization of Li ions in solution preventing either co-precipitation or adsorption.

For Ca, the addition of HCl also shows a favorable effect on the determined content with the best results yielded using either HCl:HNO_3 1:3 or the mixture of HCl, HNO_3 and HF. However, the overall effect on the determined Ca content is less pronounced as compared to other elements.

Using either HCl or HF during the digestion, Sr starts to be quantifiable as the result using nitric acid only is <LOQ. Similar to Li, Sr shows the highest quantified results with the combination of HCl, HNO_3 and HF.

Comparing the results for Bi, the addition of HCl to the digestion has little to no effect on the quantified content of about 3.5 $\mu g\,g^{-1}$ showing that Bi neither suffers from co-precipitation nor from adsorption or at least the addition of HF or HCl has no effect.

For element Na, the addition of HCl shows a great effect on the quantifiable content compared to the mere use of HNO_3 and HF resulting in a factor two greater content of ca. 90 $\mu g\,g^{-1}$ which fits with the result of the external lab.. This increase in quantifiable Na content most likely results from the stabilization of Na ions within solution instead of adsorbing to the residual silica which results in a higher Na content in solution after digestion.

For Mg and Al as well, the addition of HCl shows a great influence compared to the digestion using HNO_3 only. As expected, the addition of HF results in a great analyte loss due to precipitation, though this loss can be decreased by also adding HCl to the digestion mixture.

As for Cr, the addition of HCl cannot decrease the analyte loss when HF is added to the digestion. However, using HCl and HNO_3 during the digestion ca. 70 $\mu g\,g^{-1}$ can be quantified as compared to ca. 60 $\mu g\,g^{-1}$ using HNO_3 only.

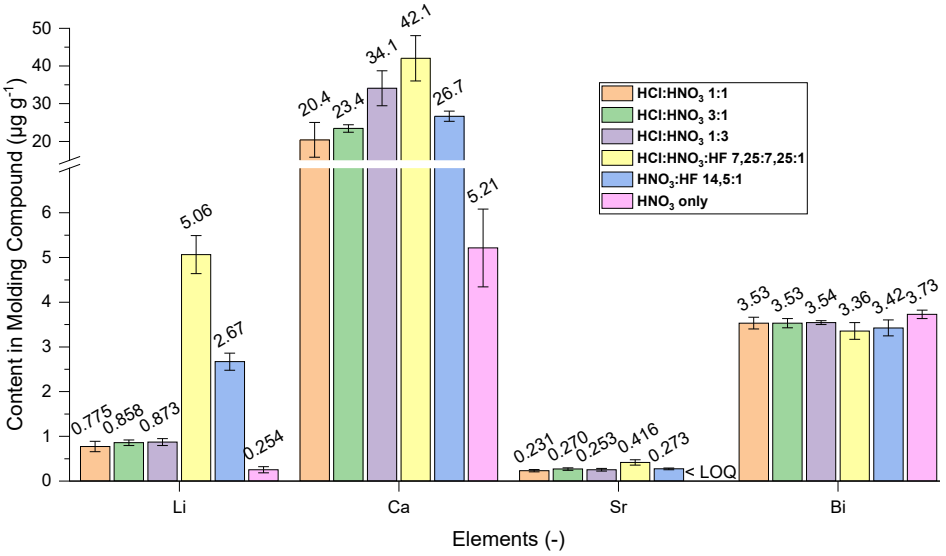

Figure 40: Quantified elemental contents for Li, Ca, Sr and Bi using mixtures of HCl and HNO_3 in ratios of 1:1(orange), 3:1 (green) and 1:3 (purple); HCl, HNO_3 and HF in a ratio of 7.25:7.25:1 (yellow); HNO_3 and HF in a ratio of 14.5:1 (blue); HNO_3 only (pink) for acid digestion at 200 °C and 45 min hold time at maximum temperature

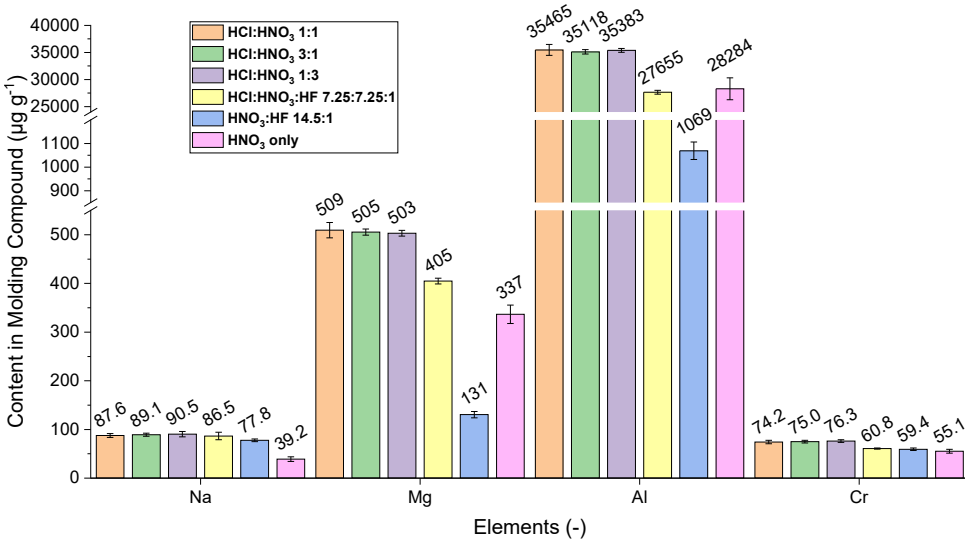

Figure 41: Quantified elemental contents for Na, Mg, Al and Cr using mixtures of HCl and HNO_3 in ratios of 1:1(orange), 3:1 (green) and 1:3 (purple); HCl, HNO_3 and HF in a ratio of 7.25:7.25:1 (yellow); HNO_3 and HF in a ratio of 14.5:1 (blue); HNO_3 only (pink) for acid digestion at 200 °C and 45 min hold time at maximum temperature

5.1.1.4 Final Digestion method

After parameter optimization using the sample MCF unmolded, a final digestion method was chosen to digest and analyze the other molding compound samples MCA to MCF (unmolded and molded). For sample digestion, 40 mg of milled molding compound sample were weighed onto weighing boats to 0.1 mg accuracy via a PP spatula using an analytical balance. The weighed sample was then put into a HVT Teflon vessel. To the sample, 3.1 mL of a 1:1 ratio

mixture of HCl and HNO_3 (1.55 mL HCl + 1.55 mL of HNO_3) was added.The closed vessels were then put into the microwave. For the temperature program, the temperature was ramped up to 220 °C for 15 min and was then held constant at 220 °C for 45 min and was afterwards cooled down to 60 °C which took about additional 20 min. The temperature program can be seen in Figure 42. The digestion was considered unsatisfactory if the temperature range at the highest temperature was grater than ±20 °C. For each round of digestion, 5 replicates were produced. After the digestion, each digested sample solution was rinsed into a 50 mL centrifuge tube. The Teflon vessel was rinsed three times with ultrapure water. The solution was then filled up to a total volume of 45 mL and homogenized. As a precipitate/ residue was visible, the samples were centrifuged at 10 000 xg for 15 min. After the centrifugation, 10 mL sample aliquote were taken for subsequent Inductively Coupled Plasma Mass Spectrometry (ICP-MS) analysis.

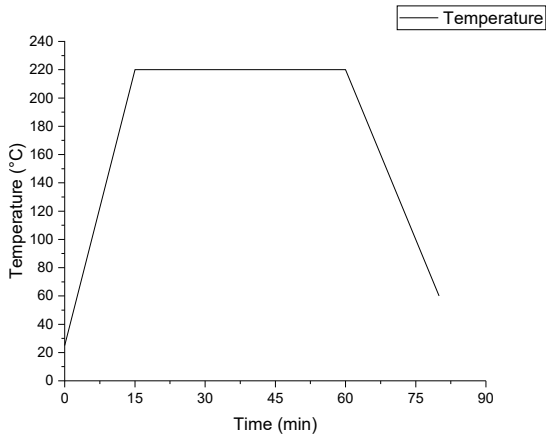

Figure 42: Applied temperature program for the finalized digestions method with a 15 min ramp to 220 °C and a hold time of 45 min with a cooling off period of 20 min to 60 °C

5.1.2 Digestion results for samples MCA to MCF using the final digestion method

Using the final digestion method, all 12 molding compound samples, 6 unmolded and 6 molded samples (split into two sub-sections), were digested and analyzed. In order to properly compare the elemental contents, the results for each element was plotted separately. Results can be seen in Figure 43 to Figure 58.

Initially, after evaluation of the various influences on digestion behavior, the digestion temperature was set to 200 °C. However, molding compounds MCA-MCE were not properly digested, as a black residue was visible, coming from the added graphite in the molding compound samples. Digestions were performed at 220 °C and all molding compound samples dissolved showed a white residue because of the embedded silica particles, as expected with the usage of a 1:3 ratio of HCl:HNO_3. Technically speaking, this does not represent a total digestion as not all sample material is digested. However, with the given complications by HF addition this was the best method when comparing the yielded results for the Na content within unmolded molding compound MCF with the results of the Wickbold combustion ($90\,\mu g\,g^{-1} \pm 5\,\mu g\,g^{-1}$ vs. $86\,\mu g\,g^{-1}$).

For the analysis of the molding compound samples, two primarily questions exist: are the different samples vastly different according to their elemental content of trace, minor and major (additives) components and is there a difference between unmolded and molded samples due to unknown processes and reactions during the curing process.

5.1.2.1 Final digestion of unmolded molding compounds

Results can be seen in Figure 43 to Figure 50. The elemental content of molded and unmolded molding compounds was expected to be fairly similar. Of course, results may differ due to additional adsorption processes or minor inhomogeneities within the milled sample material. This expectation was met for elements Li, Na, Mg, Al (except MCC), Ca (except MCF), Sr (except MCF) as well as Bi.
In the unmolded sample MCC almost additional 85 $\mu g\,g^{-1}$ ppm Al are found (+30 %) which most likely results from the variation in adsorption processes during the cooling of the digestion mixture.
For elements Ca and Sr approx. 2 times more amount can be quantified in the unmolded sample MCF when compared with the results of its molded counterpart. Apart from adsorption processes also inhomogeneity within the sample powder may cause a difference in total content. However, such behavior cannot be observed for Mg. Going further down the Periodic Table of Elements (PTE), Ba shows an almost 30 times higher content within the unmolded sample MCF.

For Cr, all molding compounds show a vast difference between unmolded and molded sample. Also elements such a Fe and Mn show similar behavior. This leads us to believe that this comes from the different approaches during milling processes of unmolded and molded samples due to their different material properties. Because of these different milling conditions, different amounts of abrasion of the steel vessel are introduced into the milled powder. This also explains a fairly equal amount of Cr within molded samples except for MCF. MCF is an exception in general, as it is the only samples which shows a higher Cr content within the unmolded as compared to the molded sample as well as other elements employed as steel alloys. A summary of the minimal, maximal and average elemental over all unmolded molding compound samples as well as the possible usage as an additive for displayed elements can be found in Table 4.

Table 4: Summary of minimal and maximal content of displayed elements Li, Na, Mg, Al, Ca, Cr, Sr and Bi, the possible usage of such elements in additives (y/n) as well as their average content over all unmolded molding compound samples

Element	Min. content ($\mu g\,g^{-1}$)	SD	Max. content ($\mu g\,g^{-1}$)	SD	Additive (y/n)	Average content
Li	0.38	0.03	1.8	0.2	n	1.1
Na	12.7	0.8	142	7	y	48.5
Mg	6.7	0.9	1028	36	y	366
Al	98	8	26647	907	y	8684
Ca	3.8	0.9	16	2	n	7.2
Cr	5	1	283	20	y	59
Sr	0.038	0.001	0.166	0.008	n	0.087
Bi	0.0101	0.0009	462	7	y	78.8

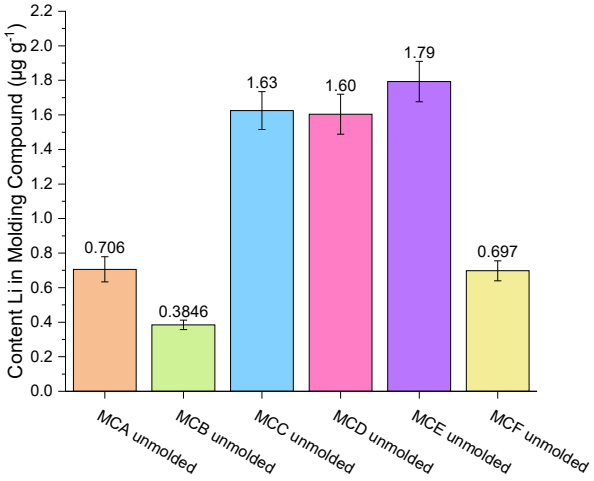

Figure 43: Results for the quantified Li content within unmolded molding compounds MCA (orange), MCB (green), MCC (blue), MCD (pink), MCE (purple) and MCF (yellow) using the final digestion method

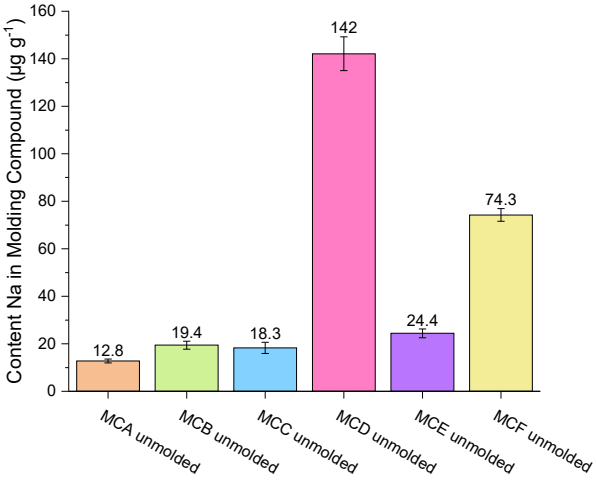

Figure 44: Results for the quantified Na content within unmolded molding compounds MCA (orange), MCB (green), MCC (blue), MCD (pink), MCE (purple) and MCF (yellow) using the final digestion method

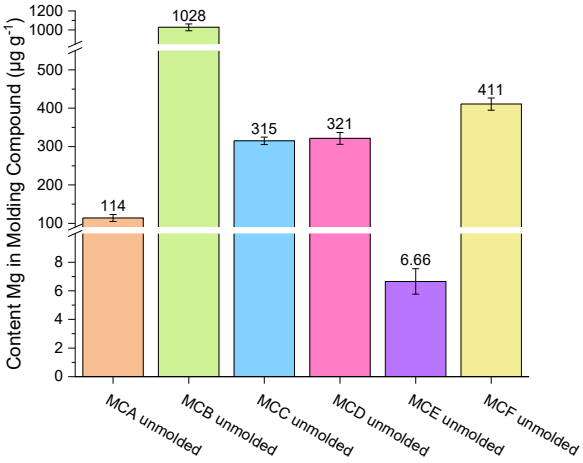

Figure 45: Results for the quantified Mg content within unmolded molding compounds MCA (orange), MCB (green), MCC (blue), MCD (pink), MCE (purple) and MCF (yellow) using the final digestion method

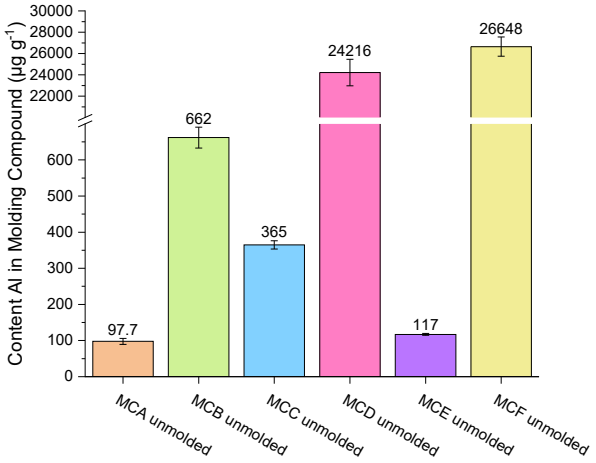

Figure 46: Results for the quantified Al content within unmolded molding compounds MCA (orange), MCB (green), MCC (blue), MCD (pink), MCE (purple) and MCF (yellow) using the final digestion method

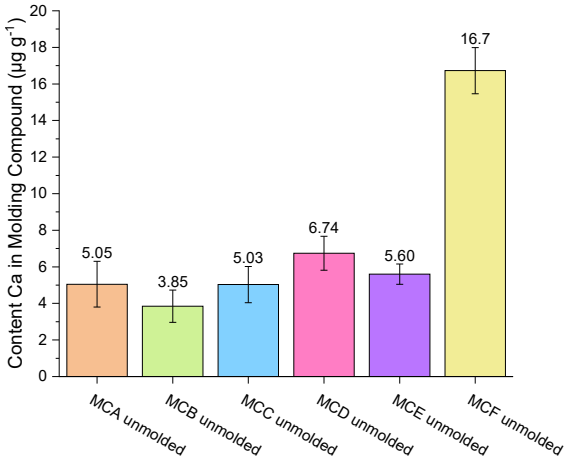

Figure 47: Results for the quantified Ca content within unmolded molding compounds MCA (orange), MCB (green), MCC (blue), MCD (pink), MCE (purple) and MCF (yellow) using the final digestion method

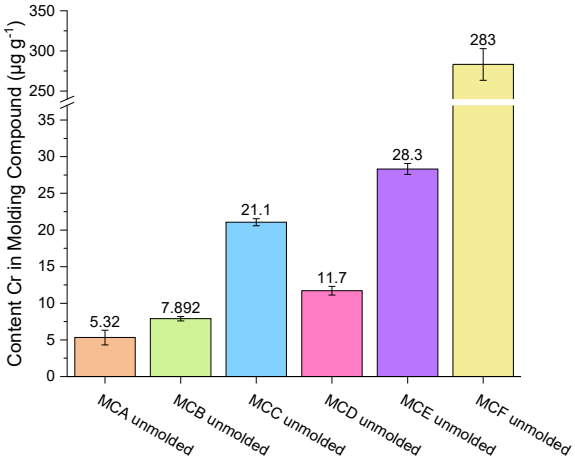

Figure 48: Results for the quantified Cr content within unmolded molding compounds MCA (orange), MCB (green), MCC (blue), MCD (pink), MCE (purple) and MCF (yellow) using the final digestion method

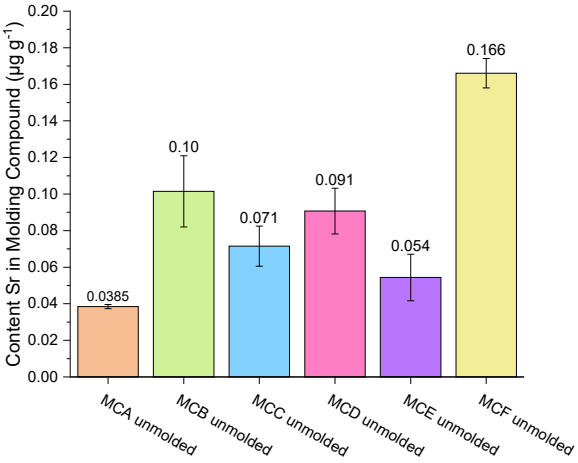

Figure 49: Results for the quantified Sr content within unmolded molding compounds MCA (orange), MCB (green), MCC (blue), MCD (pink), MCE (purple) and MCF (yellow) using the final digestion method

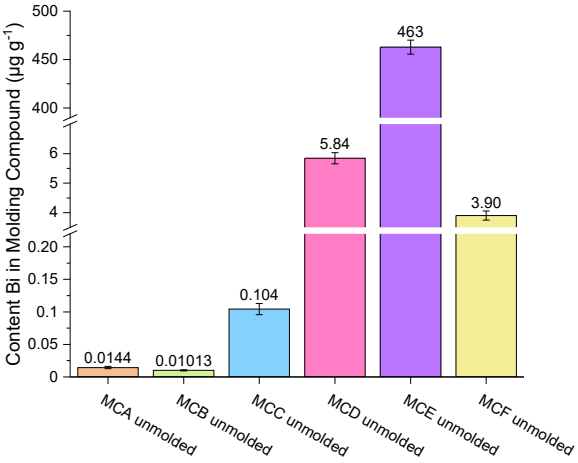

Figure 50: Results for the quantified Bi content within unmolded molding compounds MCA (orange), MCB (green), MCC (blue), MCD (pink), MCE (purple) and MCF (yellow) using the final digestion method

5.1.2.2 Final digestion of molded molding compounds

Elemental content within the molding compound samples may vary due to different contamination in different production sites as well as different additives in order to achieve desired properties. Which additives have been added to the molding compounds, of course, stays within the knowledge of the manufacturer. Results for the digestion results for the molded molding compound samples can be found in Figure 51 to Figure 58.

Comparing the results in Figure 51, one can see a similar concentration range for the Li content within the different molding compounds of $0.32\,\mu g\,g^{-1} \pm 0.04\,\mu g\,g^{-1}$ to $1.70\,\mu g\,g^{-1} \pm 0.05\,\mu g\,g^{-1}$, classifying it as trace element within all samples. However, as mentioned above, Li is an element which heavily benefits from the addition of HF during the digestion. Comparing it to Figure 30, Li contents may be at least up to 4 times higher compared to the determined results.

For Na, the concentration range is different as compared to Li. Where the lowest quantified content lays at $10\,\mu g\,g^{-1} \pm 0.9\,\mu g\,g^{-1}$ and the highest at $143\,\mu g\,g^{-1} \pm 4\,\mu g\,g^{-1}$. However, the total elemental content does not directly account for correlation with mobility.

Mg shows a broad range of concentration as well with a Mg content of up to $926\,\mu g\,g^{-1} \pm 84\,\mu g\,g^{-1}$ for MCB. Here Mg can be classified as a trace ($<100\,\mu g\,g^{-1}$) and minor component ($>100\,\mu g\,g^{-1}$)[62]. Molding compound MCE shows the lowest content of Mg with $7\,\mu g\,g^{-1} \pm 0.5\,\mu g\,g^{-1}$, which results in ca. a factor of 130 lesser Mg content when compared to sample MCB.

Al shows one of the greatest ranges showing that in some cases it represents a contamination (MCA, MCB, MCC and MCE) whereas with molding compounds MCD and MCF, the content ranges up to the wt $-$ % range with $26\,629\,\mu g\,g^{-1} \pm 983\,\mu g\,g^{-1}$. Here Al most likely was added in the form of $AlOH_3$ or korundum Al_2O_3 which in general should result in a low mobile content as both components are insoluble in water.

Results for Ca in Figure 55 show no great concentration range around $5\,\mu g\,g^{-1} \pm 1.3\,\mu g\,g^{-1}$ to $7\,\mu g\,g^{-1} \pm 0.5\,\mu g\,g^{-1}$. The high standard deviation for the Ca content results on the one hand on the rather poor sensitivity for Ca in ICP-MS, as its main isotope ^{40}Ca overlaps with ^{40}Ar making it necessary to switch to ^{44}Ca with a natural abundance of only 2.1 %. The high deviation may also results from inconsistent adsorption processes, which may differ from element to element due to its different affinities towards SiO_2.
Molding compounds MCA to MCE show all a moderately similar Cr content with a range of

$170\,\mu g\,g^{-1} \pm 9\,\mu g\,g^{-1}$ to $221\,\mu g\,g^{-1} \pm 11\,\mu g\,g^{-1}$. The only molding compound which differs from this is molding compound MCF with only $71\,\mu g\,g^{-1} \pm 5\,\mu g\,g^{-1}$. However, this close range may result from a similar steel abrasion into the sample material during milling.

Sr displays as well a trace component within the sample material with concentrations below $0.1\,\mu g\,g^{-1}$ in a range of $0.038\,\mu g\,g^{-1} \pm 0.007\,\mu g\,g^{-1}$ to $0.092\,\mu g\,g^{-1} \pm 0.006\,\mu g\,g^{-1}$.

Bi shows a wide concentration range as contents range from $0.0072\,\mu g\,g^{-1} \pm 0.0007\,\mu g\,g^{-1}$ up to $425\,\mu g\,g^{-1} \pm 11\,\mu g\,g^{-1}$ which covers a magnitude of ca. 6. For molding compound MCE with such a high Bi content, a Bi compound is most likely added to the sample during production processes. However, extraction data showed a mobile fraction <LOQ, though sensibility for Bi in ICP-OES is comparatively low compared to ICP-MS.

Chosen elements to present in this thesis were picked due to their content within the molding compound as well as their range. While some elements do not deviate significantly from sample to sample, for example Li, Ca and Sr, Cr shows a broader range (2 to 5 times deviation between samples). As for elements with a great range, e.g. Na, Mg, Al and Bi, this suggests that compounds containing these elements maybe were used as additives. A summary of the minimal, maximal and average elemental over all unmolded molding compound samples as well as the possible usage as an additive for displayed elements can be found in Table 5.

Table 5: Summary of minimal and maximal content of displayed elements Li, Na, Mg, Al, Ca, Cr, Sr and Bi, the possible usage of such elements in additives (y/n) as well as their average content over all molded molding compound samples

Element	Min. content ($\mu g\,g^{-1}$)	SD	Max. content ($\mu g\,g^{-1}$)	SD	Additive (y/n)	Average content
Li	0.32	0.03	1.7	0.05	n	1
Na	10.1	0.8	143	3	y	48
Mg	7.1	0.4	925	84	y	337
Al	94	5	26628	983	y	8515
Ca	5.2	0.9	7.4	0.5	n	6.2
Cr	71	4	221	11	y	176
Sr	0.038	0.006	0.092	0.006	n	0.068
Bi	0.0071	0.0007	425	11	y	72

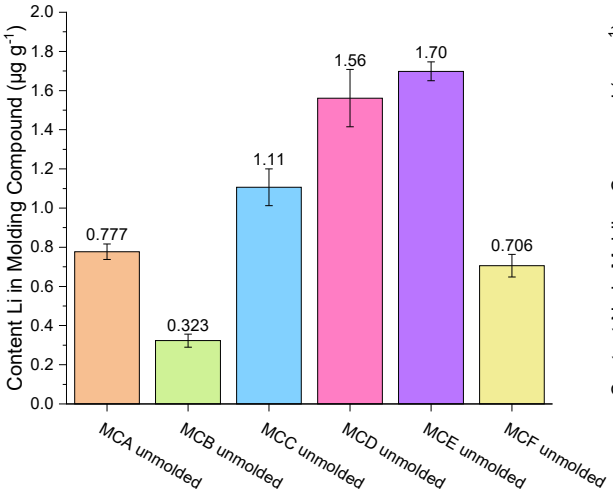

Figure 51: Results for the quantified Li content within molded molding compounds MCA (orange), MCB (green), MCC (blue), MCD (pink), MCE (purple) and MCF (yellow) using the final digestion method

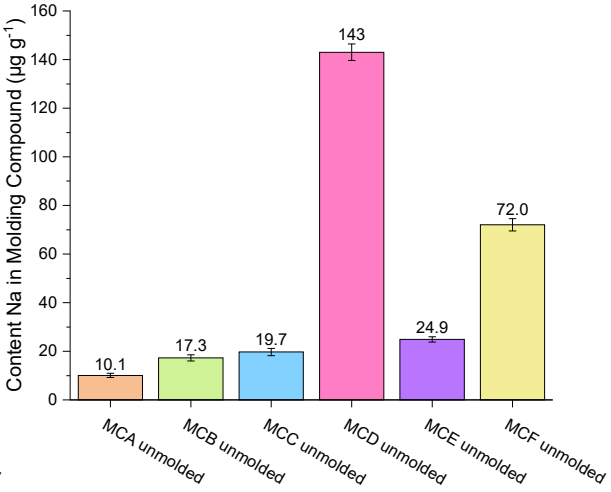

Figure 52: Results for the quantified Na content within molded molding compounds MCA (orange), MCB (green), MCC (blue), MCD (pink), MCE (purple) and MCF (yellow) using the final digestion method

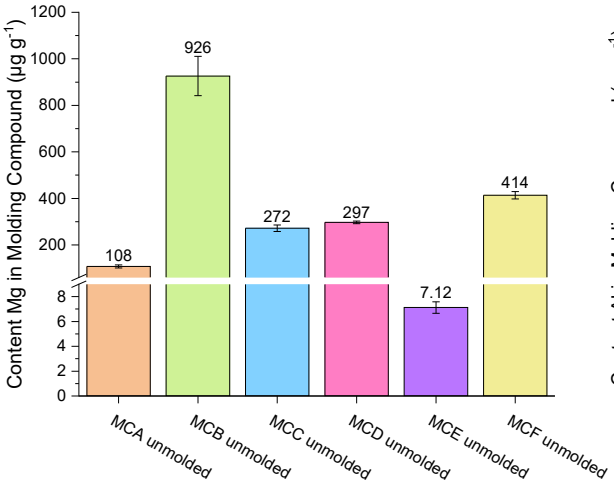

Figure 53: Results for the quantified Mg content within molded molding compounds MCA (orange), MCB (green), MCC (blue), MCD (pink), MCE (purple) and MCF (yellow) using the final digestion method

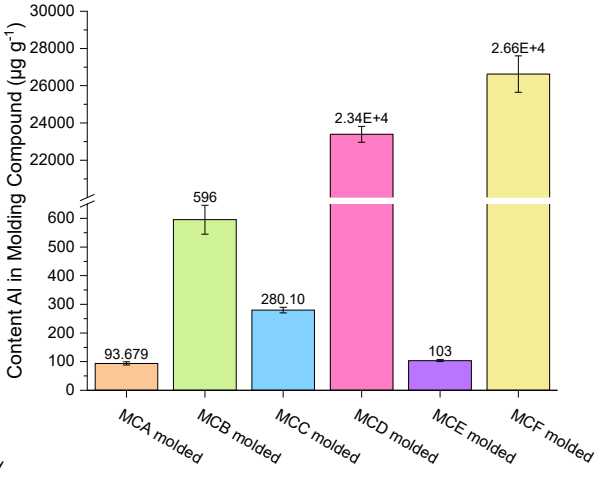

Figure 54: Results for the quantified Al content within molded molding compounds MCA (orange), MCB (green), MCC (blue), MCD (pink), MCE (purple) and MCF (yellow) using the final digestion method

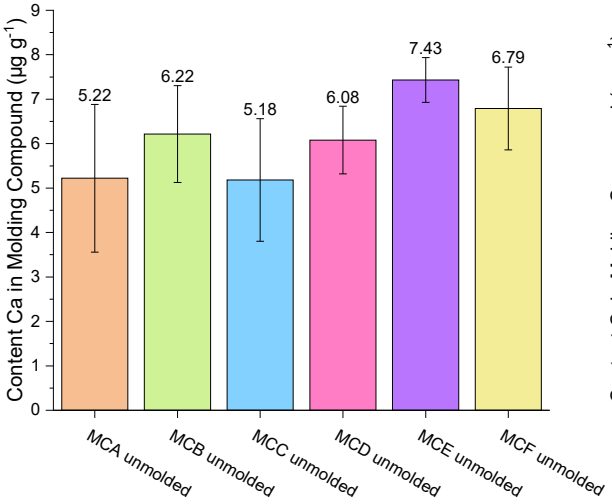

Figure 55: Results for the quantified Ca content within molded molding compounds MCA (orange), MCB (green), MCC (blue), MCD (pink), MCE (purple) and MCF (yellow) using the final digestion method

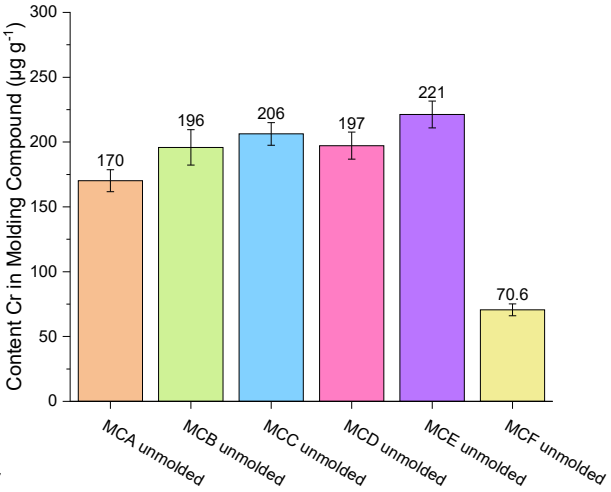

Figure 56: Results for the quantified Cr content within molded molding compounds MCA (orange), MCB (green), MCC (blue), MCD (pink), MCE (purple) and MCF (yellow) using the final digestion method

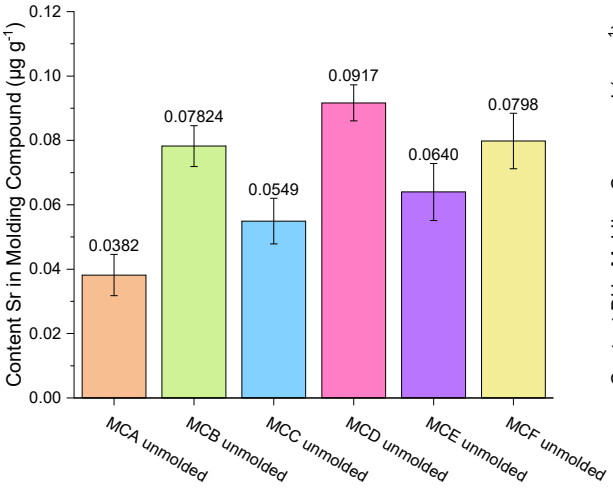

Figure 57: Results for the quantified Sr content within molded molding compounds MCA (orange), MCB (green), MCC (blue), MCD (pink), MCE (purple) and MCF (yellow) using the final digestion method

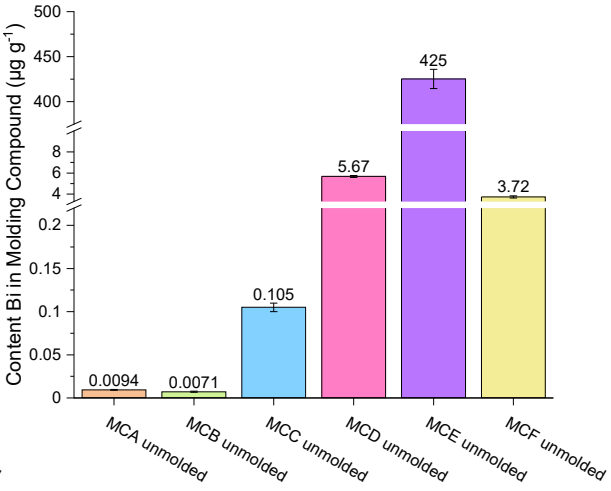

Figure 58: Results for the quantified Bi content within molded molding compounds MCA (orange), MCB (green), MCC (blue), MCD (pink), MCE (purple) and MCF (yellow) using the final digestion method

5.2 Extraction of mobile ions

In order to optimize the extraction behavior using water as a leaching agent, the influence of time and temperature needed to be investigated, as one would suspect that with higher temperature and/ or longer time increased extraction yields may be achieved. In order to compare the results to a reference point, these were compared to the results of the extraction using the SEMI G29. Experiments were carried out using two different heating sources: convective heating using an convection oven and a heating block and microwave radiation. A different heating source apart from microwave radiation was necessary as the microwave instrument should only be used for a maximum of 2 h. As the SEMI G29 foresees an extraction time of 48 h a convective heating source was necessary. In addition, the heating block itself was necessary as using merely the convection oven, the comparison of stirring vs. not stirring during the experiment could not have been investigated. For the extraction results, also 8 elements (Li, C, Na, Mg, K, Ca, Mn and Sr) were chosen to display the different extraction behaviors. Additionally, the results of the IC measurement (ions Lactate, Acetate, Formate, $Cl^-, {NO_3}^-, {SO_4}^{2-}$ as well as the data of the measurement of pH value and electric conductivity) are plotted for each experiment. Using the current IC system, it was not possible to resolve Acetate and Formate which resulted in the treatment of both analytes as a sum parameter.

Discussion on the extraction results will be split into two parts: heating block plus convection oven experiments and the microwave assisted extraction. Heating block experiments were necessary as for the comparison to the standard SEMI G29. Also, first experiments on the influence of extraction temperature and shorter extraction times were carried out. However, results for temperature dependency on the extraction behavior of heating block experiments and microwave assisted extractions cannot be compared as the extraction times differed vastly in comparison.

5.2.1 Heating block experiments

For heating block experiments, temperature and time were varied. The temperature ranged from 60 °C to up to 150 °C which was the upper temperature limit due to the maximal pressure of the extraction vessels of 20 bar. Extraction time was varied from as short as 6 h to up to 48 h at different extraction temperatures. In addition to temperature and time variation also the conditions of the SEMI G29 were applied (120 °C for 48 h). In Figure 68 to Figure 74 the data points for extraction at 90 °C and 24 h has been excluded due to wrong sample treatment for the IC and pH value/ conductivity measurement. All data points represent the means of 3 repeats and their standard deviation.

5.2.1.1 Heating block: influence of extraction temperature

For the investigation of the influence of the extraction temperature, extraction time was held constant at 24 h.
It was expected for the extraction behavior of all elements to show a higher extractable content within solution at higher temperatures. Additionally, it was expected for the curves to show a

somewhat linear trend before the curve flattens due to the extraction equilibrium. Generally, there are three phases during extraction: the equilibrium controlled phase, transition phase and diffusion controlled phase. Ideally, for a complete extraction, it desired to reach the diffusion controlled phase with the given extraction conditions[63,64]. A typical extraction curve can be seen in Figure 59.

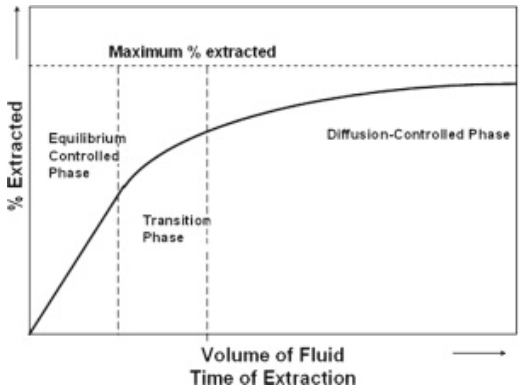

Figure 59: General extraction behavior with three defined phases: equilibrium controlled phase, transition phase and diffusion controlled phase[64]

Analytes in general showed a vastly different behavior compared to each other at temperatures of 150 °C and below. Li, C and Mn show a similar trend with the highest possible extractable content at the highest employed temperature with little to no signs of an equilibrium. However, experiments at 120 °C do not align with this trend.

For elements Na and K extraction at 60 °C showed little to now extraction efficiency as the the content in the extract was <LOQ. At temperatures above 60 °C, Na and K show no strong dependency on the extractability at temperatures of 150 °C and below.

Elements from the earth alkali group all show similar behaviors. Element Mg shows a maximal content after extraction at 120 °C as compared to Ca and Sr which show a maximal content for extraction at 90 °C. All three elements then show a decrease in quantified mobile content for extraction at 150 °C which contradicts the expectations of the extraction behavior. Also Ba behaves similarly to Mg. However, it remains unclear whether extractability actually decreased or if the elements formed a precipitate or re-adsorbed onto the sample material in the suspension. Experiments suggest that for longer extraction times, higher temperatures are not beneficial for extractability for all elements. As elements such a Mg and Ca showcase elements of interest for corrosion processes as well, this should be considered when performing long-term extraction experiments.

For the results of the IC, conductivity and pH value measurements, the extraction at 90 °C was excluded due to wrong sample treatment after work up and contamination of the extracts with nitric acid. All ions show an expected dependency on the temperature with increasing extractability for all ions except for NO_3^- which already shows signs of an equilibrium.

The pH value stays somewhat constant for all experiments at around 5.5. However, the electric conductivity behaves similar as elements Mg, Ca and Sr suggesting again either the formation of a precipitate or a decrease in extractability for higher temperatures at long-term extraction times.

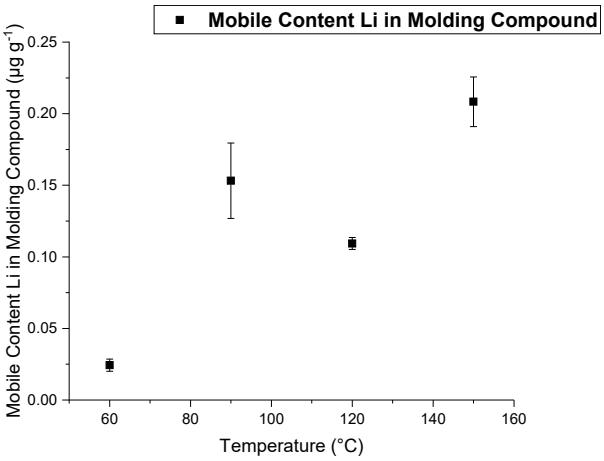

Figure 60: Dependence of the quantified mobile ion content of Li in MCF1 on the temperature applied during extraction

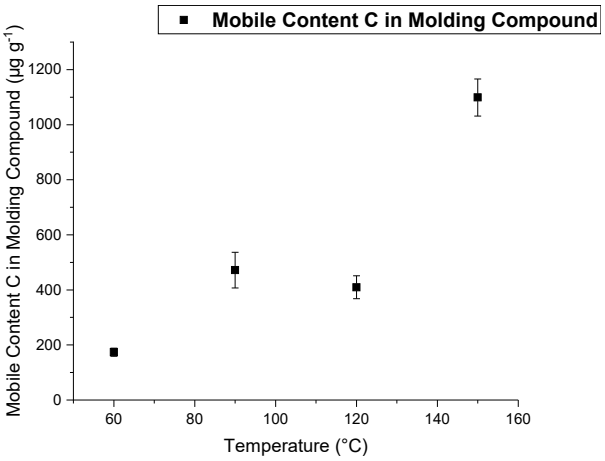

Figure 61: Dependence of the quantified water soluble content of C in MCF1 on the temperature applied during extraction

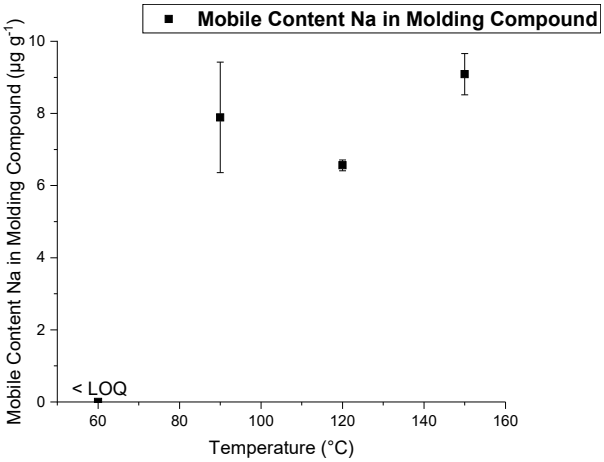

Figure 62: Dependence of the quantified mobile ion content of Na in MCF1 on the temperature applied during extraction

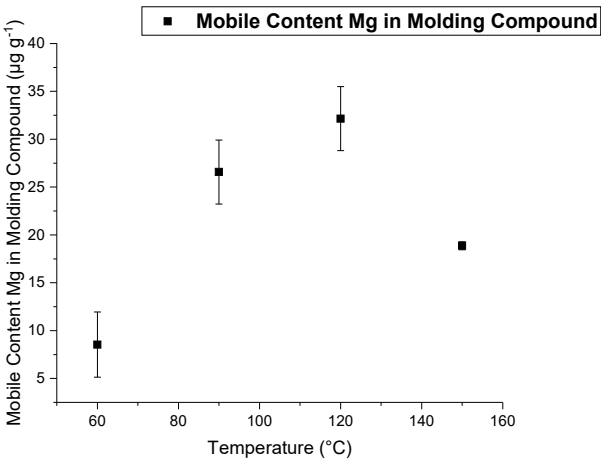

Figure 63: Dependence of the quantified mobile ion content of Mg in MCF1 on the temperature applied during extraction

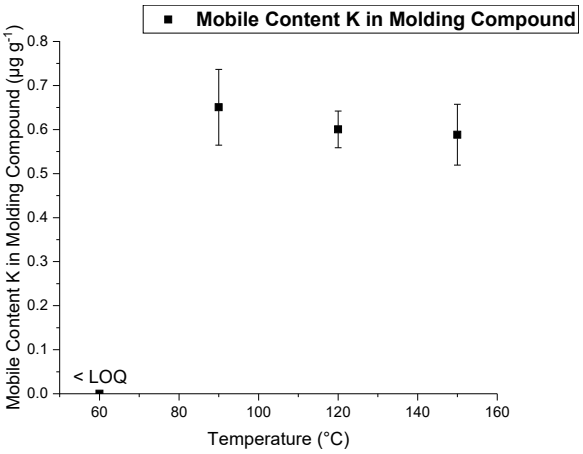

Figure 64: Dependence of the quantified mobile ion content of K in MCF1 on the temperature applied during extraction

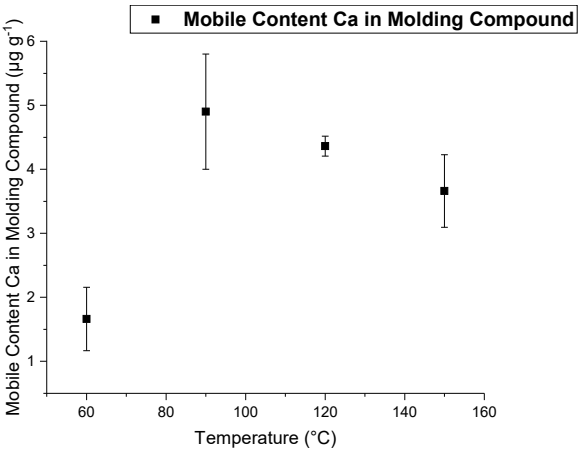

Figure 65: Dependence of the quantified mobile ion content of Ca in MCF1 on the temperature applied during extraction

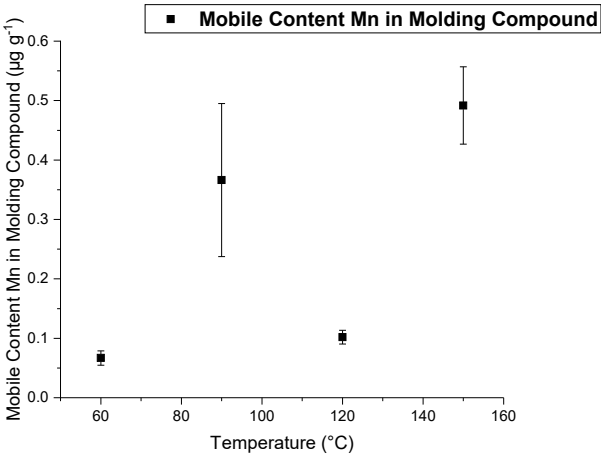

Figure 66: Dependence of the quantified mobile ion content of Mn in MCF1 on the temperature applied during extraction

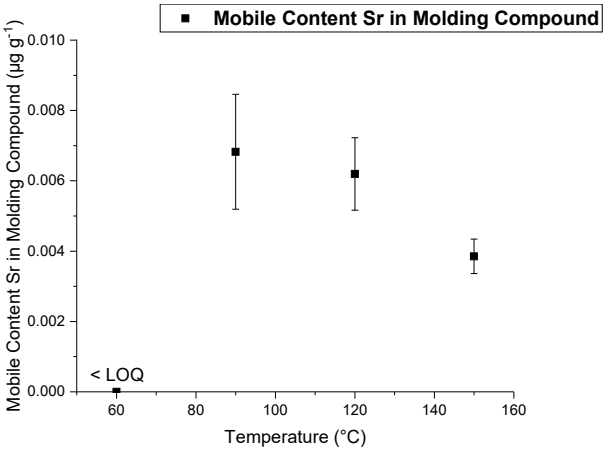

Figure 67: Dependence of the quantified mobile ion content of Sr in MCF1 on the temperature applied during extraction

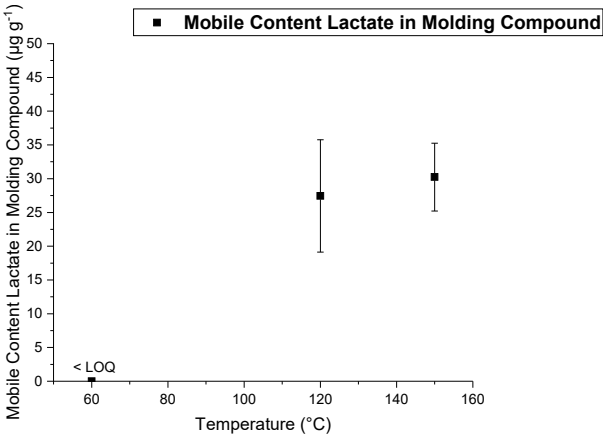

Figure 68: Dependence of the quantified mobile ion content of Lactate in MCF1 on the temperature applied during extraction

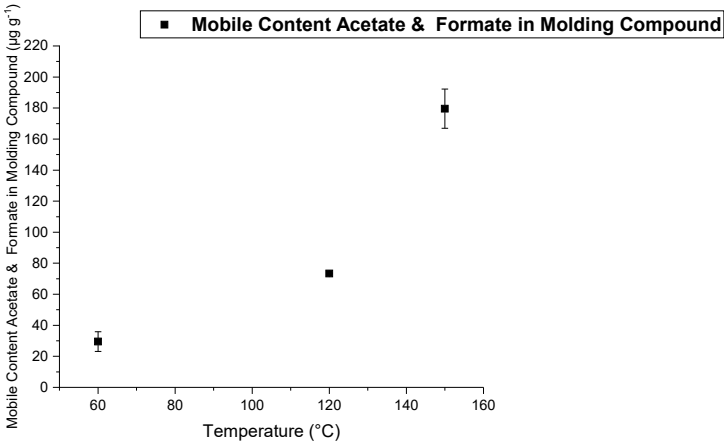

Figure 69: Dependence of the quantified mobile ion content of Acetate and Formate in MCF1 on the temperature applied during extraction

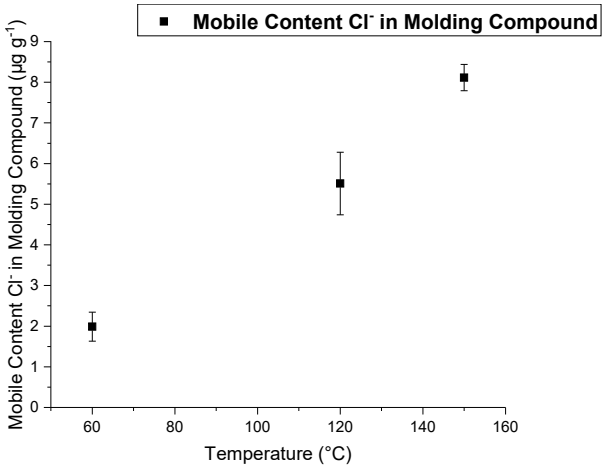

Figure 70: Dependence of the quantified mobile ion content of Cl^- in MCF1 on the temperature applied during extraction

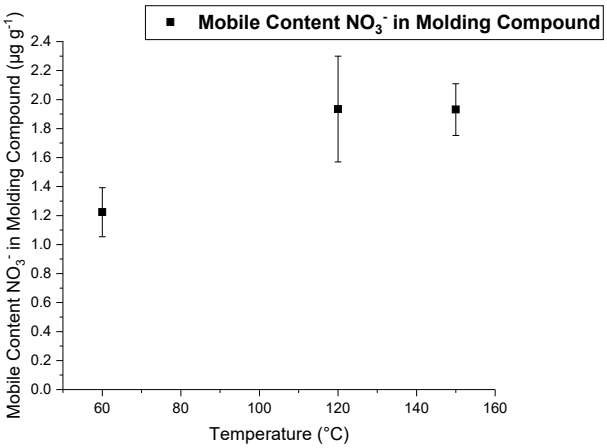

Figure 71: Dependence of the quantified mobile ion content of NO_3^- in MCF1 on the temperature applied during extraction

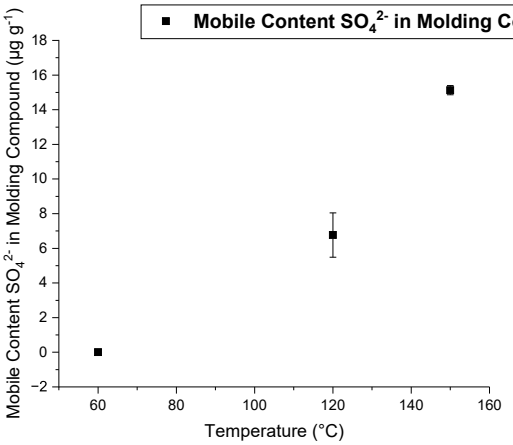

Figure 72: Dependence of the quantified mobile ion content of $SO_4{}^{2-}$ in MCF1 on the temperature applied during extraction

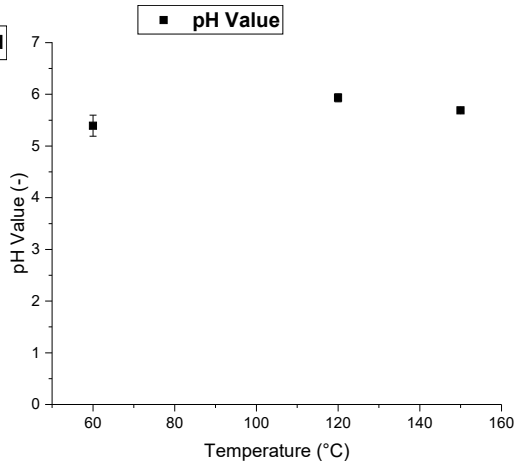

Figure 73: Dependence of the determined pH value in the extracts of MCF1 on the temperature applied during extraction

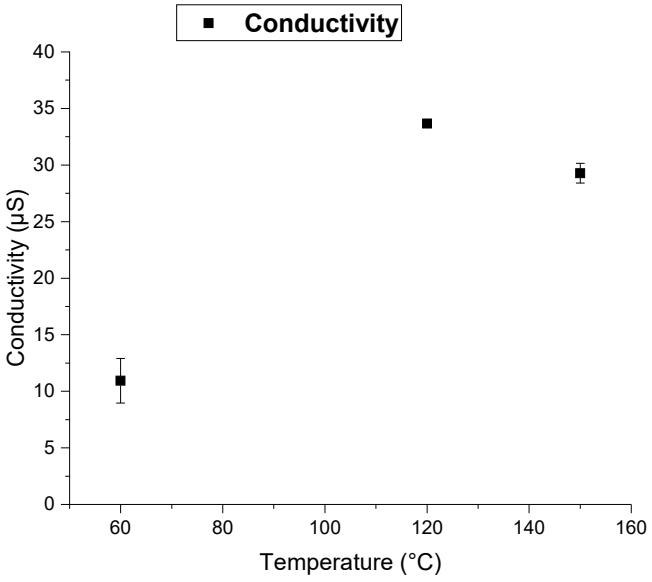

Figure 74: Dependence of the determined electric conductivity in the extracts of MCF1 on the temperature applied during extraction

5.2.1.2 Comparison to SEMI G29

For a better comparability, the results for the extraction according to SEMI G29 (120 °C; 48 h) were plotted together with results at different extraction conditions: 120 °C; 24 h stirred and unstirred as well as 150 °C; 24 h stirred and unstirred. In addition, a first try for the investigation of the short term extraction behavior was carried out at 150 °C for 6 h as a pre-experiment for the afterward microwave assisted extraction.

The focus laid upon the quantification of the mobile ions (Mobile Content) as well as the relative extractability (Mobile Fraction). Hence, both results are plotted below. However, for elements C and K no mobile fraction can be calculated as the total carbon content can not be determined using wet digestion. Using an Ar sustained plasma for ICP-MS, only the isotope ^{39}K can be measured as $^{40}K^+$ cannot be separated from $^{40}Ar^+$ using only a single quadrupole instrument. Due to the addition of HCl during the digestion, a highly abundant isobaric interference forms with m/z 39 which cannot be eliminated using the collision cell technology. Although it is unclear what this isobaric interference is exactly, it may be suggested that $^{37}Cl^1H^1H^+$ forms in the plasma, additionally to $^{38}Ar^1H$ which forms independently from the addition of HCl.

By knowing the total quantified content of an element $c_{element;total}$ and its mobile content $c_{element;mobile}$, the mobile fraction $w_{element;mobile}$ can be easily calculated as can be seen in Equation 20.

$$w_{element;mobile} = \frac{c_{element;mobile}}{c_{element;total}} \tag{20}$$

Different experiments were conducted to further understand and/ or optimize the extraction behavior of the sample material. Firstly, it was of interest whether stirring during the extraction, has a strong influence at different temperatures (120 °C and 150 °C). Additionally, results were compared to the extraction according to SEMI G29 (120 °C for 48 h). After all experiments using the heating block were conducted, the question remained whether short extraction times at a higher temperature compared to SEMI G29 are favorable or already show a high extraction efficiency, showcasing whether a shorter extraction time may lead to comparable results and thus higher sample throughput. Results can be found in Figure 75 to Figure 89.

Comparing results for the extractions at 120 °C stirred and unstirred, elements Li, C, Na, K, Ca and Sr showed a slightly higher quantified mobile/ water soluble content of about 20 % when stirring was employed. Mg showed a higher extractability when the extraction is not stirred (30 %) and Mn showed a strong benefit of stirring with a 4 times greater quantified mobile content. Ions Lactate and Chloride showed a higher mobile content of 40 % and 10 % when the extraction is not stirred. Sum mobile content for Acetate and Formate showed no great influence whether the suspension is stirred or not. For NO_3^-, error bars are too high as to properly compare the results. Only SO_4^{2-} of all quantified ions showed a higher mobile content while stirring of the extraction, though error bars are high as well.

At 150 °C extraction temperature, elements Li, Na, K, Ca and Sr showed a slight increase in the mobile content while stirring during the extraction of again ca. 20 %. Elements C and Mg showed higher mobile contents by 10 % when the suspension was not stirred during extraction. For Mn, stirring showed again a higher mobile content, though the effect was not as pronounced as compared to the influence of stirring at 120 °C with a factor of only approx. 1.5. Additionally, extraction at 150 °C without stirring delivered a similar or higher mobile content as compared to a stirred extraction at 120 °C for elements Li, C, Na and Mn and the opposite for K, Mg, Ca and Sr. For all quantified ions, extraction at 150 °C without stirring showed a higher or similar mobile content as compared to its stirred counterpart. The pH value again decreased slightly at the stirred extraction and electric conductivity increased as well.

Comparing results for the extractions at 120 °C (24 h and 48 h extraction time unstirred), elements Li, C, Na and Sr showed a similar mobile content thus no further increase in extractability towards longer extraction times can be observed. Elements Mg, K and Ca showed a higher mobile content after extraction for 24 h compared to 48 h which may result from precipitation or adsorption onto the extraction residue. Only Mn showed in increase in extractability at longer extraction time. $SO_4{}^{2-}$ showed a similar mobile content at both extraction times. Ions Cl^- and $NO_3{}^-$ showed a higher mobile content at 24 h extraction time and ions Lactate, Acetate and Formate showed in increase in mobile content at longer extraction time. The pH value as well as the electric conductivity both showed a decrease with longer extraction time.

For the unstirred extraction at 150 °C for 24 h an increase in mobile content was expected compared to the results of SEMI G29. Elements Li, C, Mg, K and Mn showed the expected behavior. For Na and Ca, the extractability stayed somewhat the same. Only Sr showed a decrease in mobile content at higher extraction temperature. Ions Cl^-, $NO_3{}^-$ and $SO_4{}^{2-}$ showed an increase in mobile content at higher extraction temperature. Acetate and Formate showed a similar behavior at both extraction conditions and the quantified mobile content of Lactate decreased at higher temperature due to possible degradation. The pH value increased at 150 °C while the electric conductivity showed neither increase nor decrease.

To further compare long term and short term extraction behavior, extractions at 150 °C for 6 h were conducted. In comparison to the SEMI G29, elements Na, K and Sr showed similar extractability at higher temperature and shorter extraction time. Elements Li, C, Mg, Ca and Mn even showed a higher extractability, though the extraction time was shortened by a factor of 8 (48 h to 6 h). Ions Cl^-, $NO_3{}^-$ and $SO_4{}^{2-}$ also showed a greater mobile content at shorter extraction time. Merely ions Lactate, Acteta and Formate showed an increase in mobile content with longer extraction time. The pH value and conductivity increased with decreased extraction time as well.

Comparing the unstirred results at 150 °C with 24 h and 6 h extraction time, elements Na and K showed similar mobile contents. Elements Mg, Ca and Sr showed an increased mobile content

at shorter extraction time. Li, C and Mn showed a decreased mobile content, though already 70 % of ions are already mobile within the first 6 h of extraction. Ions Cl^- and NO_3^- showed similar mobile contents at both extraction times. Lactate showed an increase in mobile content by a factor of almost 2 at 6 h of extraction time. Acetate and Formate showed a decrease of mobile content, resulting in 40 % of ions being mobile within the first 6 h. SO_4^{2-} showed the same behavior as Li, C and Mn as it showed a decrease in mobile content and again 70 % of ions were mobile within the first 6 h of extraction. The pH value and the electric conductivity increased as well with shorter extraction times.

Comparison to SEMI G29: mobile content

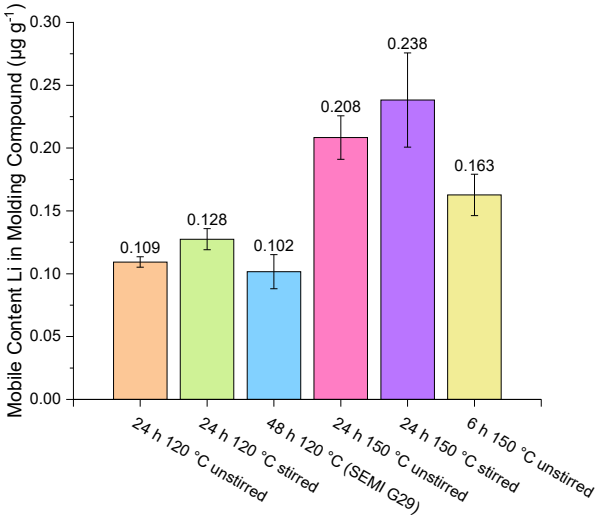

Figure 75: Quantified mobile content of Li in molding compound MCF1 at different extraction conditions: 120 °C; 24 h unstirred (orange), 120 °C; 24 h stirred (green), SEMI G29 120 °C; 48 h (blue), 150 °C; 24 h unstirred (pink), 150 °C; 24 h stirred (purple) and 150 °C; 6 h unstirred (yellow)

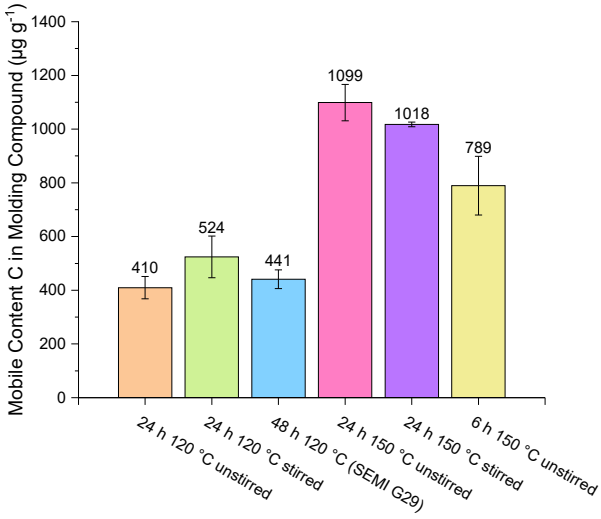

Figure 76: Quantified water soluble content of C in molding compound MCF1 at different extraction conditions: 120 °C; 24 h unstirred (orange), 120 °C; 24 h stirred (green), SEMI G29 120 °C; 48 h (blue), 150 °C; 24 h unstirred (pink), 150 °C; 24 h stirred (purple) and 150 °C; 6 h unstirred (yellow)

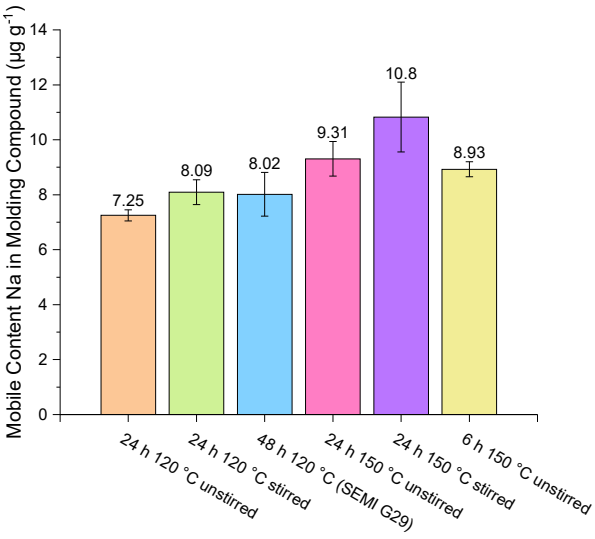

Figure 77: Quantified mobile content of Na in molding compound MCF1 at different extraction conditions: 120 °C; 24 h unstirred (orange), 120 °C; 24 h stirred (green), SEMI G29 120 °C; 48 h (blue), 150 °C; 24 h unstirred (pink), 150 °C; 24 h stirred (purple) and 150 °C; 6 h unstirred (yellow)

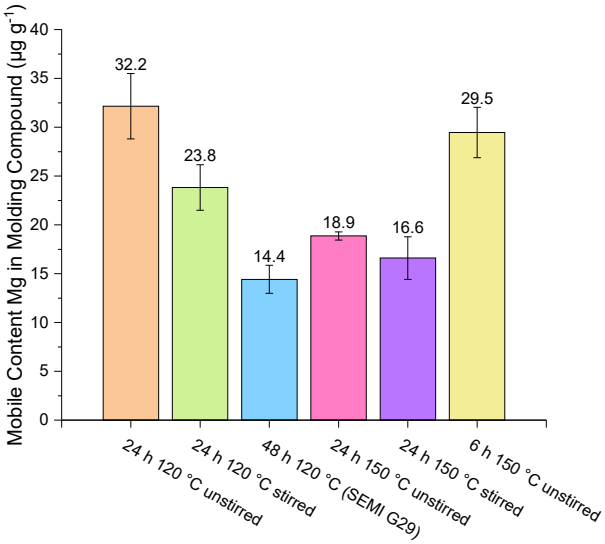

Figure 78: Quantified mobile content of Mg in molding compound MCF1 at different extraction conditions: 120 °C; 24 h unstirred (orange), 120 °C; 24 h stirred (green), SEMI G29 120 °C; 48 h (blue), 150 °C; 24 h unstirred (pink), 150 °C; 24 h stirred (purple) and 150 °C; 6 h unstirred (yellow)

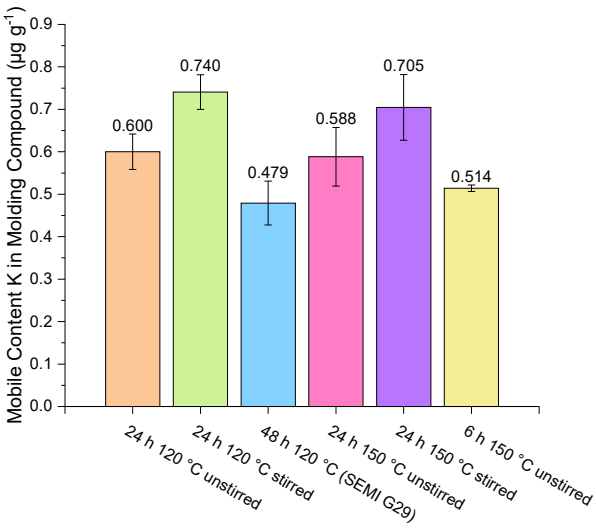

Figure 79: Quantified mobile content of K in molding compound MCF1 at different extraction conditions: 120 °C; 24 h unstirred (orange), 120 °C; 24 h stirred (green), SEMI G29 120 °C; 48 h (blue), 150 °C; 24 h unstirred (pink), 150 °C; 24 h stirred (purple) and 150 °C; 6 h unstirred (yellow)

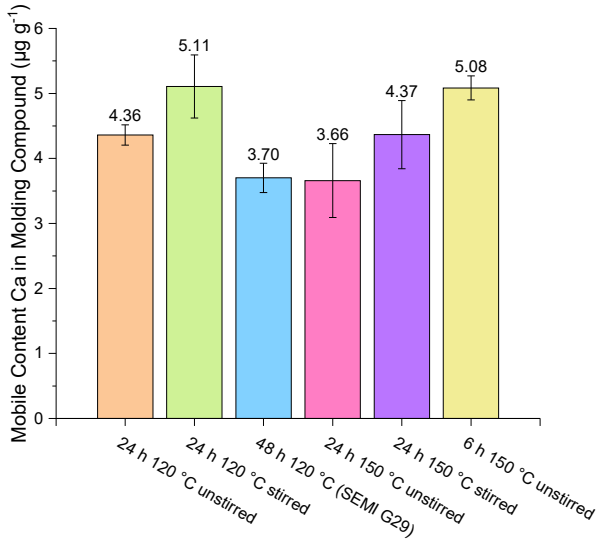

Figure 80: Quantified mobile content of Ca in molding compound MCF1 at different extraction conditions: 120 °C; 24 h unstirred (orange), 120 °C; 24 h stirred (green), SEMI G29 120 °C; 48 h (blue), 150 °C; 24 h unstirred (pink), 150 °C; 24 h stirred (purple) and 150 °C; 6 h unstirred (yellow)

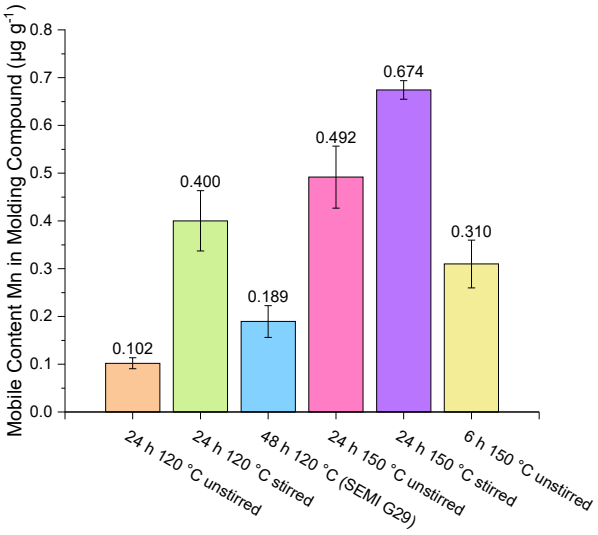

Figure 81: Quantified mobile content of Mn in molding compound MCF1 at different extraction conditions: 120 °C; 24 h unstirred (orange), 120 °C; 24 h stirred (green), SEMI G29 120 °C; 48 h (blue), 150 °C; 24 h unstirred (pink), 150 °C; 24 h stirred (purple) and 150 °C; 6 h unstirred (yellow)

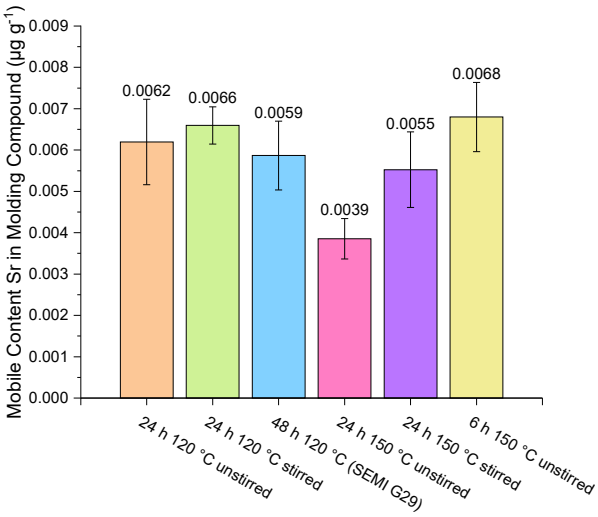

Figure 82: Quantified mobile content of Sr in molding compound MCF1 at different extraction conditions: 120 °C; 24 h unstirred (orange), 120 °C; 24 h stirred (green), SEMI G29 120 °C; 48 h (blue), 150 °C; 24 h unstirred (pink), 150 °C; 24 h stirred (purple) and 150 °C; 6 h unstirred (yellow)

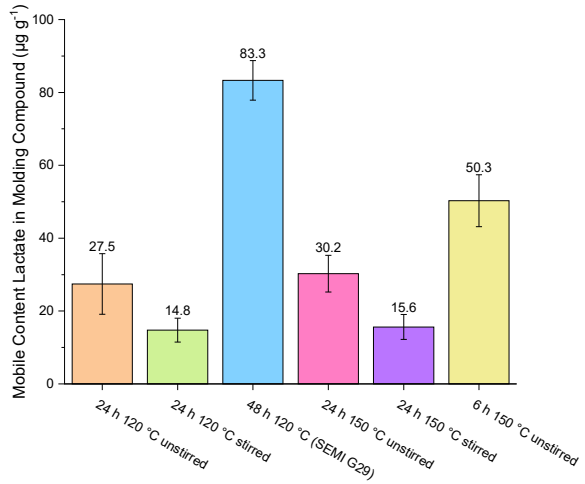

Figure 83: Quantified mobile content of Lactate in molding compound MCF1 at different extraction conditions: 120 °C; 24 h unstirred (orange), 120 °C; 24 h stirred (green), SEMI G29 120 °C; 48 h (blue), 150 °C; 24 h unstirred (pink), 150 °C; 24 h stirred (purple) and 150 °C; 6 h unstirred (yellow)

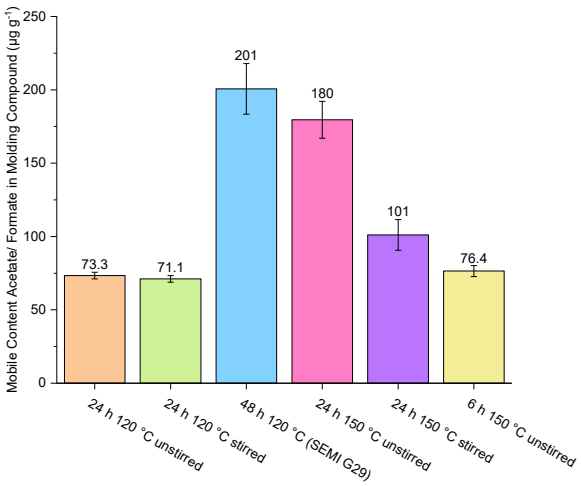

Figure 84: Quantified mobile content of Acetate and Formate in molding compound MCF1 at different extraction conditions: 120 °C; 24 h unstirred (orange), 120 °C; 24 h stirred (green), SEMI G29 120 °C; 48 h (blue), 150 °C; 24 h unstirred (pink), 150 °C; 24 h stirred (purple) and 150 °C; 6 h unstirred (yellow)

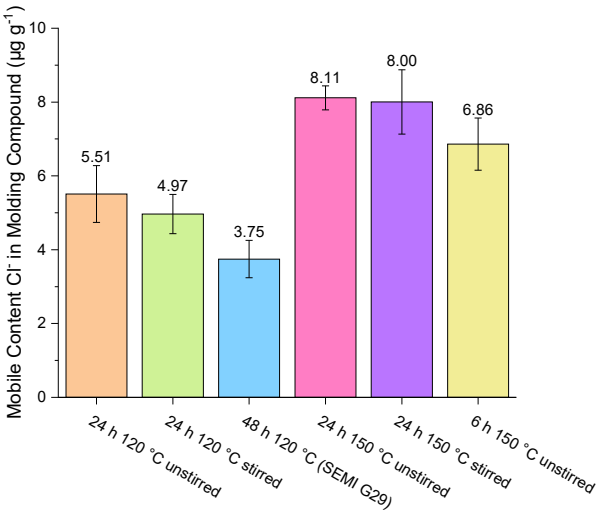

Figure 85: Quantified mobile content of Cl^- in molding compound MCF1 at different extraction conditions: 120 °C; 24 h unstirred (orange), 120 °C; 24 h stirred (green), SEMI G29 120 °C; 48 h (blue), 150 °C; 24 h unstirred (pink), 150 °C; 24 h stirred (purple) and 150 °C; 6 h unstirred (yellow)

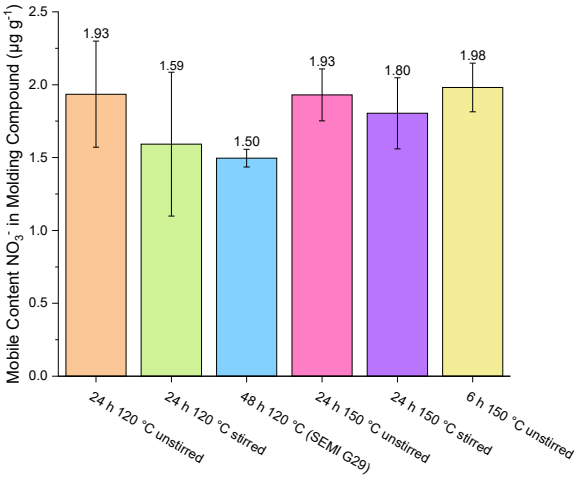

Figure 86: Quantified mobile content of NO_3^- in molding compound MCF1 at different extraction conditions: 120 °C; 24 h unstirred (orange), 120 °C; 24 h stirred (green), SEMI G29 120 °C; 48 h (blue), 150 °C; 24 h unstirred (pink), 150 °C; 24 h stirred (purple) and 150 °C; 6 h unstirred (yellow)

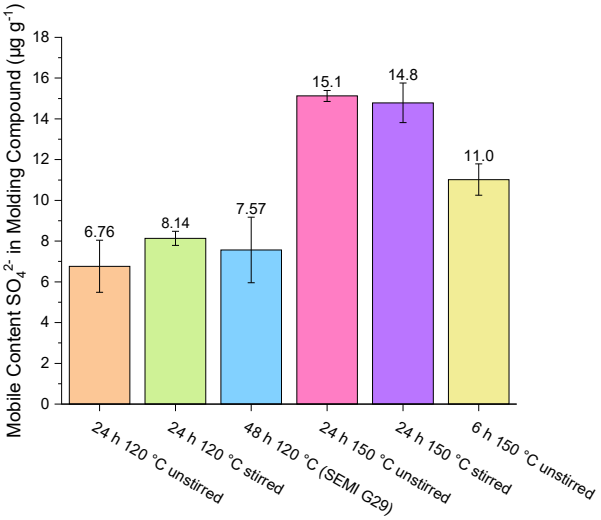

Figure 87: Quantified mobile content of SO_4^{2-} in molding compound MCF1 at different extraction conditions: 120 °C; 24 h unstirred (orange), 120 °C; 24 h stirred (green), SEMI G29 120 °C; 48 h (blue), 150 °C; 24 h unstirred (pink), 150 °C; 24 h stirred (purple) and 150 °C; 6 h unstirred (yellow)

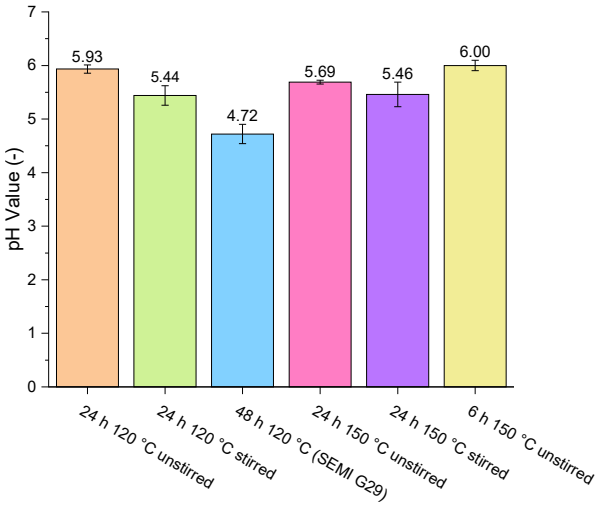

Figure 88: Determined pH value in extracts of molding compound MCF1 at different extraction conditions: 120 °C; 24 h unstirred (orange), 120 °C; 24 h stirred (green), SEMI G29 120 °C; 48 h (blue), 150 °C; 24 h unstirred (pink), 150 °C; 24 h stirred (purple) and 150 °C; 6 h unstirred (yellow)

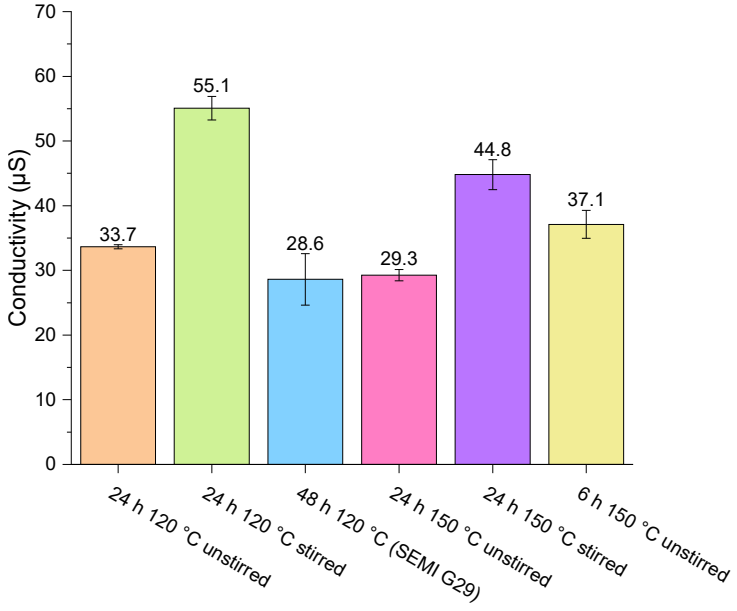

Figure 89: Determined electric conductivity in extracts of molding compound MCF1 at different extraction conditions: 120 °C; 24 h unstirred (orange), 120 °C; 24 h stirred (green), SEMI G29 120 °C; 48 h (blue), 150 °C; 24 h unstirred (pink), 150 °C; 24 h stirred (purple) and 150 °C; 6 h unstirred (yellow)

Comparison to SEMI G29: mobile fraction

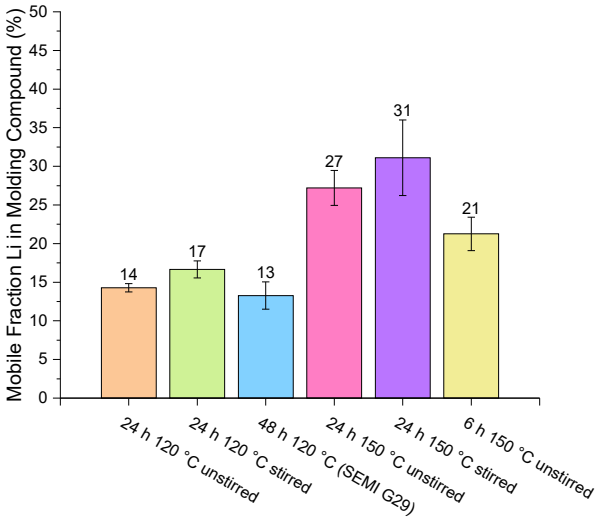

Figure 90: Quantified mobile fraction of Li in molding compound MCF1 at different extraction conditions: 120 °C; 24 h unstirred (orange), 120 °C; 24 h stirred (green), SEMI G29 120 °C; 48 h (blue), 150 °C; 24 h unstirred (pink), 150 °C; 24 h stirred (purple) and 150 °C; 6 h unstirred (yellow)

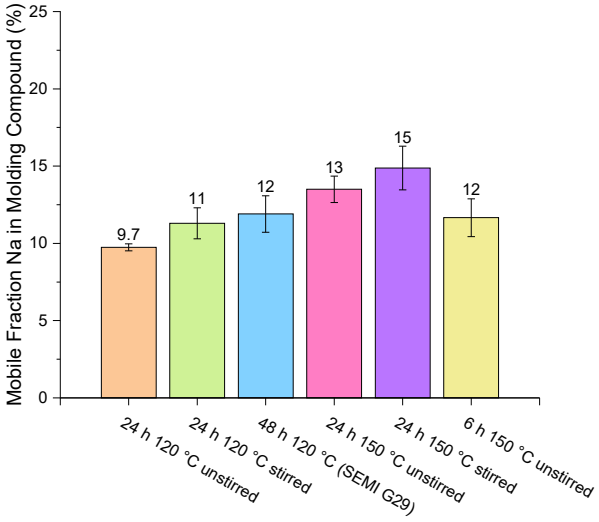

Figure 91: Quantified mobile fraction of Na in molding compound MCF1 at different extraction conditions: 120 °C; 24 h unstirred (orange), 120 °C; 24 h stirred (green), SEMI G29 120 °C; 48 h (blue), 150 °C; 24 h unstirred (pink), 150 °C; 24 h stirred (purple) and 150 °C; 6 h unstirred (yellow)

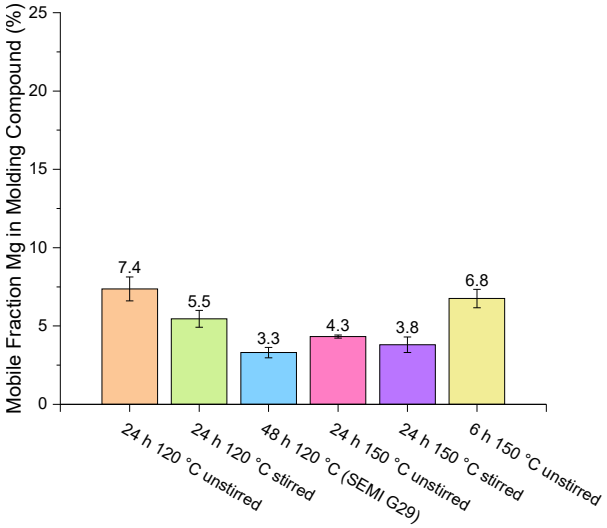

Figure 92: Quantified mobile fraction of Mg in molding compound MCF1 at different extraction conditions: 120 °C; 24 h unstirred (orange), 120 °C; 24 h stirred (green), SEMI G29 120 °C; 48 h (blue), 150 °C; 24 h unstirred (pink), 150 °C; 24 h stirred (purple) and 150 °C; 6 h unstirred (yellow)

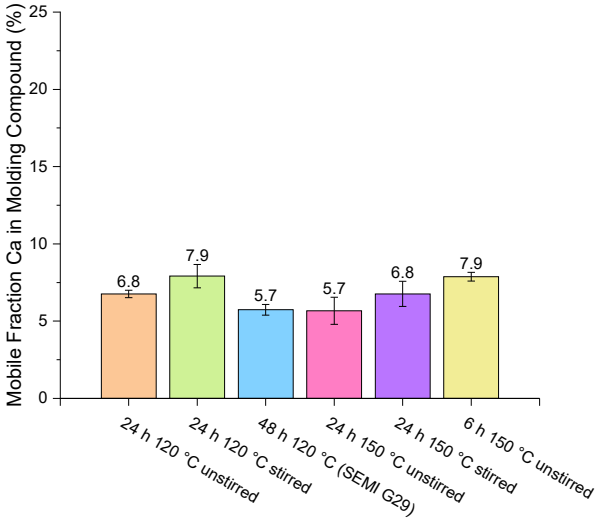

Figure 93: Quantified mobile fraction of Ca in molding compound MCF1 at different extraction conditions: 120 °C; 24 h unstirred (orange), 120 °C; 24 h stirred (green), SEMI G29 120 °C; 48 h (blue), 150 °C; 24 h unstirred (pink), 150 °C; 24 h stirred (purple) and 150 °C; 6 h unstirred (yellow)

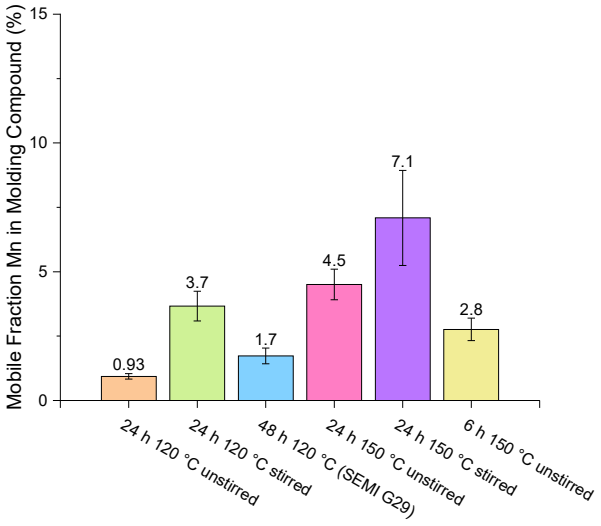

Figure 94: Quantified mobile fraction of Mn in molding compound MCF1 at different extraction conditions: 120 °C; 24 h unstirred (orange), 120 °C; 24 h stirred (green), SEMI G29 120 °C; 48 h (blue), 150 °C; 24 h unstirred (pink), 150 °C; 24 h stirred (purple) and 150 °C; 6 h unstirred (yellow)

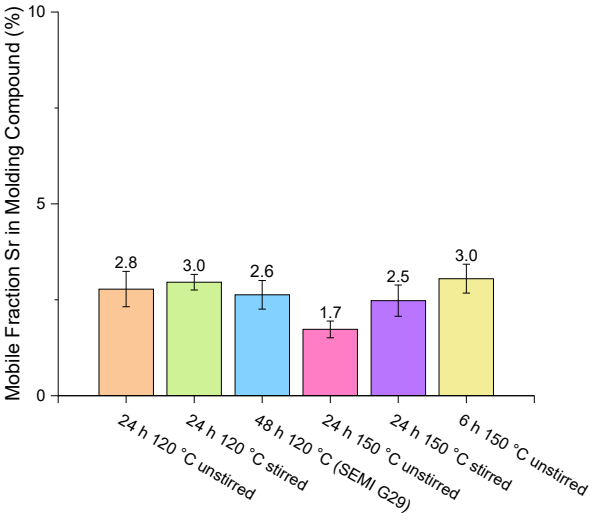

Figure 95: Quantified mobile fraction of Sr in molding compound MCF1 at different extraction conditions: 120 °C; 24 h unstirred (orange), 120 °C; 24 h stirred (green), SEMI G29 120 °C; 48 h (blue), 150 °C; 24 h unstirred (pink), 150 °C; 24 h stirred (purple) and 150 °C; 6 h unstirred (yellow)

5.2.2 Microwave assisted extraction

After the first pre-experiment for the short term leaching behavior at higher temperature (150 °C; 6 h), experiments were conducted using the microwave for temperatures above 150 °C and extraction times shorter than 2 h with the exception of the extraction at 175 °C for 180 min. Overall, 4 different influences on the extraction behavior were investigated: influence of time, temperature and particle size as well as the testing of the completeness of the extraction. For experiments in paragraph 5.2.2.1 to paragraph 5.2.2.3 the yielded powder of molding compound MCF1 after milling was used. For experiments in paragraph 5.2.2.4, the powder was sieved into two fractions: greater and smaller than 180 μm.

For the microwave assisted extraction, the same HVT Teflon vessels were used, resulting in a high contamination of the extracts with Cl^- and $NO_3{}^-$, which were not possible to eliminate even after thorough cleaning of the vessels. Latter anions had a strong affect on the measured pH value and conductivity. However, trends are still visible. As for this, the labeling of the y-axis was left out for mentioned analytes and measurements as the values itself are arbitrary due to the high contamination. All data points represent the means of 4 repeats and their standard deviation.

5.2.2.1 Microwave assisted extraction: influence of extraction temperature

For the investigation on the temperature dependency on the extraction behavior, extractions were performed as described above in a temperature range of 150 °C to 225 °C with a hold time of 90 min at maximum temperature.

Results for the influence of temperature on the microwave assisted extraction can be seen in Figure 96 to Figure 110. All elements showed a trend of increased mobile content with increasing extraction temperature, though the grade of influence differed between analytes, though all alanytes quantified using ICP-OES showed maximal extraction efficiency at 225 °C. Additionally, some elements show a somewhat linear curvature (Li, Na and Mg) as well as a sloping of the curve at higher temperatures (C, K, Ca, Mn, Sr). Influence of temperature on the mobile content was comparatively high for Li and Mn with a 4 times increase in mobile content at 225 °C compared to 150 °C. C and Na showed an increase by a factor of 3. Mg, K and Sr showed an increase by a factor of 2 and Ca showed an increase by a factor of 1.5. Again, elements Mg, Ca and Sr showed a similar behavior. As for Lactate, Cl^- and $NO_3{}^-$, these ions showed a maximal mobile content at 200 °C with an increase by a factor of 4 for Lactate. Acetate and Formate showed an increase factor of 4.5 with the maximal mobile content at 225 °C and a clear sloping of the curve. Increase of these organic anions most likely comes from degradation processes of the polymer. However, the analytes itself can also start to degrade at such high temperature, for example Lactate. $SO_4{}^{2-}$ shows a linear trend and the greatest increase factor of 14 with the maximal mobile content of $331\,\mu g\,g^{-1} \pm 41\,\mu g\,g^{-1}$ at 225 °C.Generally, no Sulfate species should be present within molding compound. Sulfides and Thiols are added to the compound and during the heating process these react to Sulfate species, resulting in a strong increase

of quantifiable mobile Sulfate content.Though with an increase in extraction temperature an increase in mobile content was expected, not all analytes showed such behavior.The pH value shows no big influence by the extraction behavior, though a decreasing trend is visible. Electric conductivity shows an increase until 200 °C and then stays somewhat constant at 225 °C.

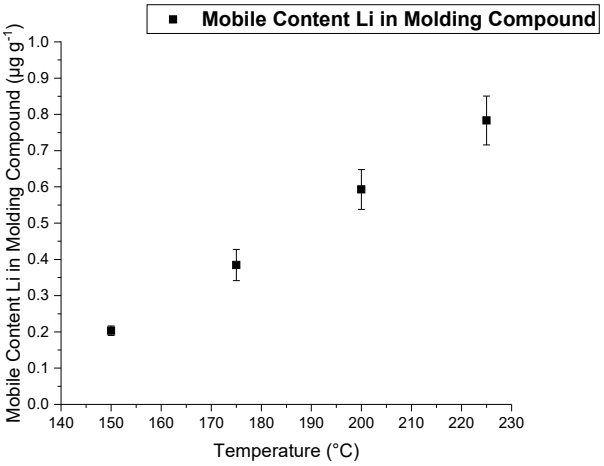

Figure 96: Temperature dependency on the quantified mobile content of Li within molding compound MCF1

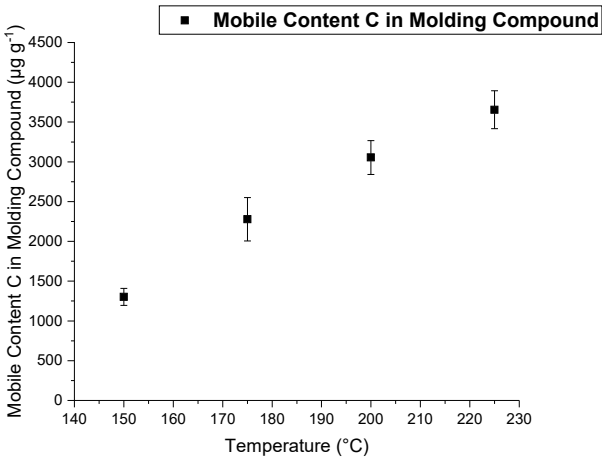

Figure 97: Temperature dependency on the quantified water soluble content of C within molding compound MCF1

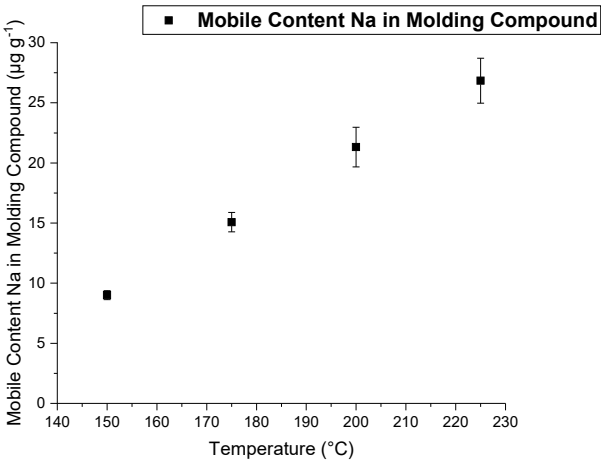

Figure 98: Temperature dependency on the quantified mobile content of Na within molding compound MCF1

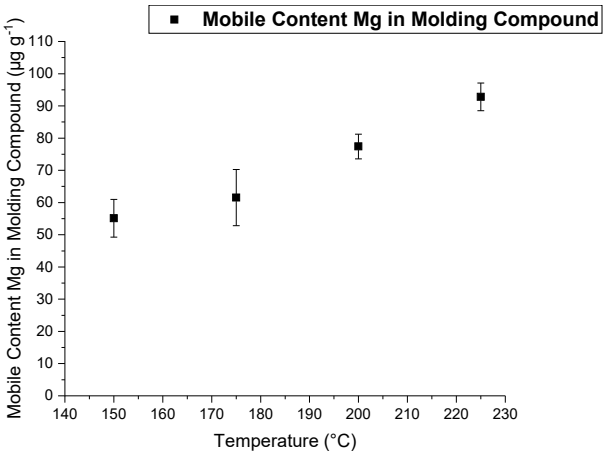

Figure 99: Temperature dependency on the quantified mobile content of Mg within molding compound MCF1

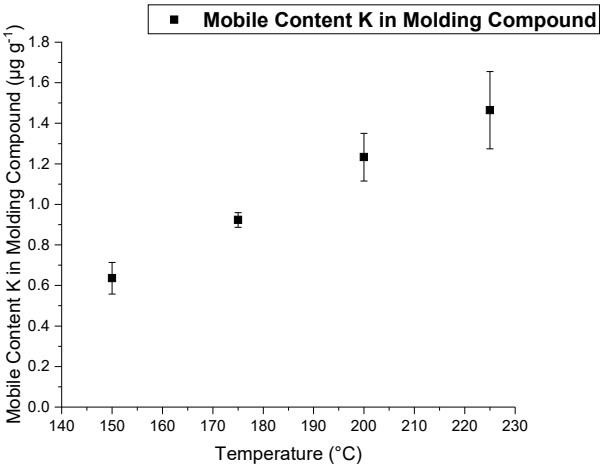

Figure 100: Temperature dependency on the quantified mobile content of K within molding compound MCF1

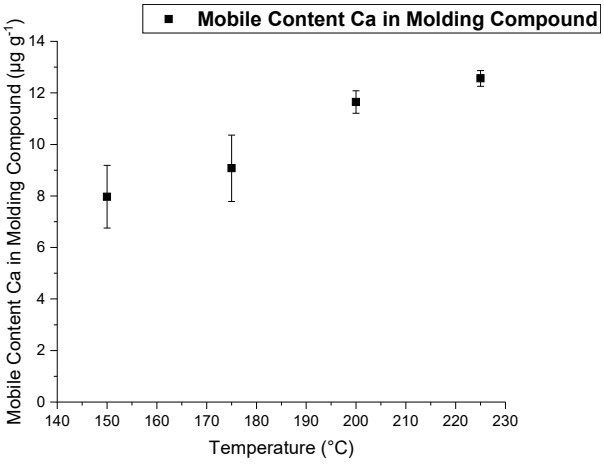

Figure 101: Temperature dependency on the quantified mobile content of Ca within molding compound MCF1

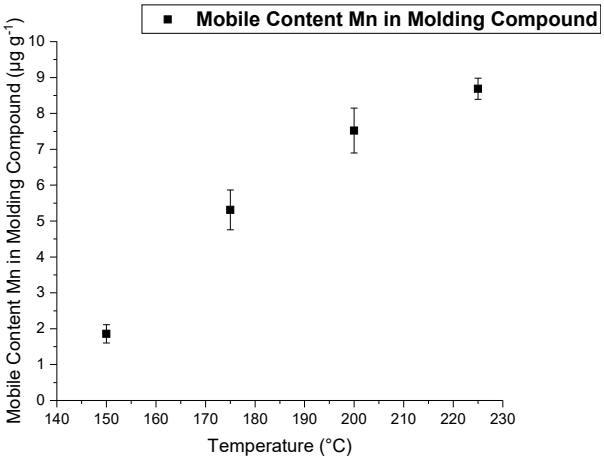

Figure 102: Temperature dependency on the quantified mobile content of Mn within molding compound MCF1

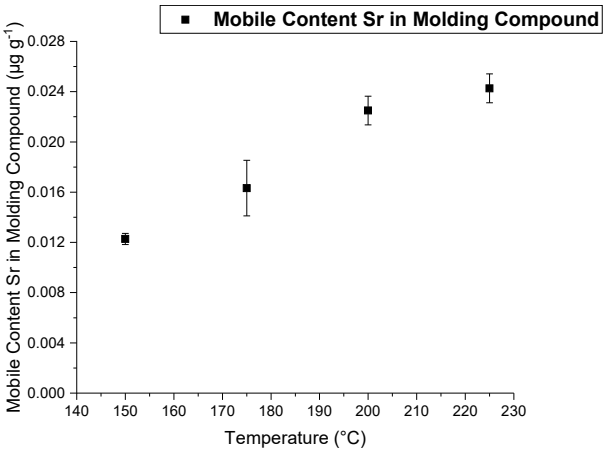

Figure 103: Temperature dependency on the quantified mobile content of Sr within molding compound MCF1

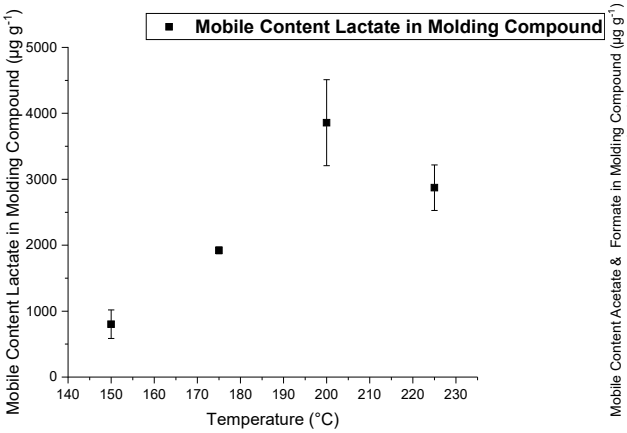

Figure 104: Temperature dependency on the quantified mobile content of Lactate within molding compound MCF1

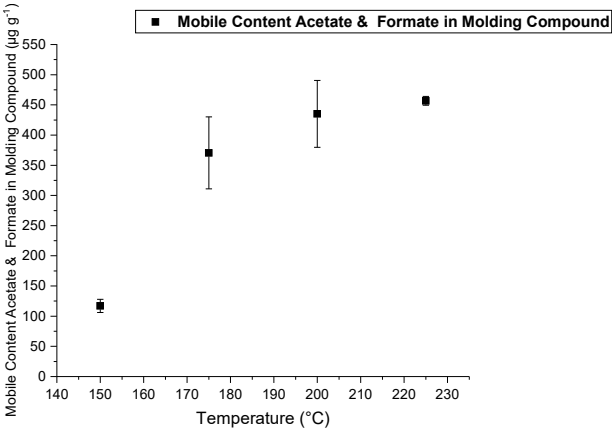

Figure 105: Temperature dependency on the quantified mobile content of Acetate and Formate within molding compound MCF1

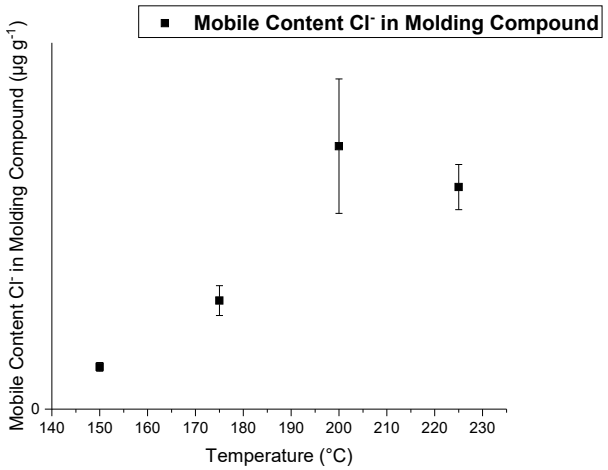

Figure 106: Temperature dependency on the mobile content of Cl^- within molding compound MCF1

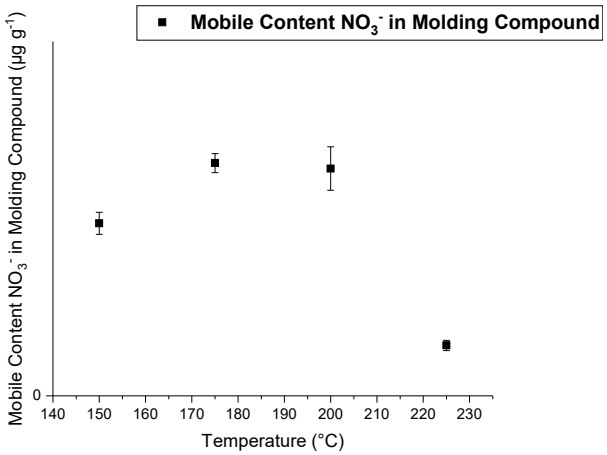

Figure 107: Temperature dependency on the mobile content of NO_3^- within molding compound MCF1

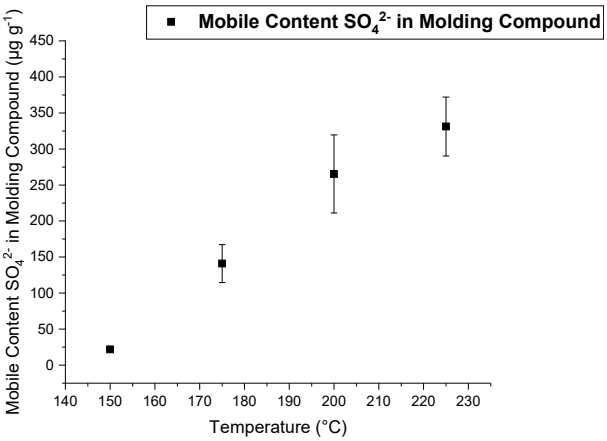

Figure 108: Temperature dependency on the quantified mobile content of SO_4^{2-} within molding compound MCF1

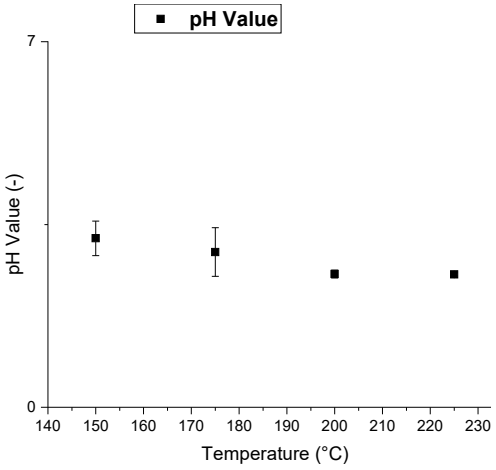

Figure 109: Temperature dependency on the determined pH value in the extracts of molding compound MCF1

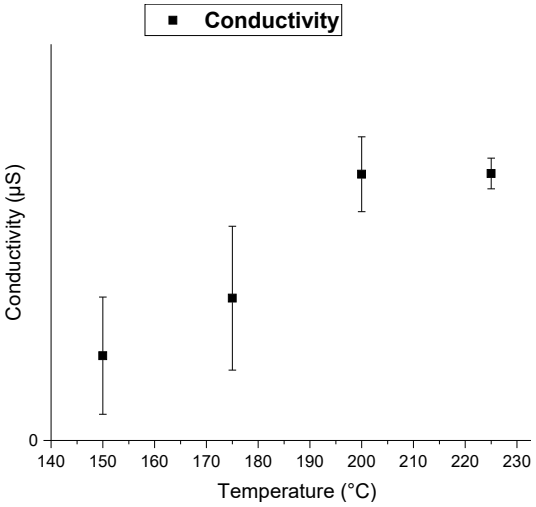

Figure 110: Temperature dependency on the determined electric conductivity in the extracts of molding compound MCF1

5.2.2.2 Microwave assisted extraction: influence of extraction time

For the investigation on the time dependency on the extraction behavior, extractions were performed as described above in a hold time range of 30 min to 180 min at maximum temperature with a maximum temperature of 175 °C.

Results for the time dependency on the microwave assisted extraction can be seen in Figure 111 to Figure 125. All elements showed an increase in mobile content with increasing extraction time with a factor range of 1.2 (K) to 4.5 (Mn). Elements Li and Sr showed a factor of 2 and C, Mg and Ca showed a factor of 1.5. Li showed a sloping towards higher extraction times, while elements C, Na, Mg, K, Ca, Mn and Sr showed a linear trend. K was not heavily influenced, though it showed an increasing trend. Lactate showed poor extractability at extraction times <90 min with an increasing trend for longer extraction times. Acetate and Formate showed a linear trend with an increasing factor of 4. For Acetate and Formate it seems that longer extraction times at lower temperature are favorable as at 175 °C for 180 min 743 $\mu g\,g^{-1} \pm 40\,\mu g\,g^{-1}$ are extractable as compared to 456 $\mu g\,g^{-1} \pm 8\,\mu g\,g^{-1}$ at 225 °C, most likely due to the degradation at such high temperatures. Additionally, Acetate and Formate show a sloping in Figure 105 for temperature dependency, though Figure 120 shows a linear trend for time dependency. Cl^- shows a linear trend as compared to $NO_3{}^-$ which shows a sloping in Figure 122. $SO_4{}^{2-}$ shows a linear trend with an increase factor of 3. The pH value also shows little to no time dependency, though a decreasing trend is visible. The electric conductivity shows a linear trend, though RSD is up to 50 %. Generally, the RSD for the time dependency experiments are much greater as compared to temperature dependency. This may result from unstable extraction conditions at 175 °C which may suggest a transition phase in the extraction.

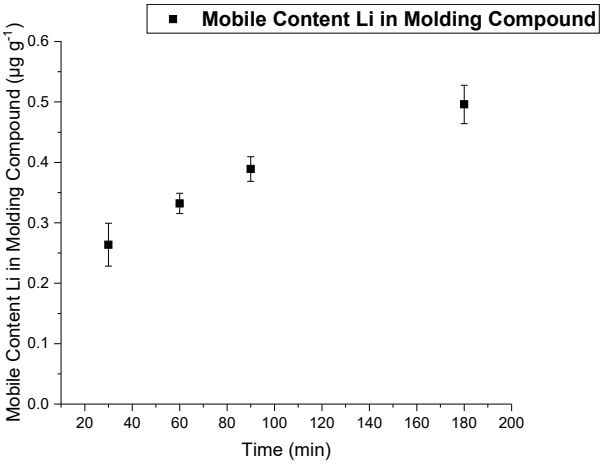

Figure 111: Time dependency on the quantified mobile content of Li within molding compound MCF1

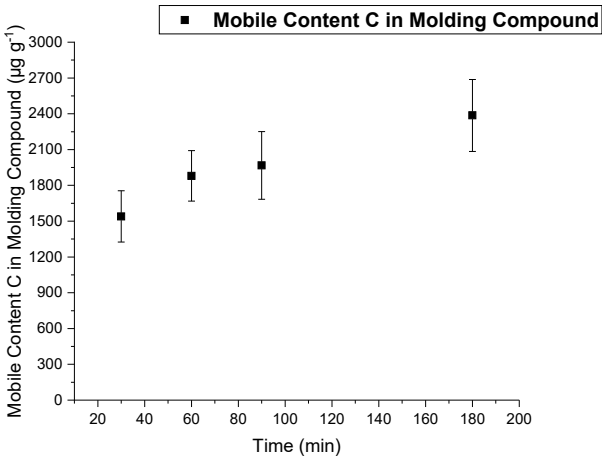

Figure 112: Time dependency on the quantified water soluble content of C within molding compound MCF1

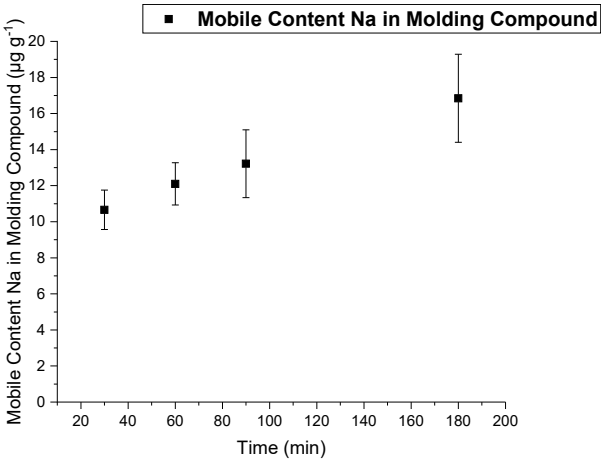

Figure 113: Time dependency on the quantified mobile content of Na within molding compound MCF1

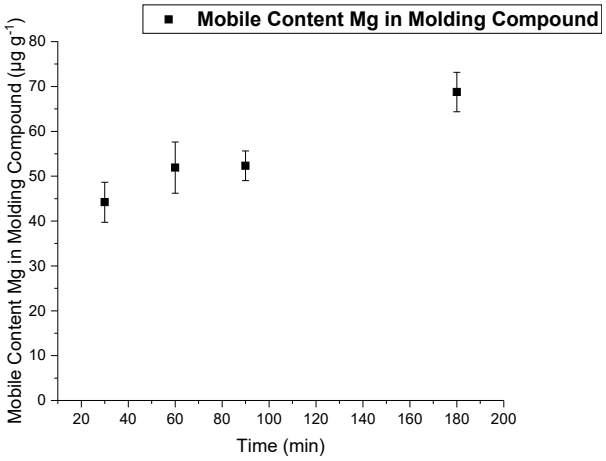

Figure 114: Time dependency on the quantified mobile content of Mg within molding compound MCF1

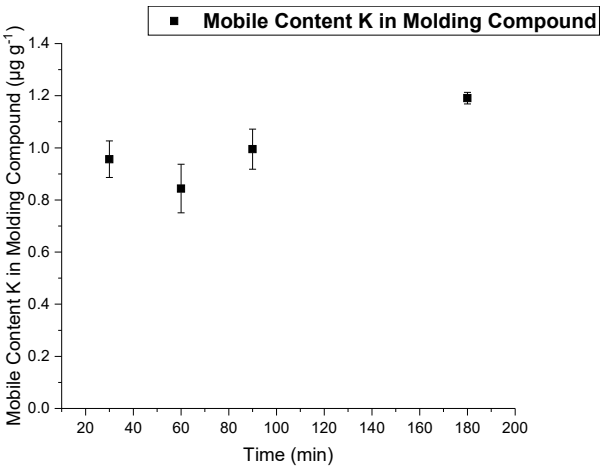

Figure 115: Time dependency on the quantified mobile content of K within molding compound MCF1

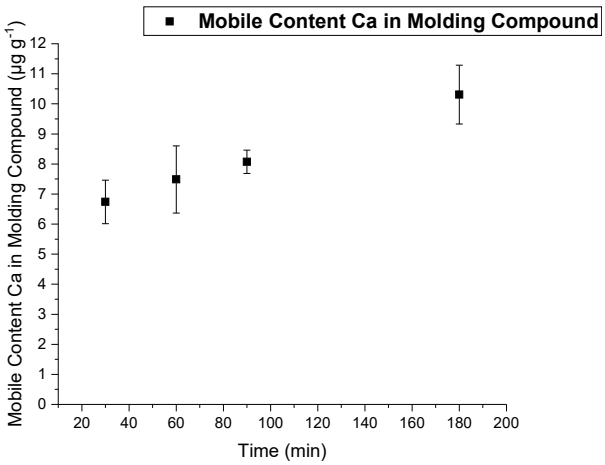

Figure 116: Time dependency on the quantified mobile content of Ca within molding compound MCF1

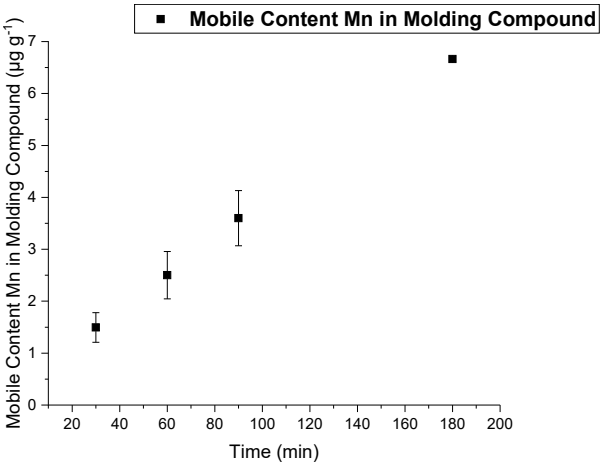

Figure 117: Time dependency on the quantified mobile content of Mn within molding compound MCF1

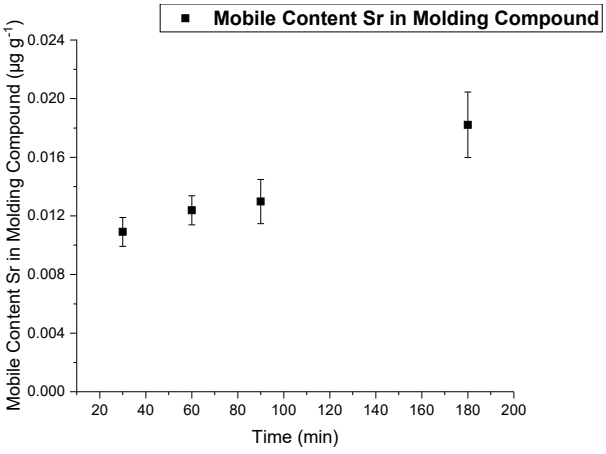

Figure 118: Time dependency on the quantified mobile content of Sr within molding compound MCF1

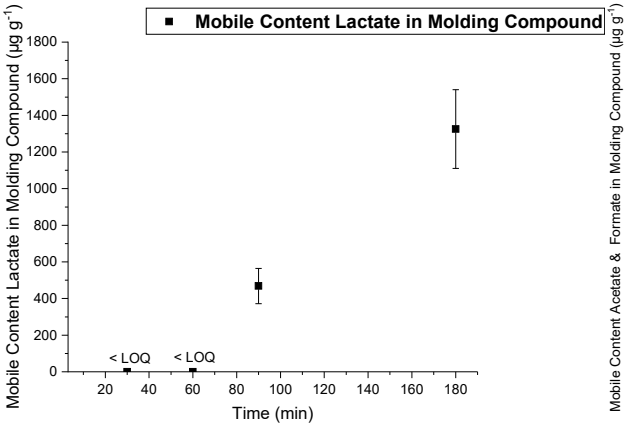

Figure 119: Time dependency on the quantified mobile content of Lactate within molding compound MCF1

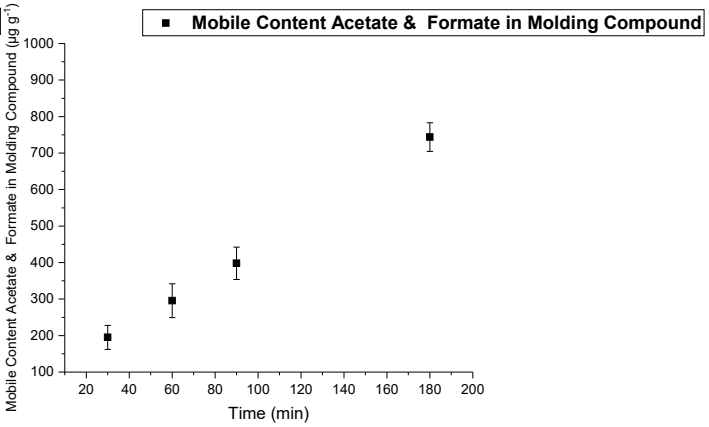

Figure 120: Time dependency on the quantified mobile content of Acetate and Formate within molding compound MCF1

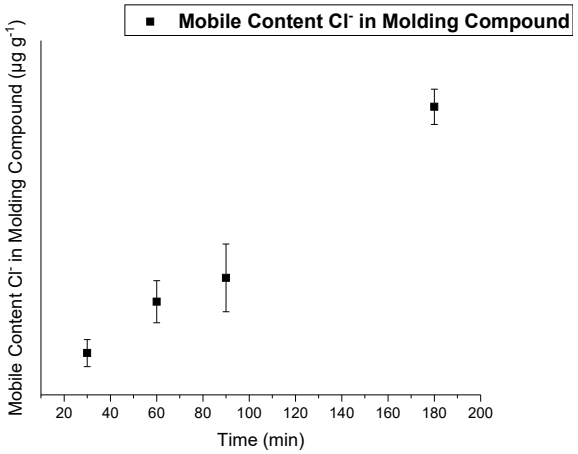

Figure 121: Time dependency on the quantified mobile content of Cl^- within molding compound MCF1

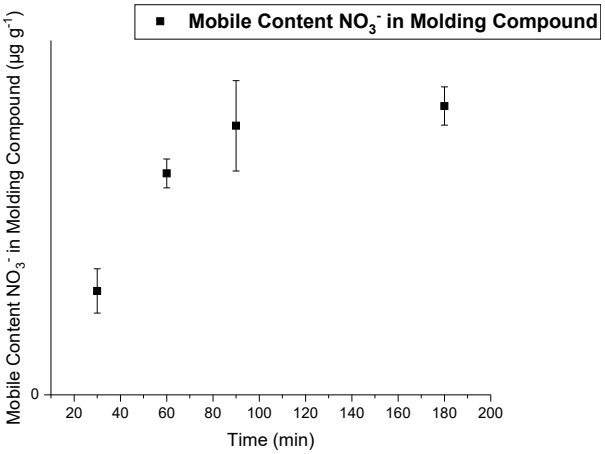

Figure 122: Time dependency on the quantified mobile content of NO_3^- within molding compound MCF1

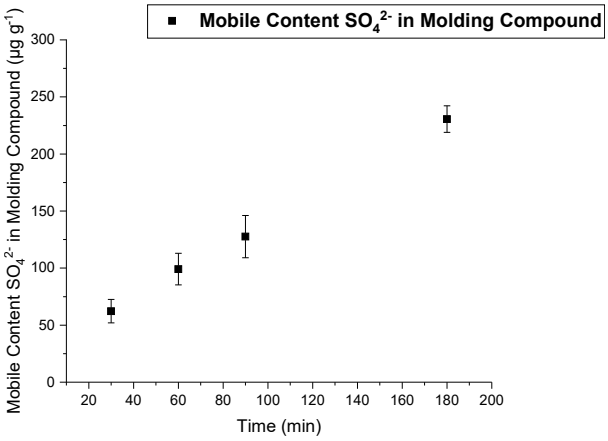

Figure 123: Time dependency on the quantified mobile content of $SO_4{}^{2-}$ within molding compound MCF1

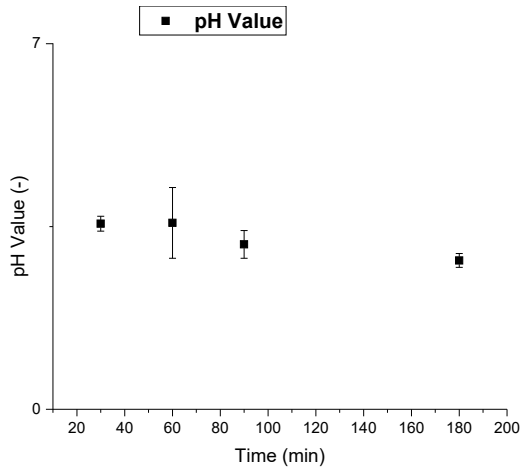

Figure 124: Time dependency on determined pH value in the extracts of molding compound MCF1

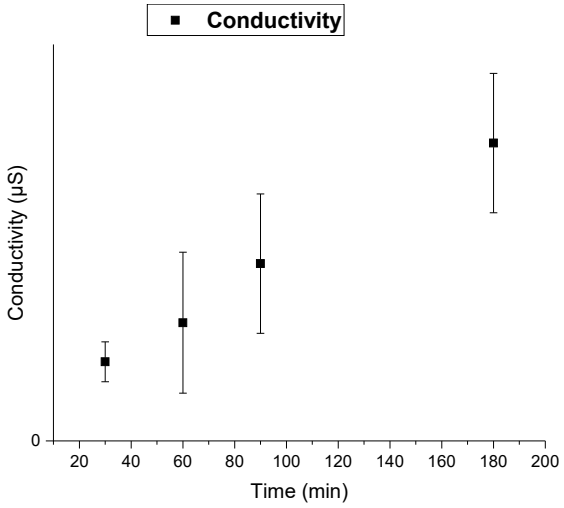

Figure 125: Time dependency on determined electric conductivity in the extracts of molding compound MCF1

5.2.2.3 Testing of completeness of extraction

In order to investigate the completeness of extraction, the molding compound MCF1 underwent 4 consecutive extractions to determine the residual mobile content. Extraction were carried out at 225 °C with 90 min hold time at maximum temperature.

Performing extractions of different sample types, completeness of extraction is always an issue. In order to investigate this, 4 consecutive extractions were performed as described in paragraph 4.6.2.3. Aim of this was not the optimization of the completion but rather to understand the leaching behavior when consecutive extraction were performed. Results for the testing of completeness of extraction can be seen in Figure 126 to Figure 140. Besides the decrease in mobile content, also the accumulative mobile content is of interest as this is also an indicator for the extraction behavior of various analytes. Accumulative extraction curves of the consecutive extraction can be seen in Figure 141 to Figure 153.

Li showed a decrease in leachable content after the 2^{nd} extraction of 63 % and showed a minor increase in mobile content after the 4^{th} extraction with a total decrease in mobile content of 80 % after 4 extractions.
C behaved similarly to Li concerning leachable content after 2^{nd} and 4^{th} extraction, though no increase in further leachable content after four extractions was visible.
Na showed a decrease by 63 % after 2^{nd} extraction and no Na could be quantified after four extractions.
Mobile content for Mg and Ca decreased by 66 % after the 2^{nd} extraction and showed overall a decrease of greater 80 % after 4 extractions. K showed the poorest behavior for completeness, as it only decreased by 40 % after the 2^{nd} extraction and then showed no further decrease in leachable content but stayed somewhat constant at around $1\,\mu g\,g^{-1}$.
Mn showed a decrease of 75 % after the 2^{nd} extraction and the mobile content decreased by 95 % after four extractions.
Leachable content of Sr decreased by 83 % after the 2^{nd} extraction and no Sr content was measurable in the extract after four extractions.
Lactate showed little to no decrease after two extractions and had a strong decrease of 80 % after the 3^{rd} extraction. Leachable content then stayed constant after four extractions, making its behavior unique among all analytes.
Cl^- showed a decreasing linear trend which may results from the leaching of the contamination of Cl^- out of the used HVT teflon vessels. Ions Cl^- and $NO_3{}^-$ do not behave similar, though they both are contaminants due to the beforehand performed acid digestions. This most likely results from a different affinity of the anions towards Teflon. $NO_3{}^-$ shows, similar to K, a decrease after the 2^{nd} extraction and then the leachable content stayed at a constant level.
$SO_4{}^{2-}$ showed a flat decline in leachable content with a decrease of only 40 % after the 2^{nd} extraction as compared to most analytes which showed a deacrease of at least 60 %. After 4 extractions, $SO_4{}^{2-}$ showed a total decrease of 70 % which is also lesser compared to other analytes.

The pH value stayed constant for all extractions, which was expected as the number of extractions should not have a strong influence on the pH value as parameters temperature and time also showed only little influence.
Electric conductivity showed a decreasing linear trend with increasing number of extractions. A decrease in general was expected, as leached ion content decreases as well. However, as most analytes showed an exponential decrease, it was also expected that the electric conductivity showed such behavior.

Analytes show vastly different extraction behaviors comparing the accumulative curves in Figure 141 to Figure 153.
Li, Acetate and Formate show a somewhat linear curvature, though accumulative content almost reaches the total quantified Li content using the final digestion method. This underlines the fact that for solely Li, addition of HF to the digestion would benefit the total quantification as this linear behavior suggests an even higher extractability of greater 100 % when being normalized to the quantified total content employing the final digestion method. However, to further investigate this, more extractions have to be conducted as more data points are necessary.
C, Cl^- and $SO_4{}^{2-}$ also show a linear curvature. However, a certain flattening of the curvature is visible, suggesting a possible saturation after further extractions.
Na shows a clear saturation after the 3^{rd} extraction. This indicates that not all of the contained Na is mobile within the molding compound.
Mg, Ca and Lactate show a similar behavior where a clear flattening of the curvature can be seen in Figure 144, Figure 146 and Figure 149. This suggests, similar to C, that the mobile content may reach saturation after a couple more extraction, though experiments need to be conducted.
On the other hand, K shows a strong linear curvature, suggesting a low mobility within the molding compound MCF1. However, due to the overall low content of K within molding compound MCF1 it is difficult to draw conclusions. To further understand the extraction behavior of K, another molding compound with a higher K content should be investigated. Unfortunately, no sample type of delivered molding compound shows an increased mobile K content.
Mn shows a clear saturation of the curvature as it approaches an extractability of nearly 100 %.
Data for Sr suggests that after two extractions, no significant amount of Sr is further extractable. This results in a high mobility for the mobile Sr within the molding compound while this also shows that a maximum of 30 % of Sr may be mobile within the molding compound using water as leaching agent.
$NO_3{}^-$ shows a linear accumulative curve, suggesting that quantified mobile contents may really just result from the leaching out of the extraction vessel. To further investigate this, extractions in newly purchased vessels are necessary.

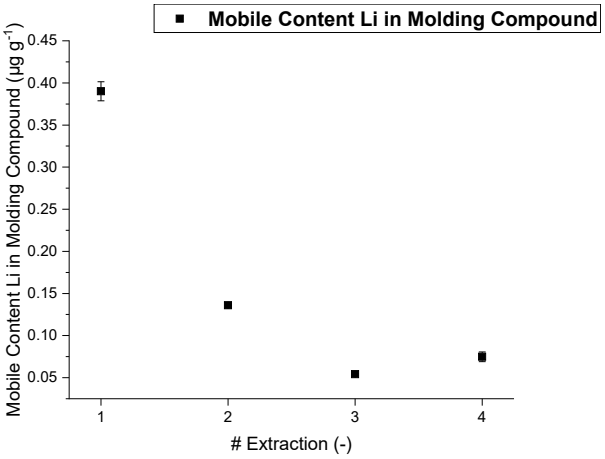

Figure 126: Extraction behavior of Li during 4 consecutive extractions of molding compound MCF1

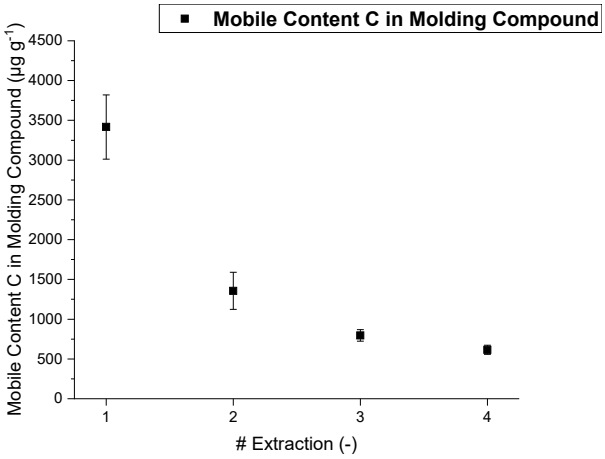

Figure 127: Extraction behavior of C during 4 consecutive extractions of molding compound MCF1

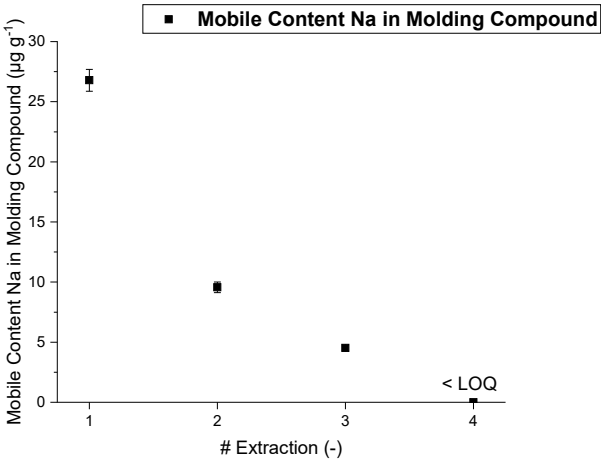

Figure 128: Extraction behavior of Na during 4 consecutive extractions of molding compound MCF1

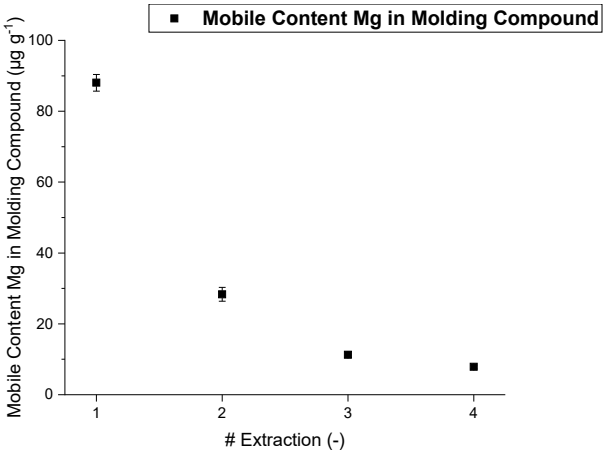

Figure 129: Extraction behavior of Mg during 4 consecutive extractions of molding compound MCF1

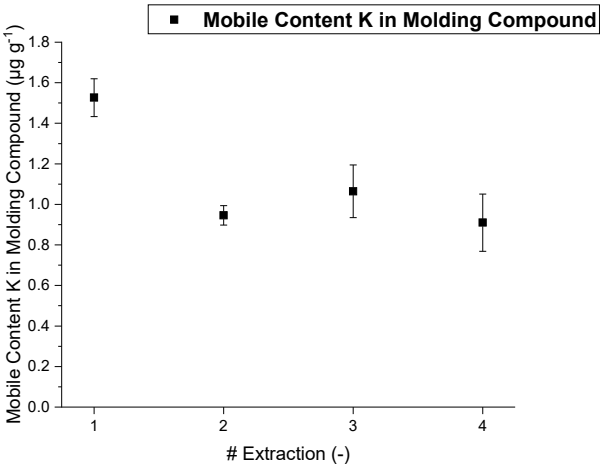

Figure 130: Extraction behavior of K during 4 consecutive extractions of molding compound MCF1

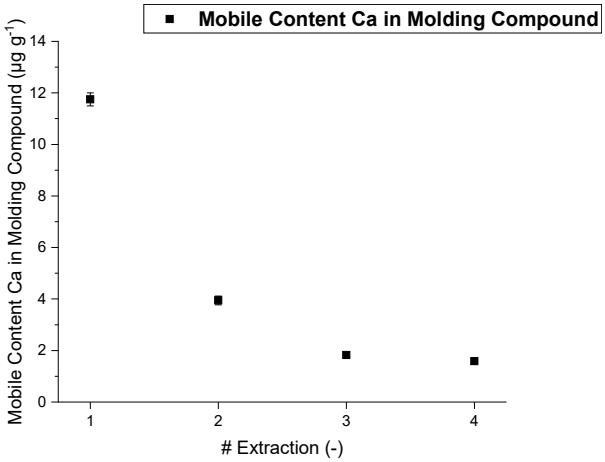

Figure 131: Extraction behavior of Ca during 4 consecutive extractions of molding compound MCF1

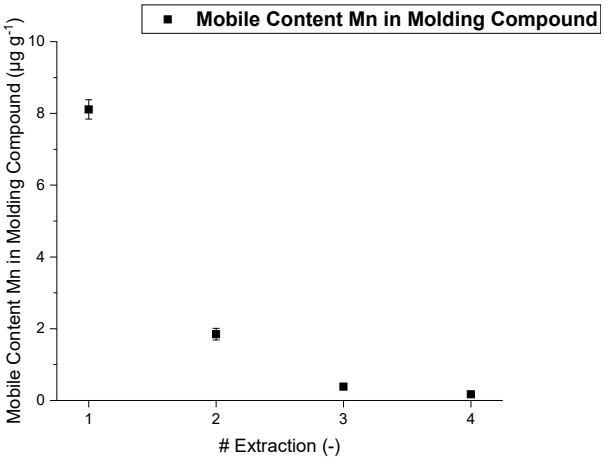

Figure 132: Extraction behavior of Mn during 4 consecutive extractions of molding compound MCF1

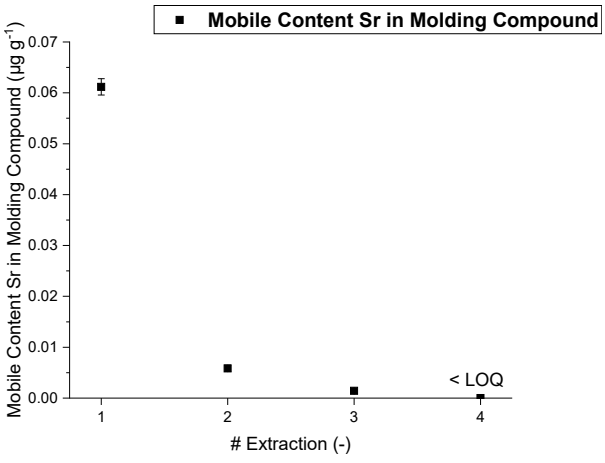

Figure 133: Extraction behavior of Sr during 4 consecutive extractions of molding compound MCF1

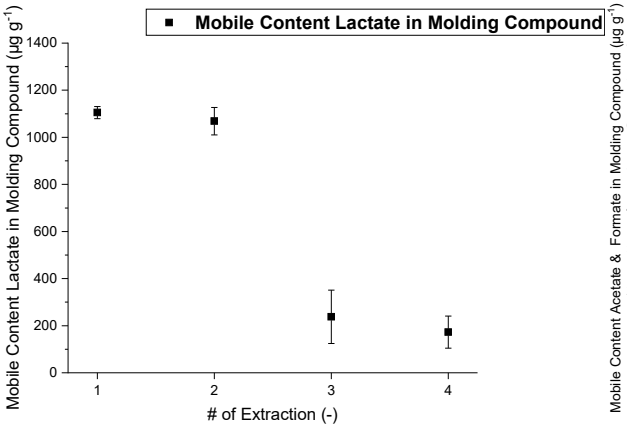

Figure 134: Extraction behavior of Lactate during 4 consecutive extractions of molding compound MCF1

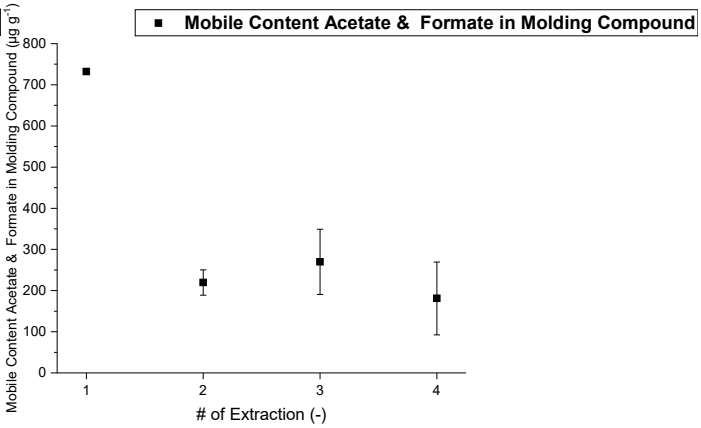

Figure 135: Extraction behavior of Acetate and Formate during 4 consecutive extractions of molding compound MCF1

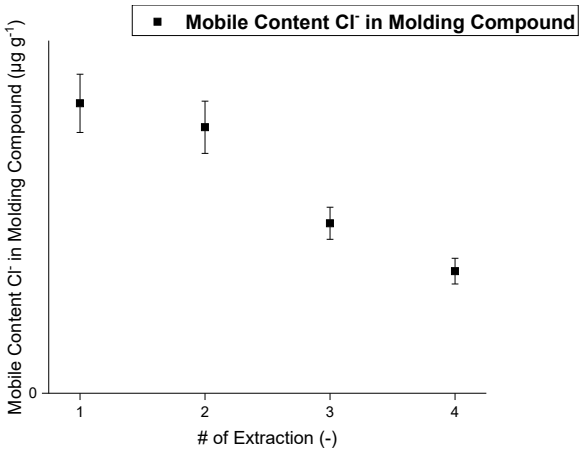

Figure 136: Extraction behavior of Cl^- during 4 consecutive extractions of molding compound MCF1

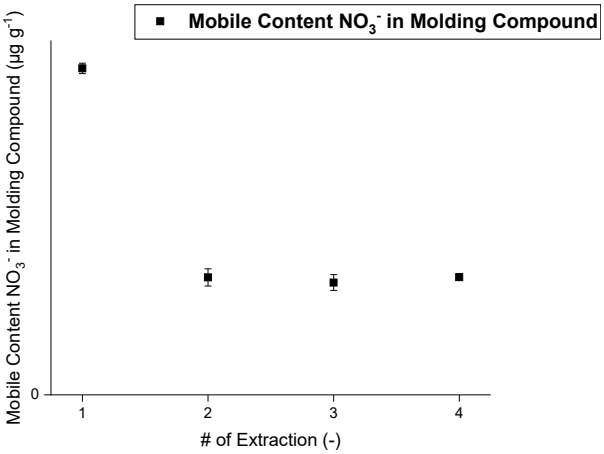

Figure 137: Extraction behavior of NO_3^- during 4 consecutive extractions of molding compound MCF1

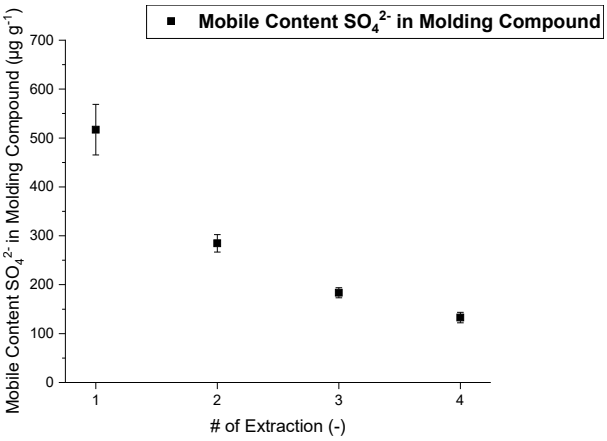

Figure 138: Extraction behavior of $SO_4{}^{2-}$ during 4 consecutive extractions of molding compound MCF1

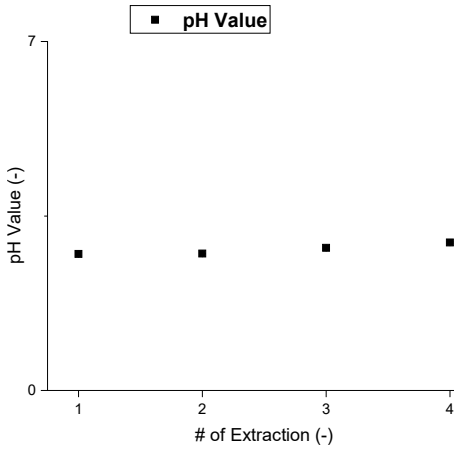

Figure 139: Course of the determined pH value during 4 consecutive extractions of molding compound MCF1

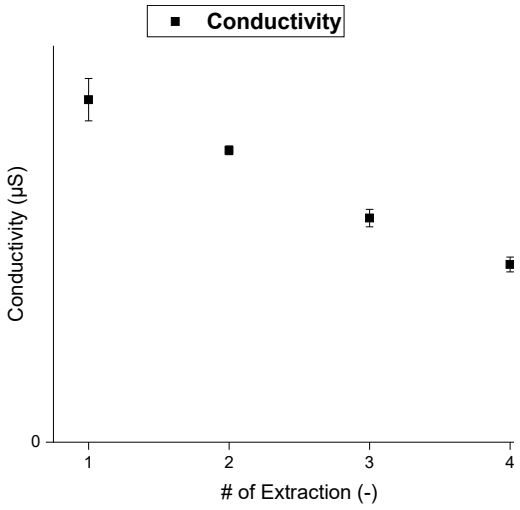

Figure 140: Course of the determined electric conductivity during 4 consecutive extractions of molding compound MCF1

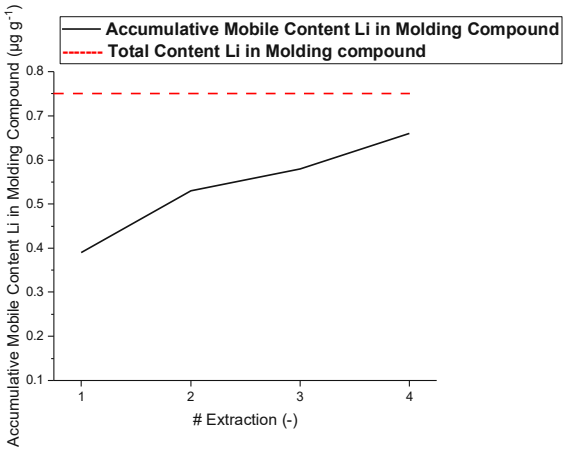

Figure 141: Accumulative extraction behavior of Li during 4 consecutive extractions of molding compound MCF1; the black curve represents the extraction behavior; the red line marks the quantified total content using the final extraction method

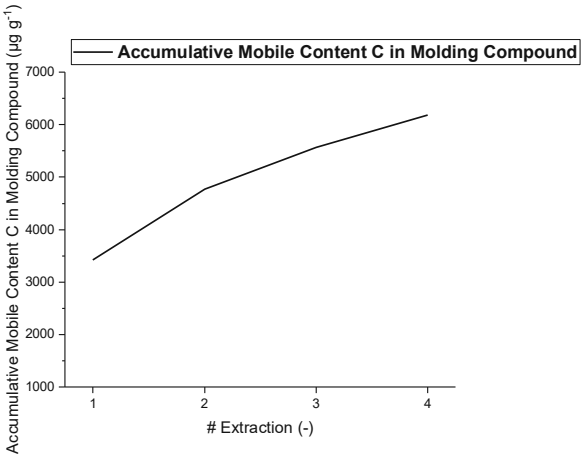

Figure 142: Accumulative extraction behavior of C during 4 consecutive extractions of molding compound MCF1

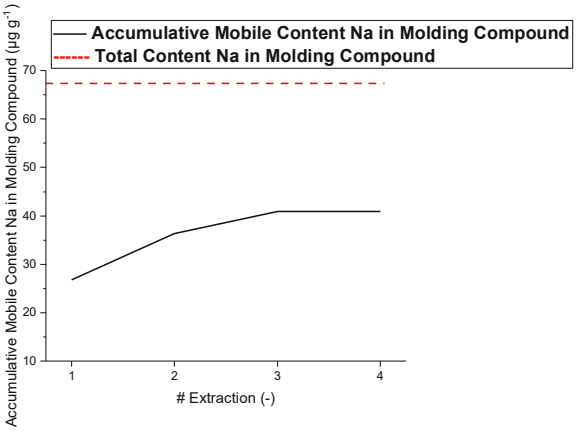

Figure 143: Accumulative extraction behavior of Na during 4 consecutive extractions of molding compound MCF1; the black curve represents the extraction behavior; the red line marks the quantified total content using the final extraction method

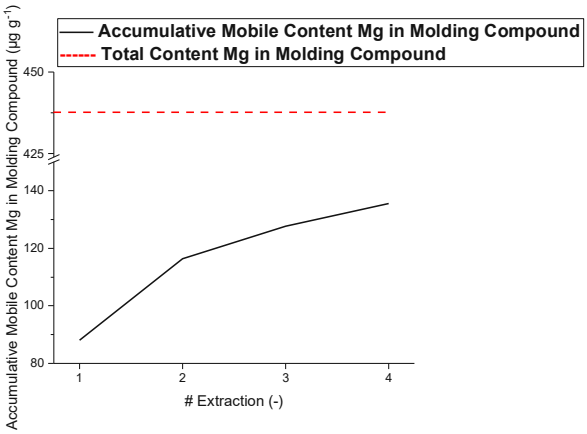

Figure 144: Accumulative extraction behavior of Mg during 4 consecutive extractions of molding compound MCF1; the black curve represents the extraction behavior; the red line marks the quantified total content using the final extraction method

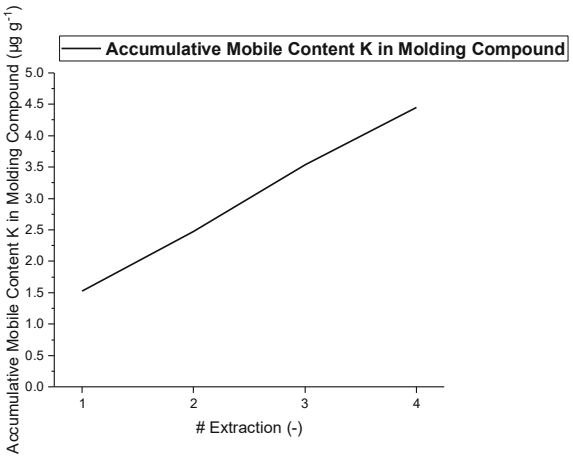

Figure 145: Accumulative extraction behavior of K during 4 consecutive extractions of molding compound MCF1

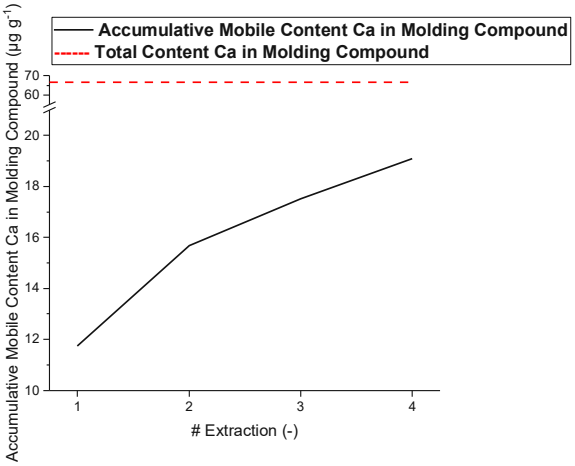

Figure 146: Accumulative extraction behavior of Ca during 4 consecutive extractions of molding compound MCF1; the black curve represents the extraction behavior; the red line marks the quantified total content using the final extraction method

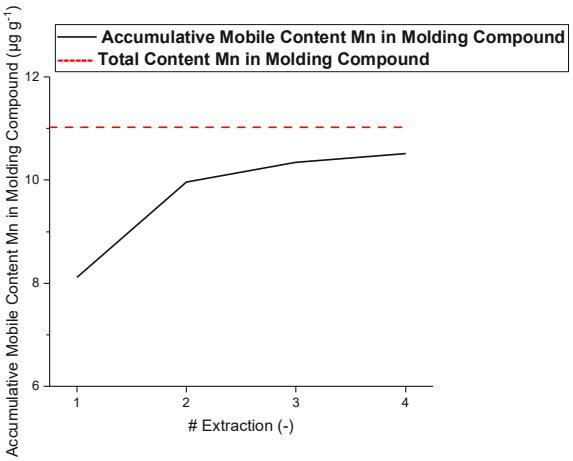

Figure 147: Accumulative extraction behavior of Mn during 4 consecutive extractions of molding compound MCF1; the black curve represents the extraction behavior; the red line marks the quantified total content using the final extraction method

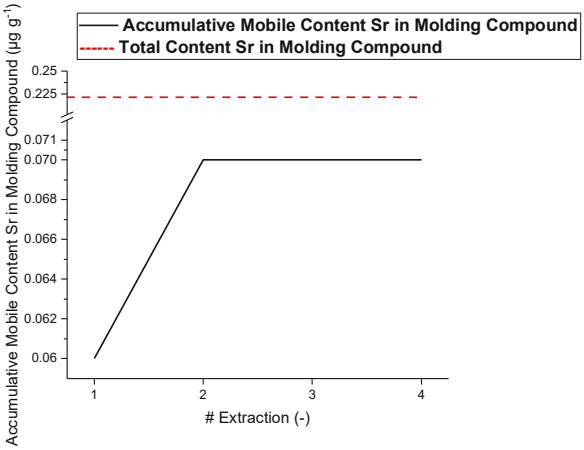

Figure 148: Accumulative extraction behavior of Sr during 4 consecutive extractions of molding compound MCF1; the black curve represents the extraction behavior; the red line marks the quantified total content using the final extraction method

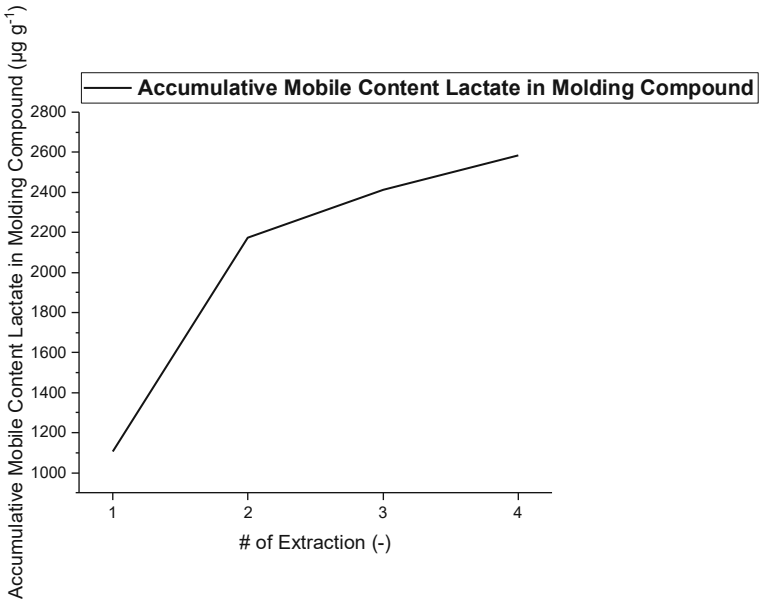

Figure 149: Accumulative extraction behavior of Lactate during 4 consecutive extractions of molding compound MCF1

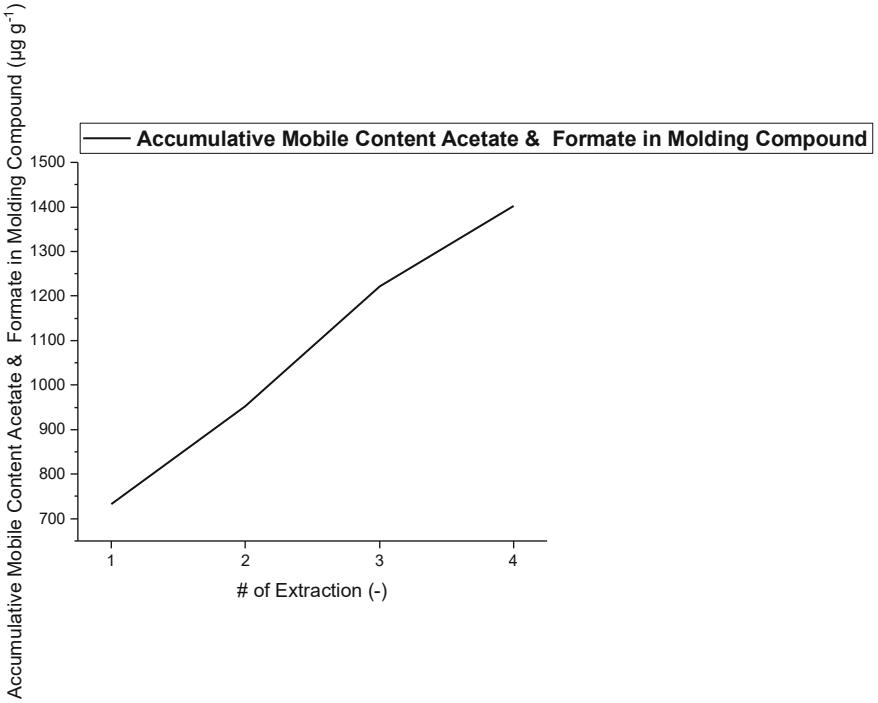

Figure 150: Accumulative extraction behavior of Lactate during 4 consecutive extractions of molding compound MCF1

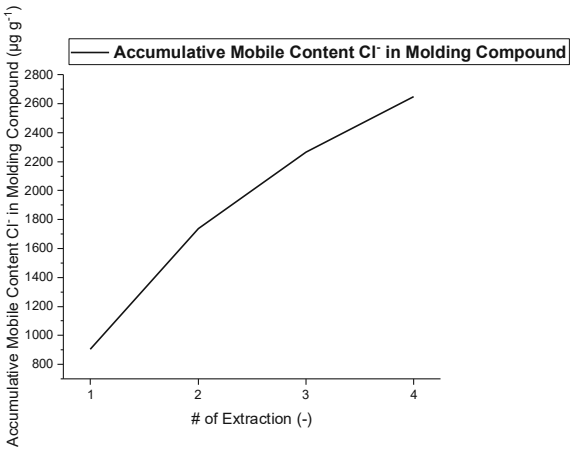

Figure 151: Accumulative extraction behavior of Cl^- during 4 consecutive extractions of molding compound MCF1

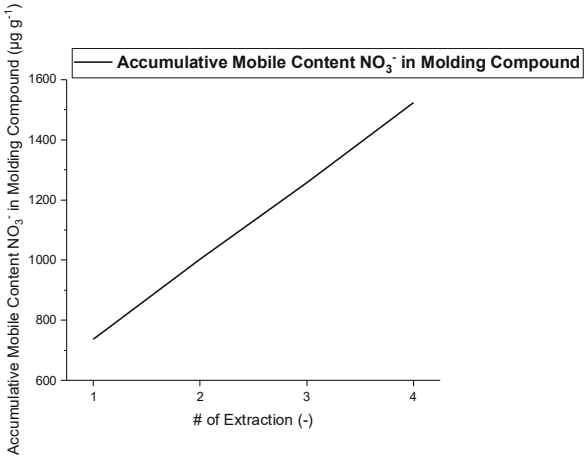

Figure 152: Accumulative extraction behavior of NO_3^- during 4 consecutive extractions of molding compound MCF1

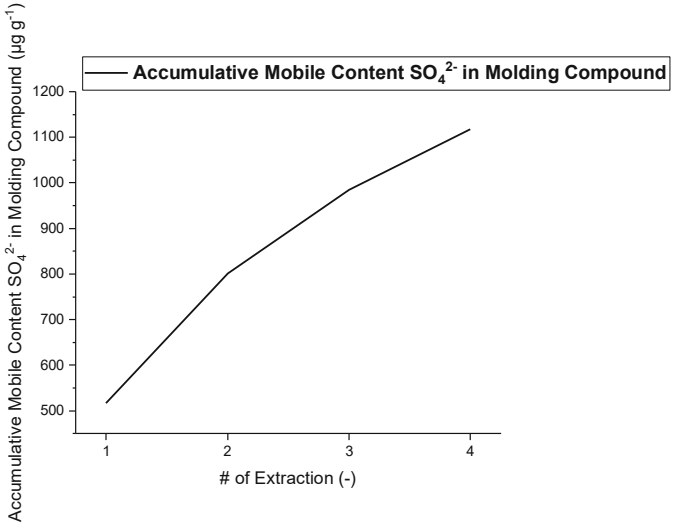

Figure 153: Accumulative extraction behavior of SO_4^{2-} during 4 consecutive extractions of molding compound MCF1

5.2.2.4 Influence of particle size

The standard SEMI G29 foresees a particle size distribution of 150 μm to 400 μm for the milled molding compound. For major parts of this thesis, the aspect of size distribution of the milled powder was ignored. This can be seen in Figure 154. In order to have a clearer picture of the actual size distribution, it was measured for the milled powder of molding compound MCF1 as mentioned in subsection 4.1. As extraction efficiency not only depends on the temperature and time but also the wetability of the sample material and its surface area, the particle size is expected to have an influence on the extraction behavior for molding compound as well. As for the experiment, the milled powder of MCF1 was sieved into 2 fractions, smaller and greater 180 μm. These powders were then extracted at 225 °C with 90 min hold time at maximum temperature. As the size distribution in Figure 154 shows that 90 % of all particles are 395 μm of size or smaller, it was enough for the powder so be split on the lower end of the classification according to SEMI G29. Generally, the powder did not fulfill the criteria of SEMI G29 as 50 % of all particles are already 101 μm in size or smaller. Leaching behavior of individual elements can be seen in Figure 155 to Figure 169.

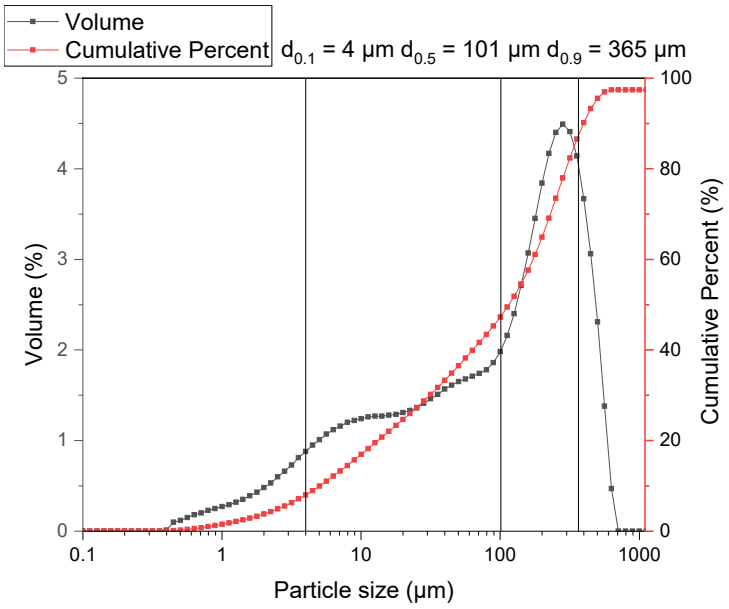

Figure 154: Measured size distribution of molding compound MCF1 with the volume curve (black) and the cumulative percent curve (red)

It was expected for the smaller particle size fraction (< 180 μm) to show a higher leachable content as compared to the greater particle size fraction. This expectation was met for elements Li, C, Na, Mg, K, Ca and Mn. For C the difference was the smallest with a higher extractability factor in the smaller particle size fraction of 1.3. Elements Li, Na, K and Ca showed an increased extractability of a factor of 2, Mg showed a factor of 3 and Mn even showed the highest increase with a factor of 5. Sr showed similar extractability in both size fractions which suggests a high mobility within the molding compound MCF1. Lactate showed a reverse trend, with higher mobile contents within the greater particle size fraction. Ions Acetate, Formate, NO_3^- and Cl^- showed a similar mobile content in both size fractions. SO_4^{2-} also showed an increased mobile content in the smaller size fraction with a factor of increase of 1.5. The pH value decreases with smaller particle size and conductivity increases with the smaller size fraction which was expected as of the higher elemental content within the smaller particle size fraction in general.

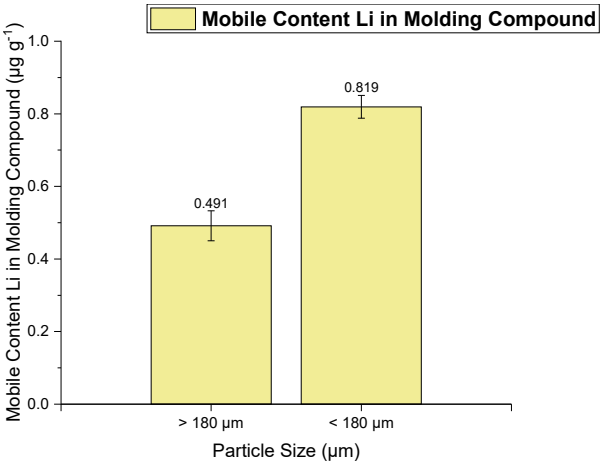

Figure 155: Comparison of the extraction behavior of Li in two different size fractions (>180 μm and <180 μm) of molding compound powder MCF1 after sieving

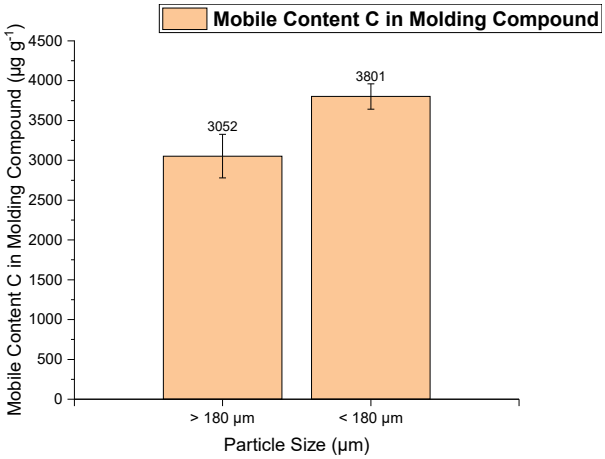

Figure 156: Comparison of the extraction behavior of C in two different size fractions (>180 μm and <180 μm) of molding compound powder MCF1 after sieving

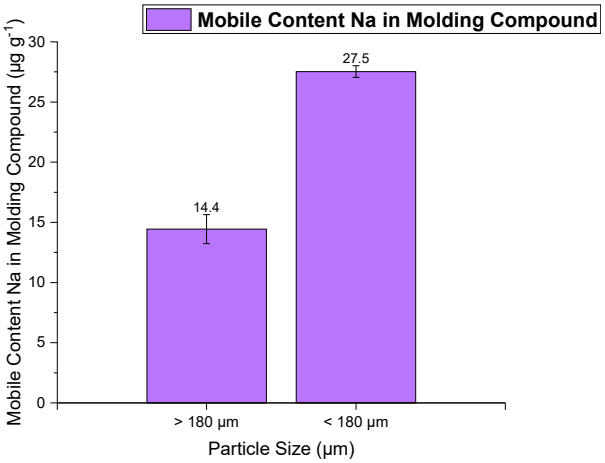

Figure 157: Comparison of the extraction behavior of Na in two different size fractions (>180 μm and <180 μm) of molding compound powder MCF1 after sieving

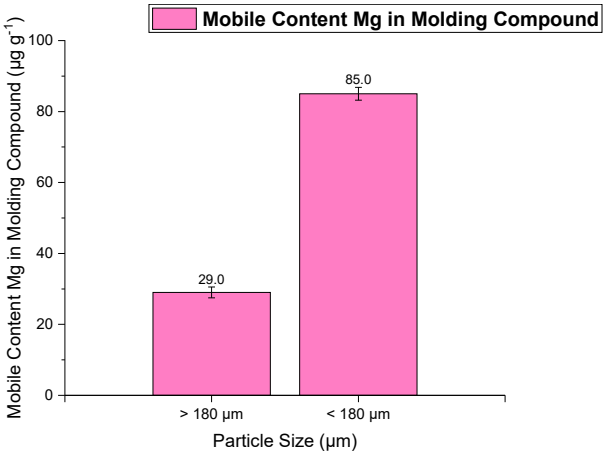

Figure 158: Comparison of the extraction behavior of Mg in two different size fractions (>180 μm and <180 μm) of molding compound powder MCF1 after sieving

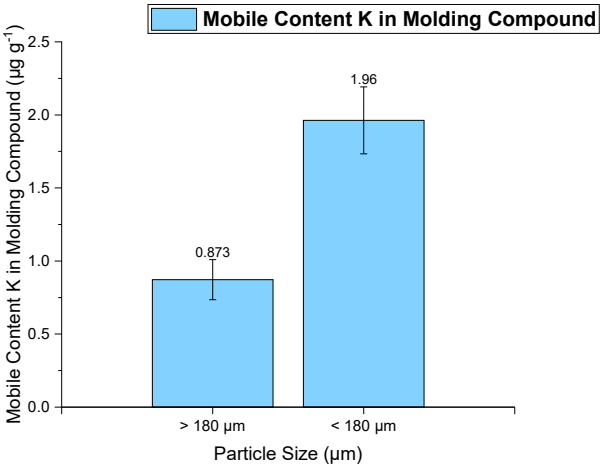

Figure 159: Comparison of the extraction behavior of K in two different size fractions (>180 μm and <180 μm) of molding compound powder MCF1 after sieving

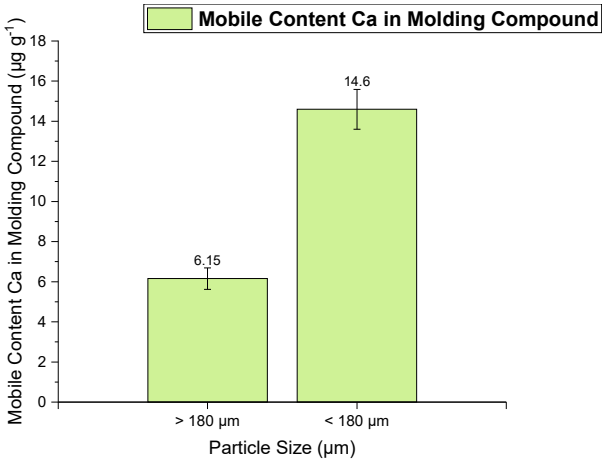

Figure 160: Comparison of the extraction behavior of Ca in two different size fractions (>180 μm and <180 μm) of molding compound powder MCF1 after sieving

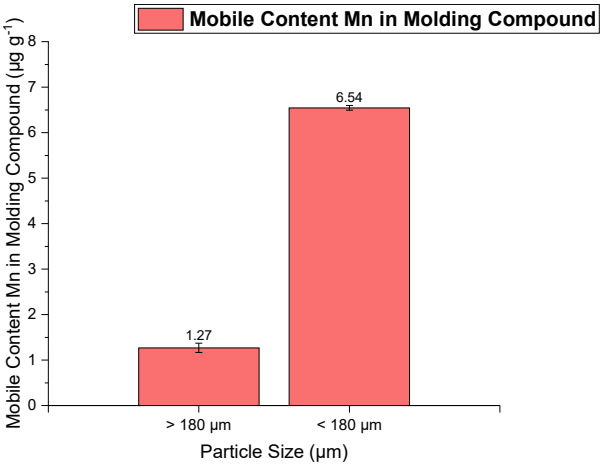

Figure 161: Comparison of the extraction behavior of Mn in two different size fractions (>180 μm and <180 μm) of molding compound powder MCF1 after sieving

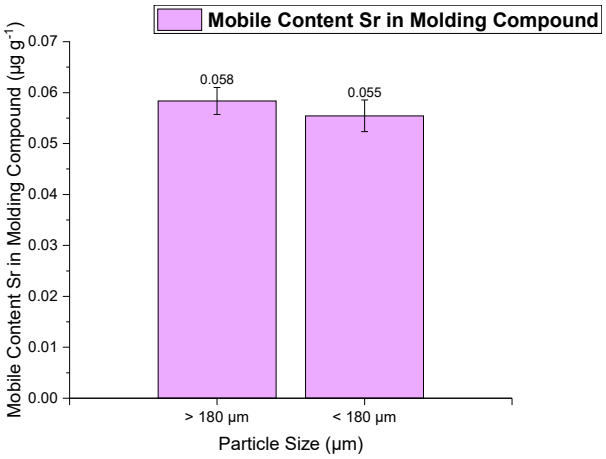

Figure 162: Comparison of the extraction behavior of Sr in two different size fractions (>180 μm and <180 μm) of molding compound powder MCF1 after sieving

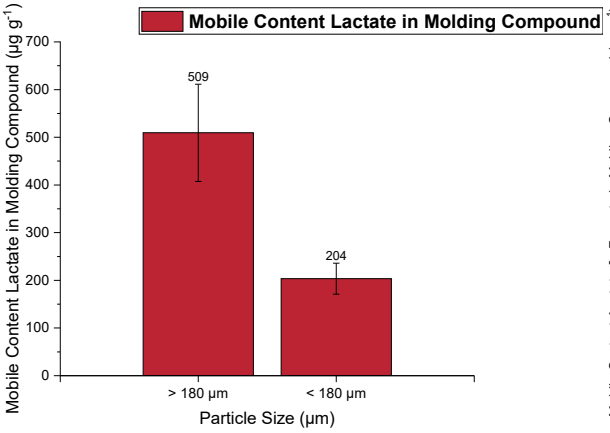

Figure 163: Comparison of the extraction behavior of Lactate in two different size fractions (>180 μm and <180 μm) of molding compound powder MCF1 after sieving

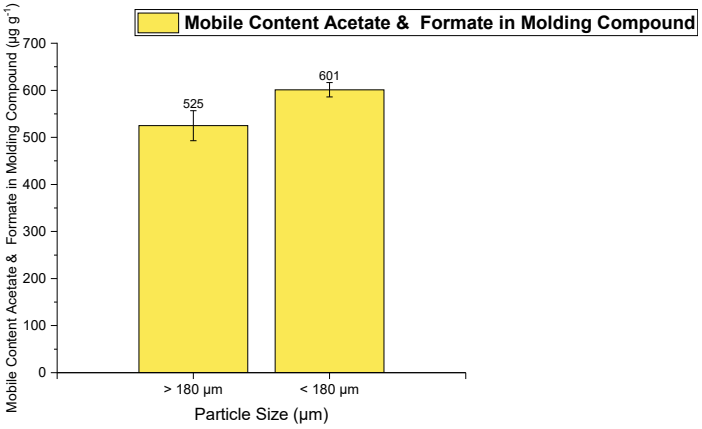

Figure 164: Comparison of the extraction behavior of Acetate and Formate in two different size fractions (>180 μm and <180 μm) of molding compound powder MCF1 after sieving

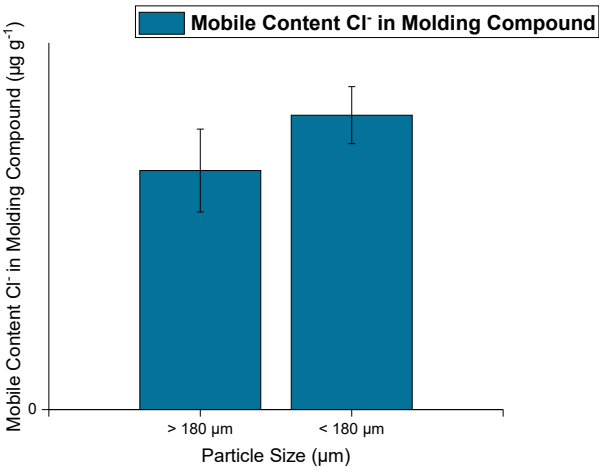

Figure 165: Comparison of the extraction behavior of Cl^- in two different size fractions (>180 μm and <180 μm) of molding compound powder MCF1 after sieving

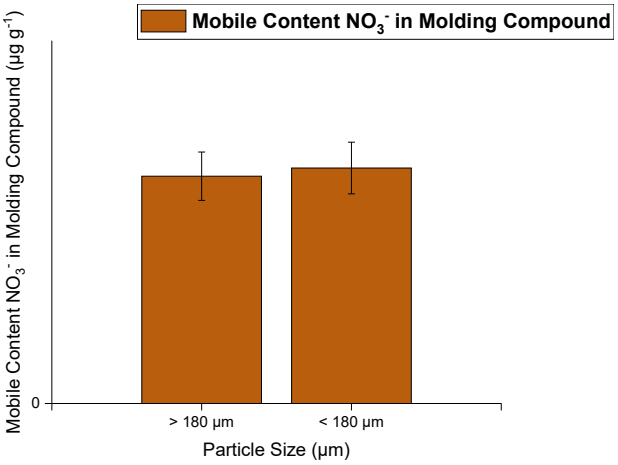

Figure 166: Comparison of the extraction behavior of NO_3^- in two different size fractions (>180 μm and <180 μm) of molding compound powder MCF1 after sieving

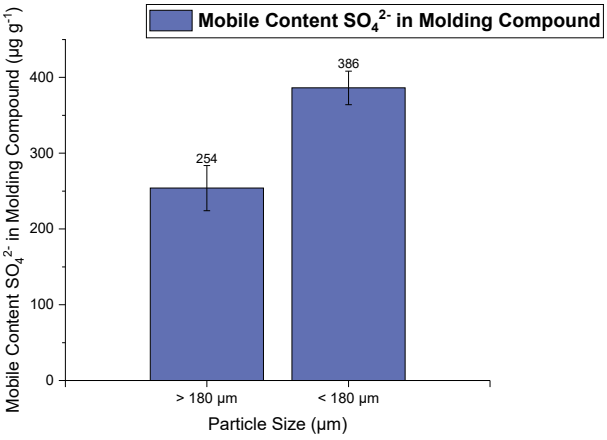

Figure 167: Comparison of the extraction behavior of SO_4^{2-} in two different size fractions (>180 μm and <180 μm) of molding compound powder MCF1 after sieving

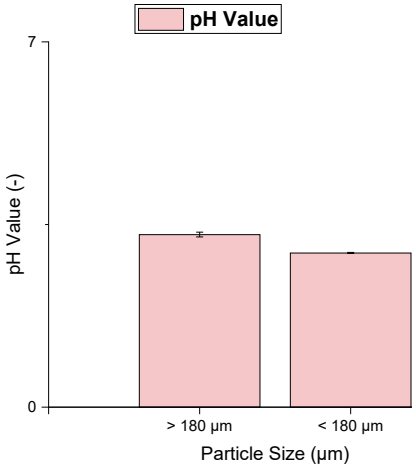

Figure 168: Comparison of the determined pH value in the extracts of two different size fractions (>180 μm and <180 μm) of molding compound powder MCF1 after sieving

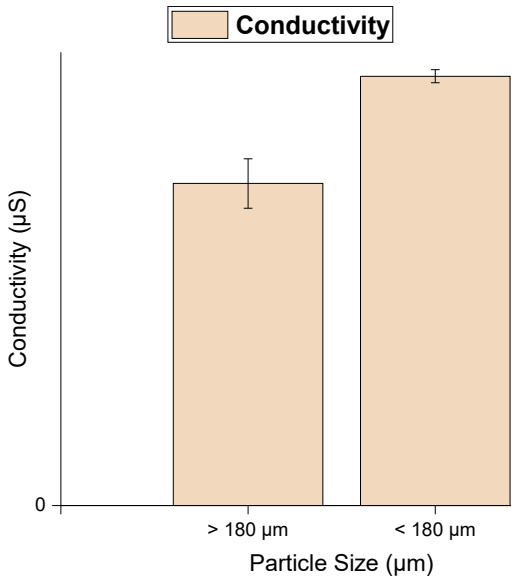

Figure 169: Comparison of the determined electric conductivity in the extracts of two different size fractions (>180 μm and <180 μm) of molding compound powder MCF1 after sieving

5.2.3 Final extraction method

After the evaluation of the influence of time and temperature as well as testing the completeness of extraction, final parameters were set in order to investigate the extraction behavior of molding compound samples MCA to MCF (molded). For the extraction, 2 g of molding compound powder were weighed into the HVT Teflon vessel to 0.1 mg accuracy using an analytical balance.To this, 20 g of ultrapure water were added. The closed HVT Teflon vessels were put into the microwave and the extraction was started. Per extraction round, 4 replicates were produced to account for reproducibility. For the temperature program, the temperature was ramped up to 200 °C in 15 min and was then held constant at 200 °C for 60 min. Afterwards the temperature was cooled to 60 °C which took additional 20 min. The employed temperature program can be seen in Figure 170. After the extraction, each yielded extract was put into a 50 mL centrifuge tube and centrifuged for 15 min at 12 000 xg. Afterwards, 14 mL were transferred into a 15 mL centrifuge tube and centrifuged for 30 min at 17 000 xg. For a final centrifugation step, 13 mL were transferred into a fresh 15 mL centrifuge tube and were centrifuged for 45 min at 18 000 xg. After that, the extracts were aliquoted for the IC, pH and conductivity measurement (9 mL) and the ICP-OES measurement (3 mL).

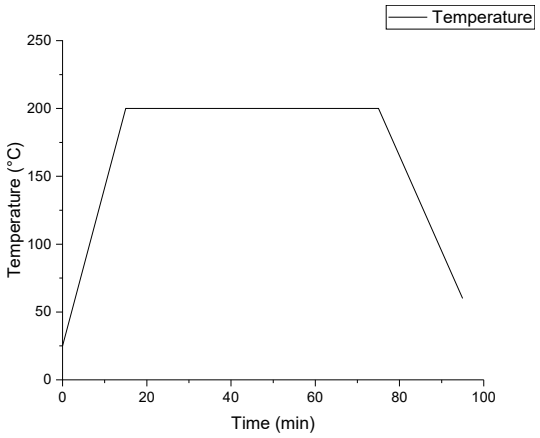

Figure 170: Applied temperature program for the finalized extraction method with a 15 min to 200 °C and a hold time of 60 min with a cooling off period of 20 min to 60 °C

5.2.4 Extraction results for molded samples MCA to MCF using the final extraction method

Only the molded molding compound is finally employed as a housing material. Thus, only the ion mobility/ extractability within the molded molding compound samples was of interest. In order to characterize and compare the different molded molding compounds, samples were extracted using the final extraction method. Again, not only the total extractable amount (Mobile Content) is of interest but also the relative extractability (Mobile Fraction). Equation 20 shows how the mobile fraction can be calculated.

As described in paragraph 5.2.1.2, the mobile fraction for elements C and K cannot be calculated due to the formation of $^{37}Cl^{1}H^{1}H^{+}$ and $^{38}Ar^{1}H^{+}$ in the plasma.

After parameter optimization, all results were considered to opt for a final extraction method. Higher extraction temperatures proved to be favorable for many analytes. However, for Lactate, temperatures above 200 °C showed a loss of analyte due to further degradation processes. Because of this, 200 °C was chosen as a final extraction temperature. As for the extraction time, analytes showed that higher extraction temperatures account for shorter extraction times. As one of the goals for the final method was easy laboratory applicability, an extraction time (hold time at maximum temperature) of 60 min was chosen as this results in an overall duration of 90 min for one extraction run, making it possible to perform up to 4 extraction runs in 8 h of work. After the final parameters were set, all molded samples MCA - MCF were extracted using the latter method. Results can be seen in Figure 171 to Figure 185 for total mobile content and in Figure 186 to Figure 191 for the mobile fraction. The results are plotted in total and relative mobile content as it is not only of interest how much was leached in total during the extraction but also how this mobile content relates to the total elemental content determined using acid digestion.
Comparing the different results for Li in Figure 171 and Figure 186, it shows that Li in all molding compounds shows a similar mobile fraction, thus making the mobile content solely depended on the total Li content within the molding compound. Though this cannot be extrapolated to other samples, it could be of interest that throughout at least 6 different samples, the mobile fraction stays comparable for Li, as no other elements showed a similar behavior.
Comparing the water soluble carbon content in Figure 172, the average carbon content lays around 1000 $\mu g\,g^{-1}$ for molding compounds MCA - MCE with only MCF showing double that amount. The water soluble carbon content comes from either water soluble additives of organic nature or degradation products of the polymer at higher temperatures such as Lactate, Acetate and Formate.
Though Na could be quantified in all molding compounds using acid digestion, the extractability draws a different picture, as Na could only be detected in the extracts of samples MCB, MCD and MCF, though MCD and MCF showed the highest Na contents of the molding compounds. However, MCB showed a similar Na content as MCA, MCC and MCE (Figure 52) showing that a certain total elemental content cannot directly be correlated to overall extractability. Com-

paring mobile fractions in Figure 187, samples MCB and MCF showed a similar mobile fraction for Na as compared to MCD which showed a Na extrability of >60 %.
Mg also showed vastly different results for all samples in Figure 174 and Figure 188. Samples MCB, MCC and MCF showed the highest mobile contents in a range of 30 $\mu g\,g^{-1}$ to 50 $\mu g\,g^{-1}$ as compared to its mobile fraction where samples MCA, MCC and MCE showed the highest extractability for Mg.
Mobile content of K within the different samples stayed within a similar range. However, ion mobility cannot be compared as the total content of K could not be quantified due to strong isobaric interference as for the addition of HCl to the digestion.
Comparing the results for Ca in Figure 176 and Figure 189, sample MCD showed the lowest mobile content as well as the lowest mobile fraction for Ca. For sample MCF, the mobile fraction of 121 % strikes as odd, as the mobile fraction should always be 100 % or below. This shows a good example whereas due to adsorption processes there is a strong loss of analyte in solution after the digestion, thus a mobile fraction above theoretical limits is calculated. As for the other samples MCA, MCB and MCC, these ranged in a similar mobile content as well as mobile fraction.
Mn showed a vastly different mobile content within the molding compound samples as well as different mobile fractions (Figure 177 and Figure 190). This is important to mention, as one would expect Mn to show a similar mobile fraction for all samples if the additional Mn in the molded samples actually came from abrasions of the steel vessel during sample preparation, as it was expected of the steel particles to also leach ions during extraction.These different mobile fractions suggest, though sample were contaminated with steel particles during sample preparation, these particles seem to not influence the extraction results.
Comparing Sr results in Figure 178 and Figure 191, Sr showed only low mobility within molding compounds MCA - MCE with mobile fractions below 20 % with MCD showing even a mobile content <LOQ. MCF showed the highest total and mobile content as well as a great mobile fraction >80 %.
Comparing the different mobile Lactate contents in Figure 179, these lay in a similar range for samples MCB - MCE. MCA showed the highest mobile content and MCF showed the lowest mobile content for Lactate. Acetate and Formate (Figure 180) showed a similar range for samples MCA - MCE with MCF having the highest mobile content of Acetate and Formate. As for Cl^- and $NO_3{}^-$ (Figure 181 and Figure 182), Cl^- showed higher mobile contents for samples MCA, MCD and MCF and similar lower content for samples MCB, MCC and MCE whereas in comparison, $NO_3{}^-$ showed similar mobile contents for all samples. However, whether the difference in mobile content com from the sample materials or a inconsistent leaching behavior out of the Teflon vessels remains unclear. $SO_4{}^{2-}$ showed a broad range for its mobile content within the samples with lower mobile contents for samples MCA - MCD with MCD having a mobile content <LOQ. Sample MCF shows the overall highest mobile content of $SO_4{}^{2-}$ of all samples analyzed. The pH value (Figure 184) also varied, though samples MCA, MCC, MCE and MCF showed similar pH values and also showed higher electric conductivity (Figure 185). Samples with higher pH values (MCB and MCD) showed lower electric conductivity.

Final extraction of molded molding compounds: mobile content

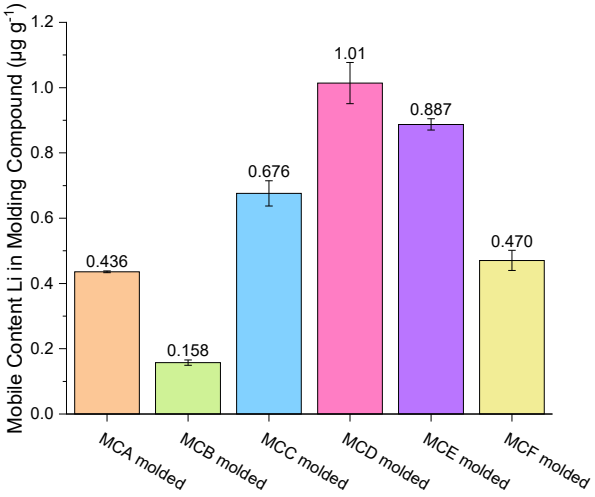

Figure 171: Results for the quantified mobile content of Li within molded molding compounds MCA (orange), MCB (green), MCC (blue), MCD (pink), MCE (purple) and MCF (yellow) using the final extraction method

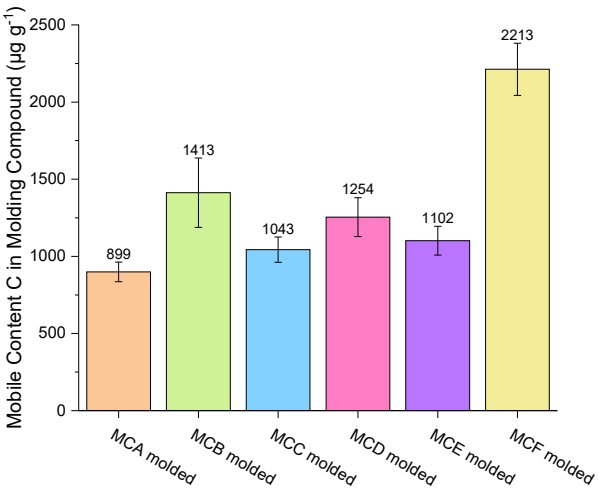

Figure 172: Results for the quantified water soluble content of C within molded molding compounds MCA (orange), MCB (green), MCC (blue), MCD (pink), MCE (purple) and MCF (yellow) using the final extraction method

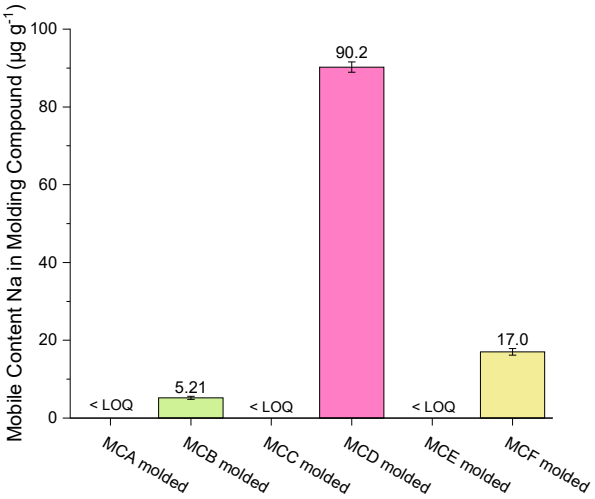

Figure 173: Results for the quantified mobile content of Na within molded molding compounds MCA (orange), MCB (green), MCC (blue), MCD (pink), MCE (purple) and MCF (yellow) using the final extraction method

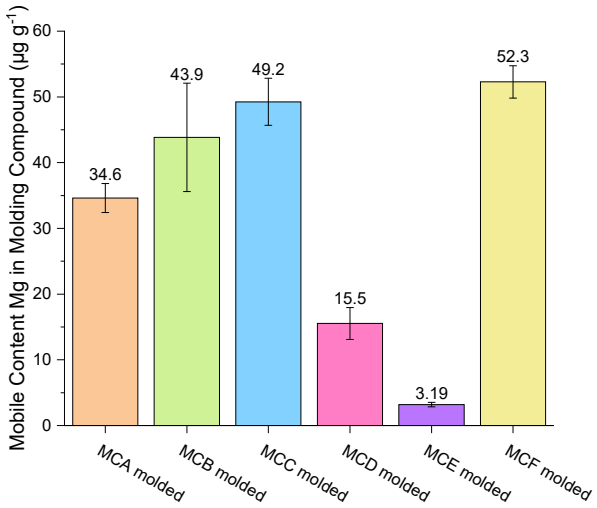

Figure 174: Results for the quantified mobile content of Mg within molded molding compounds MCA (orange), MCB (green), MCC (blue), MCD (pink), MCE (purple) and MCF (yellow) using the final extraction method

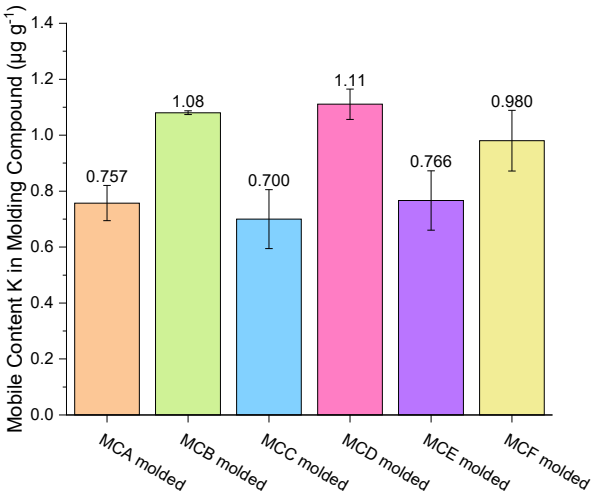

Figure 175: Results for the quantified mobile content of K within molded molding compounds MCA (orange), MCB (green), MCC (blue), MCD (pink), MCE (purple) and MCF (yellow) using the final extraction method

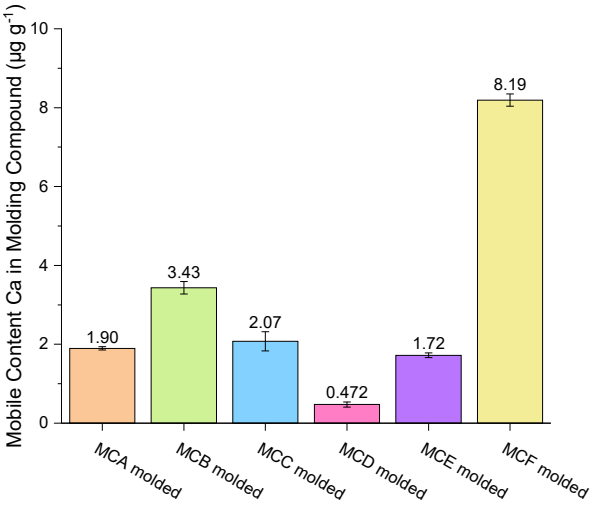

Figure 176: Results for the quantified mobile content of Ca within molded molding compounds MCA (orange), MCB (green), MCC (blue), MCD (pink), MCE (purple) and MCF (yellow) using the final extraction method

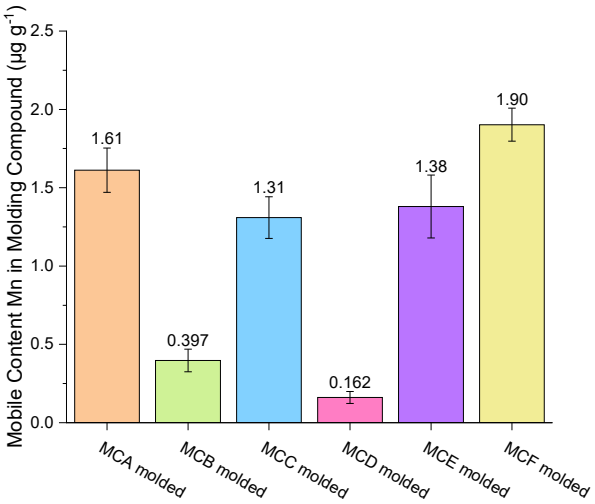

Figure 177: Results for the quantified mobile content of Mn within molded molding compounds MCA (orange), MCB (green), MCC (blue), MCD (pink), MCE (purple) and MCF (yellow) using the final extraction method

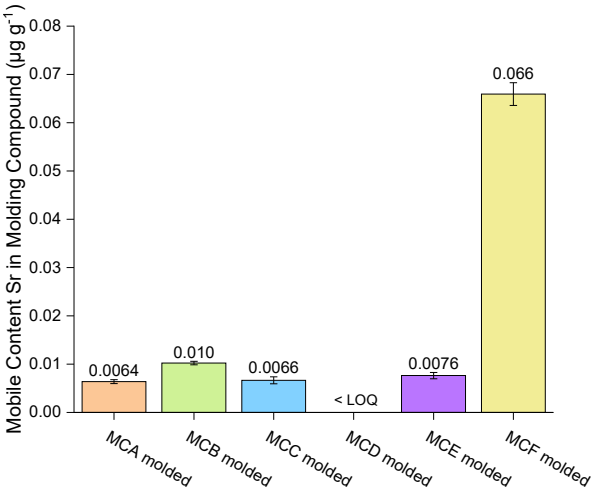

Figure 178: Results for the quantified mobile content of Sr within molded molding compounds MCA (orange), MCB (green), MCC (blue), MCD (pink), MCE (purple) and MCF (yellow) using the final extraction method

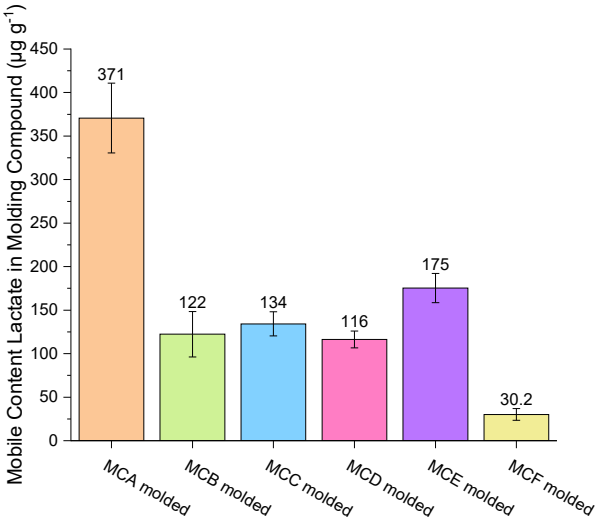

Figure 179: Results for the quantified mobile content of Lactate within molded molding compounds MCA (orange), MCB (green), MCC (blue), MCD (pink), MCE (purple) and MCF (yellow) using the final extraction method

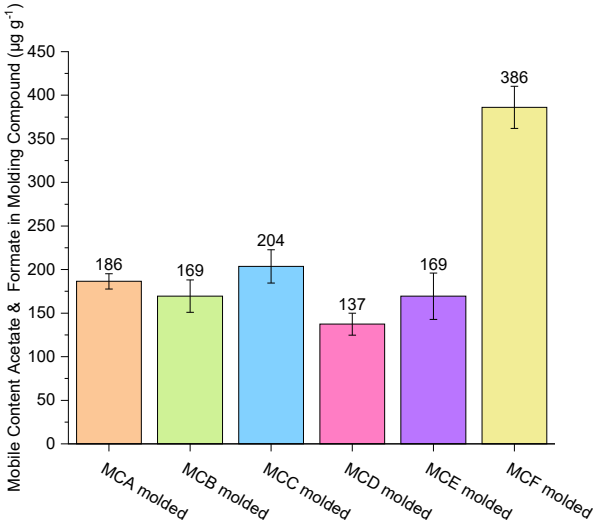

Figure 180: Results for the quantified mobile content of Acetate and Formate within molded molding compounds MCA (orange), MCB (green), MCC (blue), MCD (pink), MCE (purple) and MCF (yellow) using the final extraction method

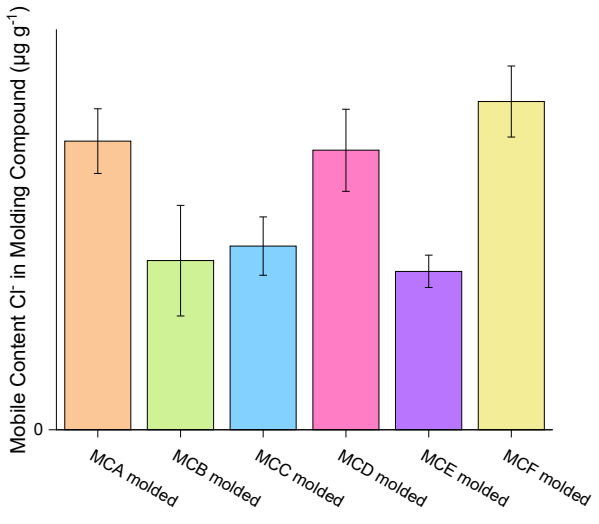

Figure 181: Results for the quantified mobile content of Cl^- within molded molding compounds MCA (orange), MCB (green), MCC (blue), MCD (pink), MCE (purple) and MCF (yellow) using the final extraction method

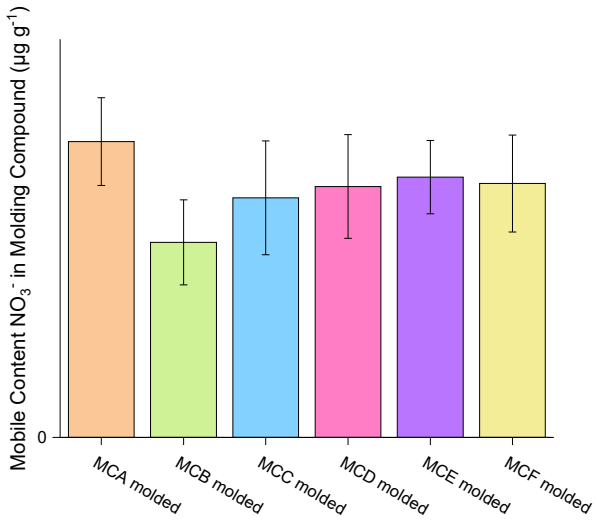

Figure 182: Results for the quantified mobile content of NO_3^- within molded molding compounds MCA (orange), MCB (green), MCC (blue), MCD (pink), MCE (purple) and MCF (yellow) using the final extraction method

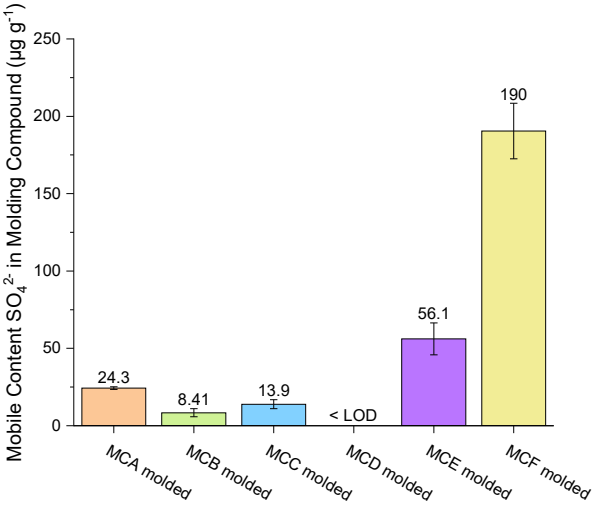

Figure 183: Results for the quantified mobile content of SO_4^{2-} within molded molding compounds MCA (orange), MCB (green), MCC (blue), MCD (pink), MCE (purple) and MCF (yellow) using the final extraction method

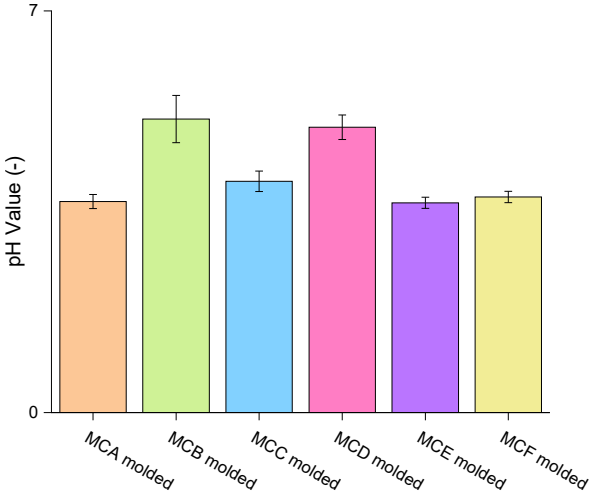

Figure 184: Results for the determined pH value in extracts of molded molding compounds MCA (orange), MCB (green), MCC (blue), MCD (pink), MCE (purple) and MCF (yellow) using the final extraction method

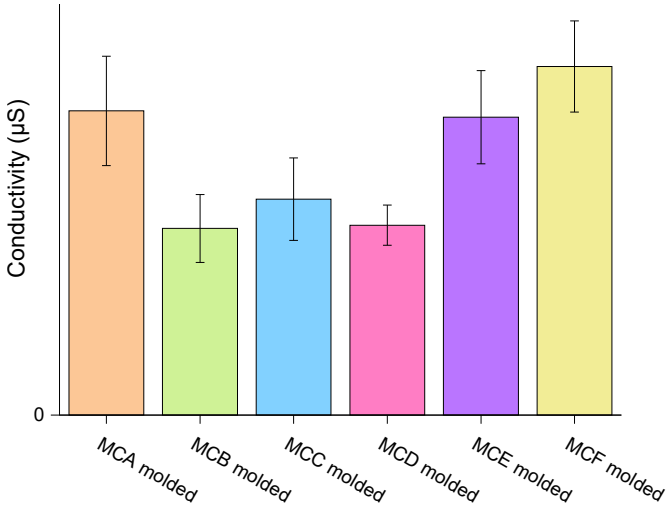

Figure 185: Results for the determined electric conductivity in extracts of molded molding compounds MCA (orange), MCB (green), MCC (blue), MCD (pink), MCE (purple) and MCF (yellow) using the final extraction method

Final extraction of molded molding compounds: mobile fraction

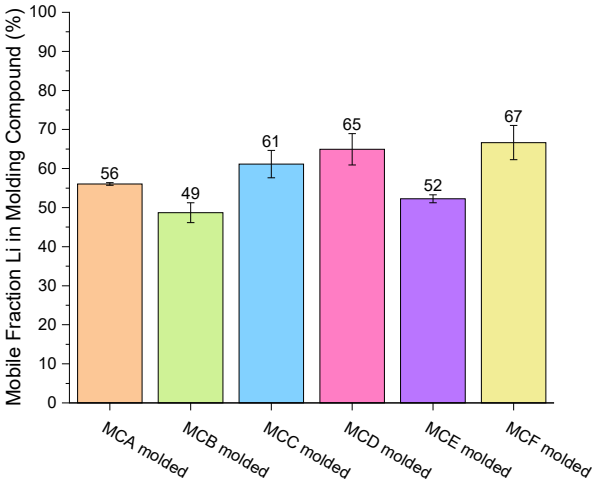

Figure 186: Results for the quantified mobile fraction of Li within molded molding compounds MCA (orange), MCB (green), MCC (blue), MCD (pink), MCE (purple) and MCF (yellow) using the final extraction method

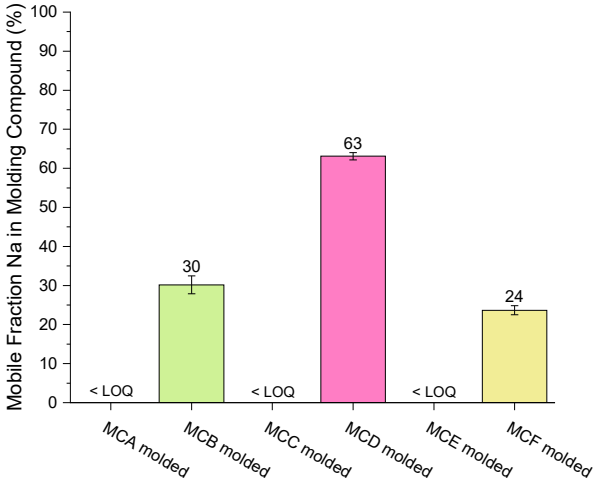

Figure 187: Results for the quantified mobile fraction of Na within molded molding compounds MCA (orange), MCB (green), MCC (blue), MCD (pink), MCE (purple) and MCF (yellow) using the final extraction method

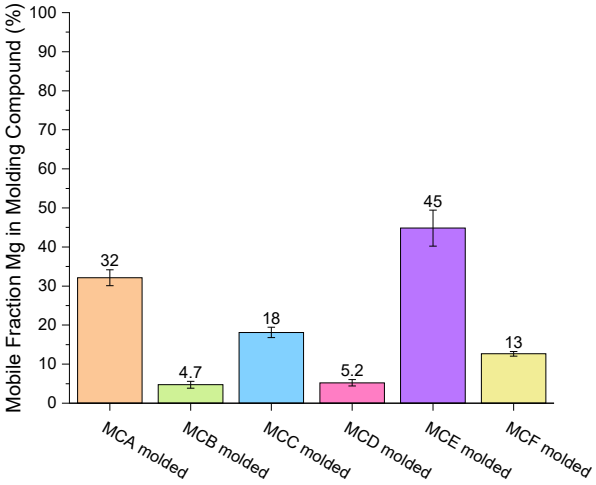

Figure 188: Results for the quantified mobile fraction of Mg within molded molding compounds MCA (orange), MCB (green), MCC (blue), MCD (pink), MCE (purple) and MCF (yellow) using the final extraction method

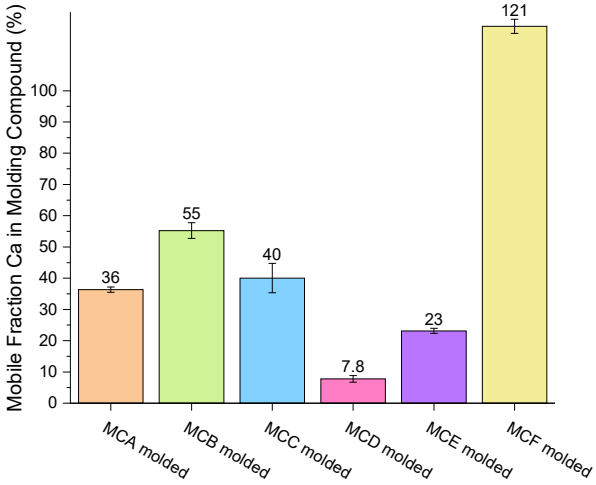

Figure 189: Results for the quantified mobile fraction of Ca within molded molding compounds MCA (orange), MCB (green), MCC (blue), MCD (pink), MCE (purple) and MCF (yellow) using the final extraction method

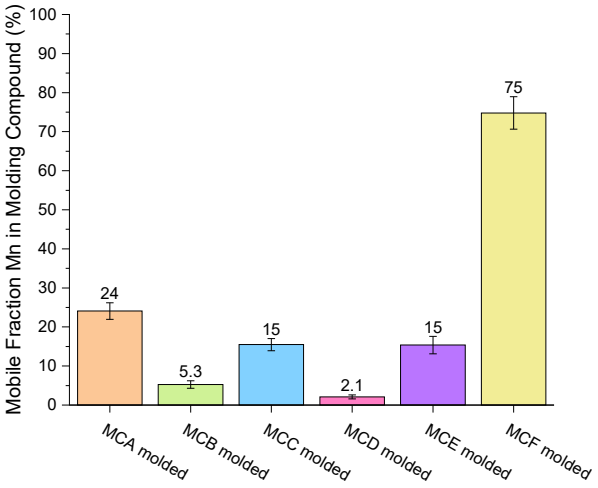

Figure 190: Results for the quantified mobile fraction of Mn within molded molding compounds MCA (orange), MCB (green), MCC (blue), MCD (pink), MCE (purple) and MCF (yellow) using the final extraction method

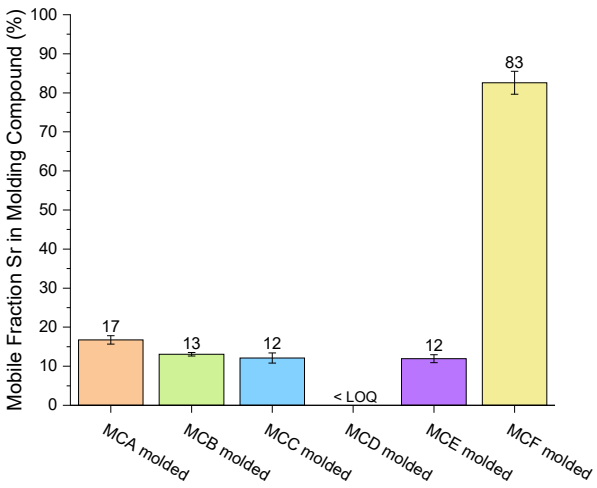

Figure 191: Results for the quantified mobile fraction of Sr within molded molding compounds MCA (orange), MCB (green), MCC (blue), MCD (pink), MCE (purple) and MCF (yellow) using the final extraction method

6 Conclusion

The goal of this thesis was to establish a total digestion method for the delivered sample material, epoxy resin based molding compound with embedded silica particles, as well as the further investigation on the leaching behavior of mobile ions within the molding compound using aqueous extraction at elevated temperatures and the final development of an extraction method. Additionally, results were to be compared to the industrial standard SEMI G29 in order to evaluate the developed extraction method. As the thesis can be split into two parts, the discussion will also split into digestion and extraction.

6.1 Digestion of molding compound

To summarize, during this thesis it was possible to show the strong influence of HF addition during digestion on the loss of analyte due to formation of insoluble Fluoride species. This lead to the exclusion of HF during digestion as for latter loss. It was possible to develop a digestion method, where the epoxy polymer could be dissolved with the silica particles remaining as residue after digestion. Though analyte loss is to be expected due to adsorption of ions onto the silica particles, it was shown that the addition of Cl^- species during digestion shows stabilization of analyte ions within digestion solution. Results for the Na content were compared with results from a reference analysis lab which performed a Wickbold combustion with afterwards acidic digestion of the residue. This showed that with the established digestion method, similar Na contents could be quantified within the sample material. This results in a method which demands less lab infrastructure to be realized.
The parameter optimization for the digestion yielded a final digestion method using 40 mg of the milled sample and 3.1 mL of an acid mixture (1:1 (v/v) HNO_3:HCl at 220 °C for 45 min hold time at maximum temperature with a temperature ramp of 15 min from room temperature to the desired 220 °C). All delivered samples were analyzed using the final digestion method and compared. Samples could be devided in a fraction of unmolded (uncured) and molded (cured) samples. 12 different molding compounds were analyzed using 6 unmolded and 6 molded samples. Unmolded and molded samples showed no difference in elemental content for most analytes. However, elements which are employed in steel alloys showed a significant higher content within the molded samples. This results from a greater abrasion process during milling using a steel vessel, as the molded samples needed to be milled 2 min longer compared to their unmolded counterpart. However, main elements of interest were Na, Mg and Ca which all showed no variance between both sample types. Between different molding compound samples MCA-MCF, elemental content varied a lot for various elements e.g. Na, Mg and Al, which indicates the employment of additives containing these elements in molding compound materials. However, for some elements, content stayed within a similar concentration range such as Li, Ca and Sr. Strong variation in the elemental content either comes from the use of additives or simply a difference in contamination due to the different production sites of the sample material.
To conclude, during this thesis it was possible to develop a digestion method which properly dissolves the synthetic material employed in molding compound. However, it was not possible

to develop a total digestion method as the silica particles remained as residue.

6.2 Extraction of mobile ions

In order to better understand the leaching behavior of the mobile ions in molding compound, time and temperature studies were conducted. Using a metal block with resistance heating, long time extractions (6 h to 48 h) were carried out to firstly investigate the extraction behavior. Results showed, that at longer extraction times and higher temperatures are not favorable due to possible precipitation or adsorption onto the sample material. However, short extraction times showed promising results as >90 % of Na are already in solution after only 6 h of extraction time and Mg and Ca showed even higher levels of mobile content after 6 h at 150 °C as compared to 24 h. Further time and temperature studies were carried out using microwave assisted extraction with temperatures from 150 °C to 225 °C and 30 min to 180 min of extraction time. At shorter extraction times, higher temperature proved to be advantageous for the leaching behavior. However, higher temperatures at a shorter extraction time showed higher extraction efficiency as compared to a lower temperature at longer extraction times. It was then possible to settle on general extraction parameters to realize a final extraction method with which all molded samples were extracted afterwards.

Comparing the results of the heating block experiments, almost all elements showed a mild increase in mobile content when a higher temperature was applied, the exception being Mg, Ca, Sr and Ba which showed a decrease at longer extraction times and higher temperatures most likely due to precipitation of these elements. This also may result from the degradation of sulfur compounds to sulfate during extraction, which would suggest the formation of insoluble sulfates. However, this is contradicted by the increase of the mobile content of Mg, Ca, Sr and Ba with longer extraction times and temperatures using microwave assisted extraction. For some elements, stirring proved to be a great option in order to increase extraction efficiency, though results stay in a comparable concentration range. Comparing the results with the industrial standard SEMI G29, the necessity of an extraction of 48 h cannot be justified, as the results after 24 h showed either similar or even greater quantified mobile contents. The reduction to an extraction time of 24 h would already double the possible sample throughput. Most interestingly, ions showed a high mobility within the first 6 h of extraction for almost all elements, suggesting an even lower applicable extraction time.

Using the microwave for extraction, only short extraction times of <120 min in one run were possible. Temperature showed to have a great and positive influence on the extraction efficiency at shorter extraction times, with all elements showing an increasing trend. For some elements, still a linear trend can be seen. However, at some point, saturation should set in during extraction which is slightly visible for Mn in Figure 102 (diffusion controlled extraction). The same can be concluded to time dependency, though the effect of a longer extraction time is not as severe compared to the temperature dependency. To visualize: At 225 °C and 90 min hold time Na shows a mobile content of $26\,\mu g\,g^{-1} \pm 2\,\mu g\,g^{-1}$ as compared to 175 °C and 180 min hold time with $17\,\mu g\,g^{-1} \pm 3\,\mu g\,g^{-1}$. As Lactate showed a decrease in mobile content at 225 °C due to degradation at higher temperatures, the final extraction method opted for 200 °C and a hold

time of 60 min.

Completion of extraction showed an average decrease of 65 % after the first extraction, suggesting that with the current method, extraction is not complete. However, the need of a complete extraction can be of debate, as the quantified mobile content should only be representative of the ion mobility and it is unclear whether all ions leachable by aqueous extraction also show mobility within the molding compound when an external electric field is applied.

Particle size showed a great influence on the extraction behavior, with increased extraction efficiency with smaller particles, as it was expected that with higher wetable surface area also the extraction efficiency should increase. The effect of particle size on extraction efficiency differed from analyte to analyte. The only analyte behaving differently was Lactate which showed a higher mobile content with the particle size fraction >180 μm.

Analytes and samples showed a great variance in the mobile fraction. Some elements showed a similar mobile fraction within almost all molded samples (Li, Sr) while others showed big differences such as Na which ranged from < LOQ to a mobile fraction of 63 % ± 1 %. Ca also showed a mobile fraction > 100 % suggesting loss of analyte due to adsorption processes after digestion. Most analytes and samples showed a mobile fraction of 50 % or below with exception of Li and sample MCF for elements Ca, Mn and Sr. However, the extraction conditions were far away from any saturation, suggesting an even higher mobile fraction is possible. Question remains, whether the quantified mobile fractions can be correlated to any errors occurring with certain molding compound samples.

Goal of this thesis was to better understand the leaching behavior of mobile ions in molding compound with a focus on time and temperature dependency. In this thesis, a positive influence of higher extraction temperatures and shorter extraction times was shown. It was further possible to develop a final extraction method and perform extractions with all delivered molded samples. Comparing various results of temperature and time variation with the SEMI G29, a greater mobile content was quantified compared to the industrial standard. For example, at 200 °C and 90 min hold time (MCF1) a mobile content of Na of 22 μg g^{-1} ± 2 μg g^{-1} was quantified. According to the results for the SEMI G29 only 9 μg g^{-1} ± 1 μg g^{-1} which is 2.5 times less compared to the mobile content mentioned before. To summarize, it was possible to develop a novel extraction method which suggests higher mobile contents within molding compounds are possible as could be believed by applying the SEMI G29. Accounting for sample work-up time the developed method takes 2.5 h until analysis is possible. This presents a 19 times faster method compared to SEMI G29 and allows for 3 to 4 extraction runs per 8 h working shift.

7 Outlook

This work presents a method for microwave assisted acid digestion of epoxy resin based molding compound using HNO_3 and HCl. However, it was not possible to totally digest the sample as silica remained as residue after digestion or insoluble Fluorides formed when HF was employed. Different approaches could be investigated in order to further optimize the digestion method. Firstly, HF could be employed during the digestion. After the digestion, the solution and the residue could then be heated and the acid is evaporated. Afterwards HCl is added which reacts with the insoluble Fluorides to HF and its Chlorides. Additional HF can then again be evaporated. Afterwards the residue is dissolved in HNO_3 which then can be further diluted and analyzed. This poses as an alternative, however, it is much more labor intensive compared to the presented digestion method. Additionally, volatile elements such as As, Se or Pb could be lost using this work up method after the digestion. Another approach could be a second digestion using boric acid (H_3BO_3) to dissolve the Fluoride precipitates, which on the other hand would account for a strong B contamination of the ICP-MS system in addition to the formation of unwanted polyatomic interferences which would further decrease sensitivity, for example $^{11}B^{16}O^+$, which would have a strong influence on the quantification of ^{27}Al as it is mono-isotopic. Further stabilization of analyte ions could also be investigated using different acids such as $HClO_4$, H_2SO_4 and H_3PO_4. However, introduction of such acids may result in problems during the ICP-MS analysis due to vastly different behavior and temperature stability in the ICP.

During this work it was possible to better understand the extraction of molding compound. However, only influences of time and temperature were considered for this thesis. Further investigations could focus on the optimization of sample to water ratio as lesser sample material would be beneficial for the sample work up after extraction as this may eliminate the necessity of a 3 step centrifugation step after extraction. Furthermore, question remains what happens during extraction at longer extraction times and higher temperatures. It is suggested that analytes precipitate or re-adsorb onto the sample material. This could be looked into by filtration and drying of the residue. The residue can then be digested using the developed digestion method. By comparing the mobile content and afterwards quantified content within the residue, a better insight of the extraction process could be gained.
To gain sensitivity for the quantification of the mobile content after aqueous extraction, an ICP-MS based method could be developed. This would allow to further understand the ultra short term leaching behavior of molding compound (time resolved measurement with s to min resolution). Together with the development of a leaching cell which could be directly coupled to the ICP-MS, giving further insights in leaching behavior, whether the extraction is continuous or happens in certain stages which would suggest a complex extraction mechanism of the analytes. This leaching cell could then also be designed with a heating mantle for further shorter term temperature leaching studies.

References

[1] Sabu Thomas. *Polymer composites. : Volume 1.* Wiley-VCH, Weinheim, 1st ed.. edition, 2012.

[2] John Bjerregaard Jacobsen, Jens Peter Krog, Lars Rimestad, Annemette Riis, and Allan Hjarbaek Holm. Climate-protective packaging: Using basic physics to solve climatic challenges for electronics in demanding applications. *IEEE Industrial Electronics Magazine*, 8(3):51–59, 2014.

[3] Morten S Jellesen, Vadimas Verdingovas, Hélène Conseil, Kamila Piotrowska, and Rajan Ambat. Corrosion in electronics: Overview of failures and countermeasures. In *European Corrosion Congress*, 2014.

[4] J. D. Sinclair. Corrosion of electronics: The role of ionic substances. *Journal of The Electrochemical Society*, 135(3):89C, mar 1988.

[5] J. W. Osenbach. Water-induced corrosion of materials used for semiconductor passivation. *Journal of The Electrochemical Society*, 140(12):3667, dec 1993.

[6] Marlene Marinescu. *Elektrische und magnetische Felder : Eine praxisorientierte Einführung*, chapter 1. Elektronische Felder, page 12. Springer Berlin Heidelberg, Berlin, Heidelberg, 2009.

[7] Giorgio Montaudo. *Mass spectrometry of polymers.* CRC Press, Boca Raton, Fla. [u.a.], 2002.

[8] B Chabert, JL Gardette, G Lachenal, and I Stevenson. Applications of ft-raman and ft-ir microspectroscopy in the near infrared to polymer analysis. In *Progress in Fourier Transform Spectroscopy*, pages 399–402. Springer, 1997.

[9] Veronika Zeller. *Characterization and classification of epoxy molding compounds using LIBS and LA-ICP-MS.* Wien, 2022.

[10] Lukas Brunnbauer. *Advanced polymer characterization using LA-ICP-MS and LIBS.* PhD thesis, Wien, 2021.

[11] T Stehrer, J Heitz, JD Pedarnig, N Huber, B Aeschlimann, Detlef Günther, H Scherndl, T Linsmeyer, H Wolfmeir, and E Arenholz. La-icp-ms analysis of waste polymer materials. *Analytical and bioanalytical chemistry*, 398(1):415–424, 2010.

[12] Beatriz Fernández, Fanny Claverie, Christophe Pécheyran, and Olivier FX Donard. Direct analysis of solid samples by fs-la-icp-ms. *TrAC Trends in Analytical Chemistry*, 26(10):951–966, 2007.

[13] Henryk Matusiewicz. Systems for microwave-assisted wet digestion. In *Microwave-Assisted Sample Preparation for Trace Element Analysis*, pages 77–98. Elsevier, 2014.

[14] Robert Thomas. *Practical guide to ICP-MS : a tutorial for beginners*. CRC Press, Boca Raton, third edition. edition, 2013.

[15] Gerhard Schlemmer, Lieve Balcaen, José Luis Todolí, and Michael W Hinds. *Elemental analysis : an introduction to modern spectrometric techniques*. De Gruyter graduate. De Gruyter, Berlin, 2019.

[16] James S. (James Sherwood) Fritz and Douglas T. Gjerde. *Ion chromatography*. Wiley-VCH, Weinheim, [Germany], 3rd ed.. edition, 2000.

[17] Andreas Limbeck, Patrick Galler, Maximilian Bonta, Gerald Bauer, Winfried Nischkauer, and Frank Vanhaecke. Recent advances in quantitative la-icp-ms analysis: challenges and solutions in the life sciences and environmental chemistry. *Analytical and Bioanalytical Chemistry*, 407(22):6593–6617, 2015.

[18] Ulrich Stroth. *Plasmaphysik : Phänomene, Grundlagen und Anwendungen*, chapter 1, pages 1,8. Springer Spektrum, Berlin, 2. auflage. edition, 2018.

[19] William M Haynes. *CRC Handbook of Chemistry and Physics : a ready-reference book of chemical and physical data*. 100 Key Points. CRC Press, London, 97th edition 2016-2017. edition, 2016.

[20] Lenntech. Argon (ar). Online, 2022. Acessed: 23.12.2022; `https://www.lenntech.de/pse/elemente/ar.htm`.

[21] David Harvey. Inductively coupled plasma torch. Online, July 2013. Acessed 23.12.2022; `https://asdlib.org/imageandvideoexchangeforum/inductively-coupled-plasma-torch/`.

[22] Sabine Becker. *Inorganic Mass Spectrometry: Principles and Applications*. Wiley-Interscience, Newy York, 1. aufl. edition, 2008.

[23] Alpha Resources. A look a the moste critical component of icp-ms. Online, October 2022. Acessed 23.12.2022; `https://www.labmanager.com/in-focus/a-look-at-the-most-critical-component-of-icp-ms-28969`.

[24] Academic library free online college e tectbooks. Different coliision/reaction cell approaches. Online, 2022. Accessed 23.12.2022; `https://ebrary.net/194327/mathematics/collisionreaction_cell_approaches`.

[25] Simon Nelms. *Inductively coupled plasma mass spectrometry handbook*. Blackwell, 2005.

[26] S. Greenfield, I. Ll. Jones, and C. T. Berry. High-pressure plasmas as spectroscopic emission sources. *Analyst*, 89:713–720, 1964.

[27] Sharib Raza Khan, Babita Sharma, Pooja A. Chawla, and Rohit Bhatia. Inductively coupled plasma optical emission spectrometry (icp-oes): a powerful analytical technique for elemental analysis. *Food analytical methods*, 15(3):666–688, 2022.

[28] Xiandeng Hou, Renata S. Amais, Bradley T. Jones, and George L. Donati. *Inductively Coupled Plasma Optical Emission Spectrometry*, pages 1–25. John Wiley & Sons, Ltd, 2016.

[29] Thomas W. Barnard, Michael I. Crockett, Juan C. Ivaldi, and Peter L. Lundberg. Design and evaluation of an echelle grating optical system for icp-oes. *Analytical Chemistry*, 65(9):1225–1230, 1993.

[30] José Alfons Clement Broekaert. *Analytical atomic spectrometry with flames and plasmas*. Wiley-VCH, Weinheim, 2., completely rev. and extended ed.. edition, 2005.

[31] Sandra L. Bonchin, Grace K. Zoorob, and Joseph A. Caruso. Atomic emission, methods and instrumentation. In John C. Lindon, editor, *Encyclopedia of Spectroscopy and Spectrometry*, pages 42–50. Elsevier, Oxford, 1999.

[32] Jinliang Li, Xiao Chen, Dezheng Dai, Yunshu Gao, Min Lv, and Genxiang Chen. Tunable fiber laser with high tuning resolution in c-band based on echelle grating and dmd chip. *Micromachines*, 10(1), 2019.

[33] James M. Harnly and Robert E. Fields. Solid-state array detectors for analytical spectrometry. *Appl. Spectrosc.*, 51(9):334A–351A, Sep 1997.

[34] Helmut Schaller. Prinzip der ccd-sensoren. Online. Accessed 05.01.2023; `http://www.bnhof.de/~didactronic/CCD/CCDprinzip.htm`.

[35] Chemical Dictionary. Definition of charge coupled device (ccd). Online, 2020. Accessed 05.01.2023; `https://www.chemicool.com/definition/charge_coupled_device_ccd.html`.

[36] Zhaochu Hu. Sample digestion methods. *Reference Module in Earth Systems and Environmental Sciences. Treatise on Geochemistry Sec. Ed.*, 15:87–109, 01 2014.

[37] Tristan Zimmermann, Marcus von der Au, Anna Reese, Ole Klein, Lars Hildebrandt, and Daniel Pröfrock. Substituting hf by hbf4 – an optimized digestion method for multi-elemental sediment analysis via icp-ms/ms. *Anal. Methods*, 12:3778–3787, 2020.

[38] C. Oliver Kappe. Controlled microwave heating in modern organic synthesis. *Angewandte Chemie International Edition*, 43(46):6250–6284, 2004.

[39] Douglas A Skoog, F. James Holler, and Stanley R Crouch. *Instrumentelle Analytik : Grundlagen - Geräte - Anwendungen*. Lehrbuch. Springer Spektrum, Berlin [u.a.], 6., vollständig überarb. erw. aufl.. edition, 2013.

[40] Joachim Weiss and Oleg Shpigun. *Handbook of ion chromatography*. Wiley-VCH, Weinheim, Germany, 4th ed.. edition, 2016.

[41] Shimadzu. Inorganic anion detection. Online, 2023. Accessed 13.02.2023 `https://www.shimadzu.com/an/service-support/technical-support/analysis-basics/liquid-chromatography/ion/64intro/index.html`.

[42] Dan Wu, Yinglu Hu, Ying Liu, and Runyu Zhang. Review of chloride ion detection technology in water. *Applied Sciences*, 11(23):11137, Nov 2021.

[43] Michael Swartz. Hplc detectors: A brief review. *Journal of Liquid Chromatography & Related Technologies*, 33(9-12):1130–1150, 2010.

[44] Inst Tools. Two electrode conductivity probes principle. Online, 2023. Accessed 13.02.2023 `https://instrumentationtools.com/two-electrode-conductivity-probes-principle/`.

[45] Winfried Vonau. ph electrodes - industrial, medical, and other applications. In *Encyclopedia of Applied Electrochemistry*, pages 1521–1529. Springer New York, New York, NY, 2014.

[46] Wolfgang Goepel. Chemical sensor technologies: Empirical art and systematic research. In *Sensors*, volume 2, pages 61–118. Wiley-VCH Verlag GmbH, Weinheim, Germany, 1991.

[47] Hamilton Company. The combination ph electrode. Online, 2023. Accessed 20.03.2023 `https://www.hamiltoncompany.com/process-analytics/ph-and-orp-knowledge/the-ph-measurement-system/combination-ph-electrode`.

[48] Rachid Hsissou, Rajaa Seghiri, Zakaria Benzekri, Miloudi Hilali, Mohamed Rafik, and Ahmed Elharfi. Polymer composite materials: A comprehensive review. *Composite Structures*, 262:113640, 2021.

[49] Mohammad Asim, Mohammad Jawaid, Naheed Saba, Ramengmawii, Mohammad Nasir, and Mohamed Thariq Hameed Sultan. 1 - processing of hybrid polymer composites—a review. In Vijay Kumar Thakur, Manju Kumari Thakur, and Raju Kumar Gupta, editors, *Hybrid Polymer Composite Materials*, pages 1–22. Woodhead Publishing, 2017.

[50] Kris Bruton, Rachael Hazael, Richard Critchley, and Susanna Bloodworth-Race. Lignocellulosic natural fibers in polymer composite materials: Benefits, challenges and applications. In M.S.J. Hashmi, editor, *Encyclopedia of Materials: Plastics and Polymers*, pages 353–369. Elsevier, Oxford, 2022.

[51] Mitja Linec and Branka Mušič. The effects of silica-based fillers on the properties of epoxy molding compounds. *Materials*, 12(11):1811, Jun 2019.

[52] Farrah Noor Ahmad, Mariatti Jaafar, Samayamutthirian Palaniandy, and Khairun Azizi Mohd Azizli. Effect of particle shape of silica mineral on the properties of epoxy composites. *Composites Science and Technology*, 68(2):346–353, 2008.

[53] Haiying Wang, Yilong Bai, Sheng Liu, Jiali Wu, and C.P. Wong. Combined effects of silica filler and its interface in epoxy resin. *Acta Materialia*, 50(17):4369–4377, 2002.

[54] Fan-Long Jin, Xiang Li, and Soo-Jin Park. Synthesis and application of epoxy resins: A review. *Journal of Industrial and Engineering Chemistry*, 29:1–11, 2015.

[55] Ananyo Bandyopadhyay, Pavan K. Valavala, Thomas C. Clancy, Kristopher E. Wise, and Gregory M. Odegard. Molecular modeling of crosslinked epoxy polymers: The effect of crosslink density on thermomechanical properties. *Polymer*, 52(11):2445–2452, 2011.

[56] Roderick Ramsdale-Capper and Joel Foreman. Internal antiplasticisation in highly crosslinked amine cured multifunctional epoxy resins. *Polymer*, 146, 05 2018.

[57] C.H. Park and W.I. Lee. 3 - compression molding in polymer matrix composites. In Suresh G. Advani and Kuang-Ting Hsiao, editors, *Manufacturing Techniques for Polymer Matrix Composites (PMCs)*, Woodhead Publishing Series in Composites Science and Engineering, pages 47–94. Woodhead Publishing, 2012.

[58] Kirk M. Cantor and Patrick Watts. 12 - plastics processing. In Myer Kutz, editor, *Applied Plastics Engineering Handbook*, Plastics Design Library, pages 195–203. William Andrew Publishing, Oxford, 2011.

[59] Kun Fang. 3 - encapsulation process technology. In Haleh Ardebili, Jiawei Zhang, and Michael G. Pecht, editors, *Encapsulation Technologies for Electronic Applications (Second Edition)*, Materials and Processes for Electronic Applications, pages 123–181. William Andrew Publishing, second edition edition, 2019.

[60] Michael Kothe, Christiane Kothe, and Bernhard Weller. Epoxy resin adhesives for structural purposes – a new approach. 10 2014.

[61] Akio MAKISHIMA, Ryoji TANAKA, and Eizo NAKAMURA. Precise elemental and isotopic analyses in silicate samples employing icp-ms: Application of hydrofluoric acid solution and analytical techniques. *Analytical Sciences*, 25(10):1181–1187, 2009.

[62] General aspects of trace analytical methods—iv. recommendations for nomenclature, standard procedures and reporting of experimental data for surface analysis techniques. *Pure and Applied Chemistry*, 51(11):2243–2250, 1979.

[63] Le Wen, Zhihang Zhang, Dilip Rai, Da-Wen Sun, and Tiwari Brijesh kumar. Ultrasound-assisted extraction (uae) of bioactive compounds from coffee silverskin: Impact on phenolic content, antioxidant activity, and morphological characteristics. *Journal of Food Process Engineering*, 42, 07 2019.

[64] F. Temelli, M.D.A. Saldaña, and L. Comin. 4.18 - application of supercritical fluid extraction in food processing. In Janusz Pawliszyn, editor, *Comprehensive Sampling and Sample Preparation*, pages 415–440. Academic Press, Oxford, 2012.

List of Tables

List of Figures

List of Abbreviations

AC	Alternating Current
CCD	Charged Coupled Device
CID	Charge Injection Device
DC	Direct Current
DCP	Direct Current Plasma
DDM	4,4'-diaminodiphenyl methane
DDS	4,4'-diaminodiphenyl sulfone
ESI-MS	Electrospray Ionization Mass Spectrometry
F-AAS	Flame Atomic Absorption Spectroscopy
FT-IR	Fourier Transformation Infrared Spectroscopy
GF-AAS	Graphite Furnace Atomic Absorption Spectroscopy
IC	Ion Chromatography
ICP	Inductively Coupled Plasma
ICP-MS	Inductively Coupled Plasma Mass Spectrometry
ICP-OES	Inductively Coupled Plasma Optical Emission Spectroscopy
IZ	Induction Zone
KED	Kinetic Energy Discrimination
LA-ICP-MS	Laser Ablation Inductively Coupled Plasma Mass Spectrometry
LIBS	Laser Induced Breakdown Spectroscopy
LOD	Limit Of Detection
LOQ	Limit Of Quantification
m/z	Mass to charge ratio
MALDI-MS	Matrix Assisted Laser Desorption Ionization Mass Spectrometry
MAAD	Microwave Assisted Acid Digestion
MIP	Microwave Induced Plasma
MOS	Metal Oxide Semiconductor
PTE	Periodic Table of the Elements
PMT	Photo-multiplier Tube
PEEK	Polyether ether ketone
PCBA	Printed Circuit Board Assembly
Py-GC	Pyrolysis Gas Chromatography
RF	Radiofrequency
RSD	Relative Standard Deviation
SEM-EDX	Scanning Electron Microscopy Energy Dispersive X-ray Spectroscopy
SEM	Secondary Electron Multiplier
SIMS	Secondary Ion Mass Spectrometry
SF	Sector Field
SCD	Segmented Coupled Device
SNR	Signal to Noise Ratio

SD	SDStandard Deviation
TOF	Time Of Flight
UV	Ultra violet
VIS	Visible
WL	Wavelength

8 Appendix

8.1 Ion chromatograms of molded molding Compounds

8.1.1 MCA

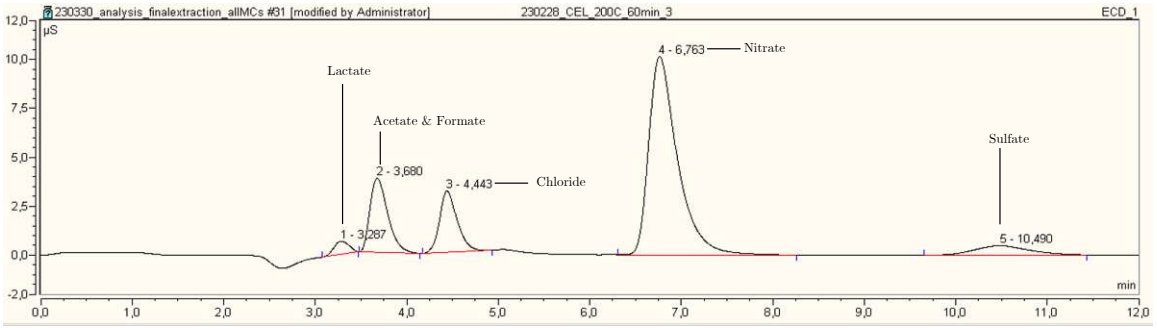

Figure 192: Ion chromatogram of molding compound MCA molded

8.1.2 MCB

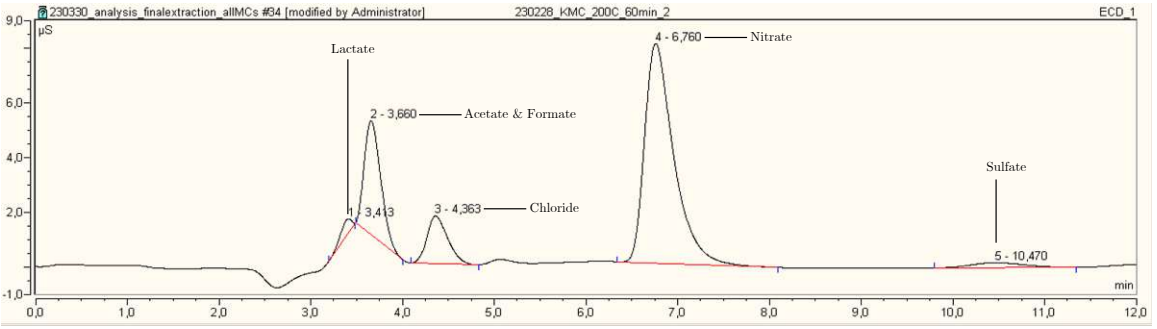

Figure 193: Ion chromatogram of molding compound MCB molded

8.1.3 MCC

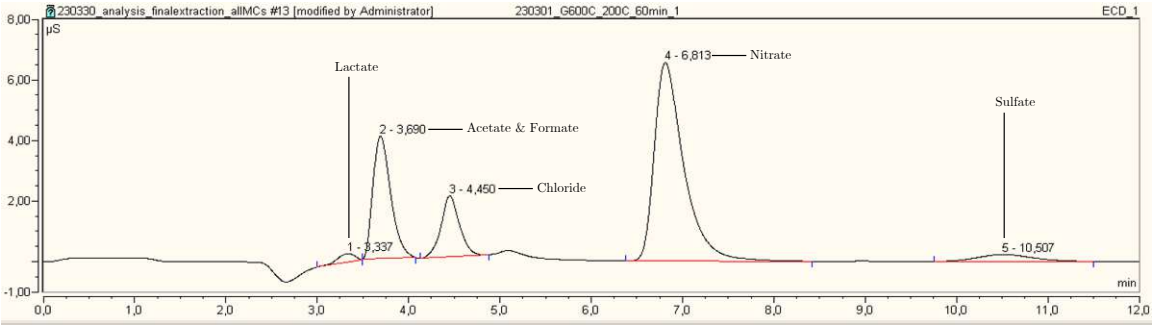

Figure 194: Ion chromatogram of molding compound MCC molded

8.1.4 MCD

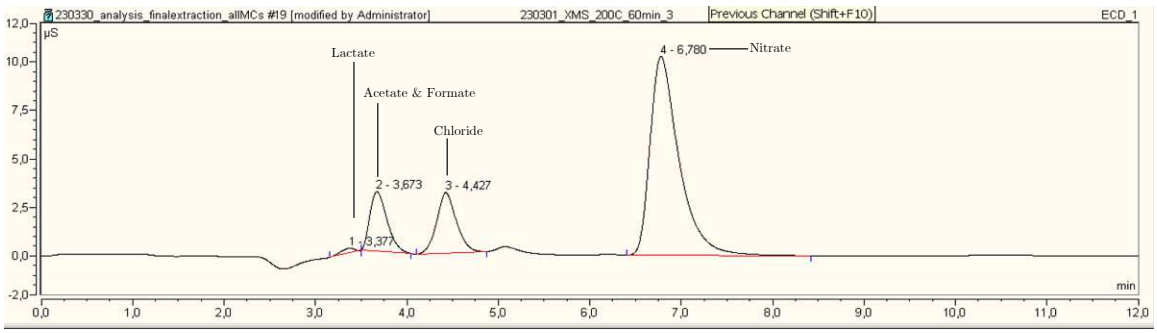

Figure 195: Ion chromatogram of molding compound MCD molded

8.1.5 MCE

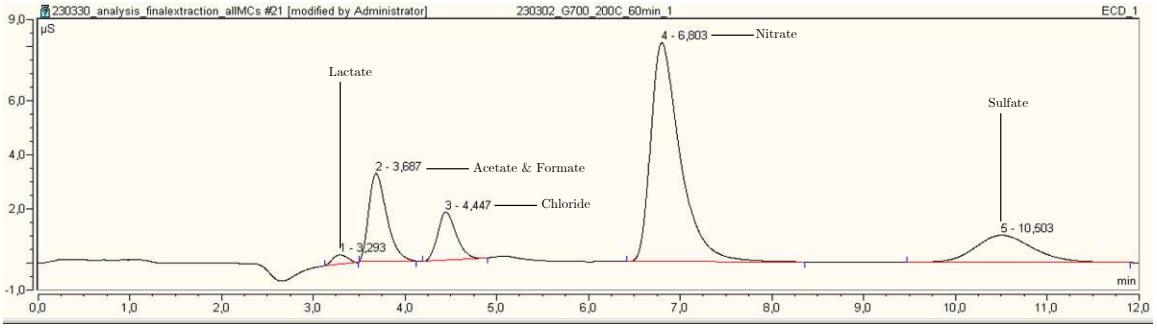

Figure 196: Ion chromatogram of molding compound MCE molded

8.1.6 MCF

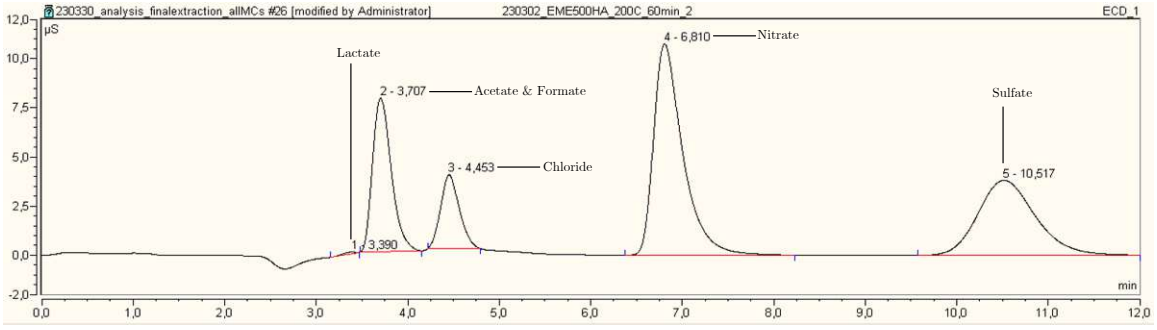

Figure 197: Ion chromatogram of molding compound MCF molded

8.2 ICP-MS: LOQs

Table 6: Determined Limits of Quantification (LOQs) for targeted isotopes of the ICP-MS measurement

Isotope	LOQ ($ng\,g^{-1}$)
^{7}Li	0.0510
^{9}Be	0.0690
^{11}B	0.344
^{23}Na	2.93
^{24}Mg	0.200
^{27}Al	0.348
^{44}Ca	0.455
^{50}Cr	0.185
^{52}Cr	0.0382
^{55}Mn	0.0418
^{56}Fe	0.0596
^{58}Ni	0.0124
^{60}Ni	0.0258
^{59}Co	0.0055
^{63}Cu	0.115
^{65}Cu	0.0705
^{64}Zn	0.176
^{66}Zn	0.0667
^{68}Zn	0.237
^{69}Ga	0.0188
^{71}Ga	0.0033
^{86}Sr	0.0465
^{88}Sr	0.0095
^{111}Cd	0.0034
^{112}Cd	0.0084
^{121}Sb	0.0089
^{125}Te	0.0165
^{126}Te	0.0177
^{137}Ba	0.0252
^{138}Ba	0.0119
^{139}La	0.0011
^{141}Pr	0.0003
^{143}Nd	0.0013
^{146}Nd	0.0029
^{178}Hf	0.0111
^{203}Tl	0.0010
^{205}Tl	0.0008
^{208}Pb	0.0061
^{209}Bi	0.0006

8.3 ICP-OES: LOQs

Table 7: Determined Limits of Quantification (LOQs) for targeted isotopes of the ICP-OES measurement

Element	WL I (nm)	LOQ ($ng\,g^{-1}$)	WL II (nm)	LOQ ($ng\,g^{-1}$)
Li	670.784	1.76	-	-
Be	313.042	0.150	234.861	1.43
B	249.773	5.60	249.678	19.9
C	193.091	1128	247.856	517
Na	589.592	296	819.482	531
Mg	279.553	0.395	280.270	0.265
Al	167.079	159	396.152	40.6
K	766.490	49.7	-	-
Ca	393.366	0.217	373.690	10.9
Cr	267.716	9.74	284.325	21.4
Mn	257.610	2.46	259.373	2.15
Fe	259.940	4.62	238.204	31.8
Co	228.616	23.8	238.892	30.4
Ni	231.604	72.0	221.647	12.7
Cu	324.754	6.36	213.598	99.5
Zn	213.856	11.4	202.548	15.5
Ga	294.364	107	-	-
Sr	407.771	0.356	421.552	0.287
Cd	228.802	15.0	226.502	8.95
Te	214.281	240	-	-
Ba	455.403	0.479	233.257	5.77
La	412.323	10.0	379.478	1.02
Pr	414.311	21.8	-	-
Nd	401.225	16.2	-	-
Tl	190.856	56.1	-	-
Pb	220.353	464	-	-
Bi	223.061	265	-	-